NOISE FROM STOCHASTICALLY EXCITED STRUCTURES

MODELLING THE NOISE FROM MARINE PROPELLERS EXCITED BY A TURBULENT BOUNDARY LAYER

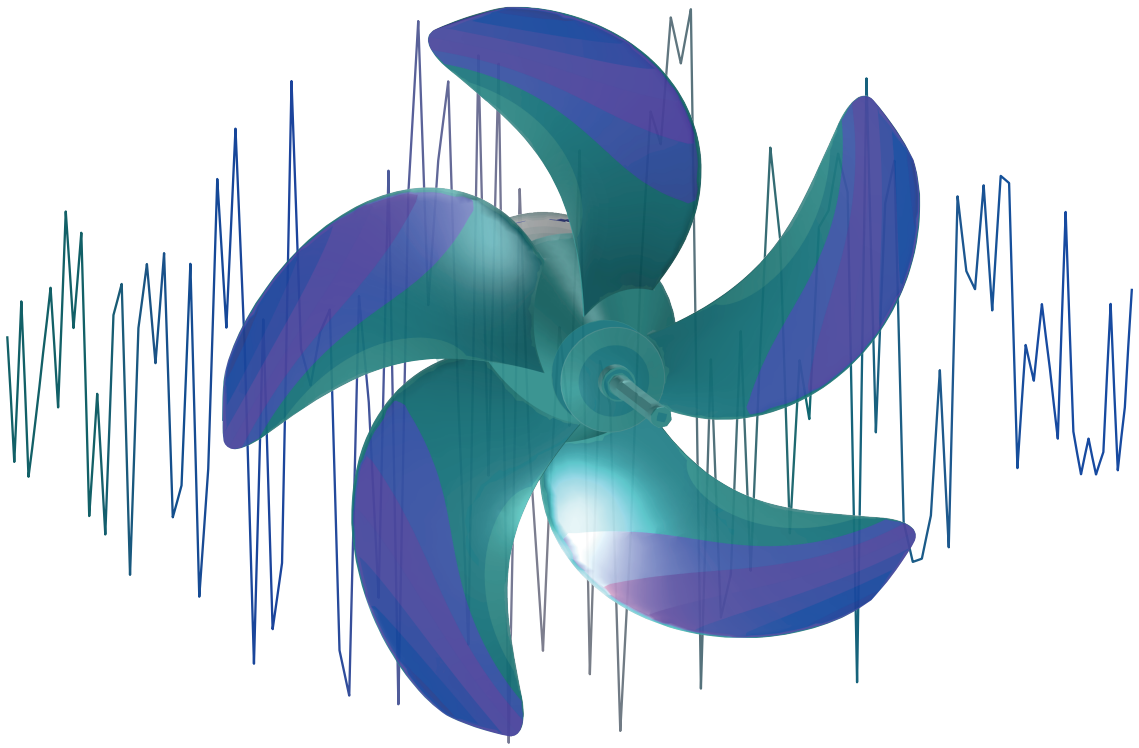

AUTHOR
Ravi de Berg BSc.
MSc. Experimental Physics
Utrecht University

SUPERVISORS
Dr.-Ing. Roel Müller
dr.ir. Ysbrand Wijnant
dr. Peter van Capel

Λεωφοροὺς ὁδους μὴ στείχειν.

Do not travel on the path of the masses.

— Pythagoras

ABSTRACT

People do not always realise sound is of great importance underwater. Marine life is strongly affected by underwater noise. The source of underwater noise this work focusses on is that of non-cavitating marine propellers. This noise is caused by pressure fluctuations on the propeller, which arise because of the turbulent inflow generated by the ship wakefield and hull, and the turbulent boundary layer on the blade. These fluctuations are so complicated, that they are basically random but with known statistical properties. Therefore, we need a stochastic approach to calculate the radiated noise. We need to first calculate the response to this stochastic excitation and consequently the radiated noise.

To this end, we first show that we can calculate the response of a multi-degree-of-freedom system under stochastic excitation. We demonstrate that we can calculate the response of proportionally damped linear systems through a modal approach. A modal approach is a valid approach, because the resonances of a system dominate the response. Apart from this, we also show that we can calculate the response through modal analysis for non-proportionally damped systems. This approach uses state-space to allow for modal analysis.

These multi-degree-of-freedom systems are the basis of further calculations on real geometries. The finite element method is employed to calculate the response of systems with arbitrary geometries. A finite element system behaves largely in the same way as a multi-degree-of-freedom system. We show that we can calculate the response of both the proportionally and non-proportionally damped systems. These calculations are verified for very simple systems by using analytical computations. One limitation of the non-proportional finite element method is that a point loading seems to give deviating results for COMSOL Multiphysics and our state-space approach. However, this is not a large limitation, as real world applications mostly use surface loads. Also, this difference does not arise for proportionally damped systems.

Finally, to calculate the radiated noise of a system, we show that we can use structural-acoustic coupled systems. A modal analysis using the state-space approach, allows us to calculate the response of the structure, and the pressure response in the fluid. Integrating the cross-spectra of these responses at the interface gives the radiated sound intensity spectrum. It turns out however, that the resulting pressure and structural response are not the same for our calculations and the one done by COMSOL Multiphysics. Especially for high density fluids (such as water), the results deviate significantly.

Further research into this topic should focus on finding an explanation for this difference, for example by using an open-source software package to calculate system matrices, or by finding the system matrices of a simple system by oneself, using the (semi-analytical) expressions for a simple system. Experimentally verifying the results would bring this part of the research to a close. Additionally, more research on characterising the pressure spectrum caused by the inflow turbulence and turbulent boundary layer on a marine propeller would make the calculations relevant for real-world applications.

ACKNOWLEDGMENTS

My time at Utrecht University has come to an end with the completion of this thesis. This work is the final step in graduating from the Experimental Physics Master's programme.

First off, I would like to thank Roel Müller for the great guidance and warm welcome at TNO. The conversations we had about LaTeX packages and Python scripts have taught me many things. I thoroughly enjoyed my time at the Acoustics and Sonar group. They are a great group of people, whether in the office or outside struggling during the boot camp sessions. In particular, I would like to mention Christ de Jong, Elisabeth van Pruissen, and Victor Oppeneer as part of the PANPA project. I also want to thank all the other people from the PANPA project for their suggestions and discussions.

Another person that rightly deserves my thanks is Ysbrand Wijnant from the University of Twente. After Yorick de Valk left the project, he made sure there was a smooth transition. He also helped a great deal by always coming up with new suggestions and ways of tackling problems. I would also like to thank Yorick, who greatly helped me in the beginning of this project with all the things I knew nothing about.

I am also grateful to Peter van Capel, my supervisor from Utrecht University. It is quite unusual in the Experimental Physics programme to do a project outside the university, but Peter was immediately enthusiastic about supervising me during my time at TNO. He was always ready to help and give feedback when I needed it. Apart from Peter, I would like to thank Gerhard Blab for being my second supervisor from Utrecht University.

I would also like to thank my friends and family. Especially my parents, whom I have called many times throughout the year with random questions about LaTeX, Ipe, and for general advice about life. Lastly, I would like to thank Salma for her support throughout the process. We were in the same boat most of the year writing our theses simultaneously, side by side at our desks. Thank you for everything you have done for me!

CONTENTS

NOMENCLATURE

For further information on notation and definitions see also Section 2.1.

General

$\mathscr{A}$	integration area for a continuous 2D system
A	area
a	length of a plate in the x-direction
b	width of a plate in the y-direction
c	speed of sound
$\boldsymbol{C}$	damping matrix
c_k	damping constant of the k^{th} damper in a system
e	mathematical constant, approximately 2.71828
E	Young's modulus of elasticity
$\vec{f}$	force vector
$\boldsymbol{G}$	diagonal matrix of frequency response functions
G_k	frequency response function associated with mode k
g_k	impulse response function associated with mode k
$\vec{h}$	modal force vector
h	thickness of a plate
$\boldsymbol{I}$	identity matrix
i	the imaginary unit
$\boldsymbol{K}$	stiffness matrix
k, l, r, s	dummy indices
k_k	spring constant of the k^{th} spring in a system
K_x	chord-wise wave number ω / U_∞
k_y	span-wise wave number
$\mathscr{L}$	integration path for a continuous 1D system
L	length of a 1D system
$\boldsymbol{M}$	mass matrix
M	Mach number U_∞ / c

m	density per unit length
m_k	mass of the k^{th} object in a system
n	number of masses in a discrete system
$\vec{p}$	pressure part of a solution vector for coupled systems
P_{rad}	radiated acoustic power
$\vec{q}$	displacement vector
q	displacement of a continuous system
R_x	correlation function for some process x, can also be a cross-correlation between two processes
S_x	two-sided power spectral density for some process x, mostly used in the displacement/force spectral density (S_q/S_f)
$\boldsymbol{U}$	matrix of modal vectors, where each column represents one modal vector
$\vec{u}_k$	k^{th} eigenvector of a system corresponding to ω_k
U_∞	mean far-field velocity
$\mathscr{V}$	integration volume for a continuous 3D system
$\boldsymbol{X}$	right eigenvector matrix in state-space
$\vec{x}_k$	k^{th} right eigenvector of a system in state-space corresponding to λ_k
x, y, z	Cartesian coordinates
$\boldsymbol{Y}$	left eigenvector matrix in state-space
$\vec{y}_k$	k^{th} left eigenvector of a system in state-space corresponding to λ_k

Greek Symbols

α	damping proportionality constant for the mass matrix
β	damping proportionality constant for the stiffness matrix
γ	airfoil response function
Γ	integration surface for a 3D system
ζ_k	damping factor of the k^{th} mode
η_k	displacement of a system in the k^{th} mode
$\vec{\eta}$	modal displacement vector
λ_k	k^{th} eigenfrequency in state-space
$\boldsymbol{\Lambda}$	diagonal matrix of eigenvalues in state-space
μ, κ, χ	dummy variables
ν	Poisson's ratio
$\vec{v}$	modal force vector in state-space

$\vec{\xi}$	modal displacement vector in state-space
π	mathematical constant, approximately 3.14159
ρ	density per unit area or volume
σ_x	standard deviation of a process x
Φ_{ww}	two-dimensional wave number spectrum of the inflow turbulence
ψ_k	k^{th} mode shape of the continuous system
$\boldsymbol{\Omega}$	diagonal matrix of eigenfrequencies
ω	angular frequency
ω_k	k^{th} eigenfrequency

Functions

$\varkappa$	the unit step function
erf [.]	the error function
E [.]	the Fresnel integral function
δ	Dirac delta function

Operators

det [.]	determinant of a matrix
diag[.]	diagonal matrix of a given vector
$\mathcal{F}[.]$	Fourier transform
$\mathcal{F}^{-1}[.]$	inverse Fourier transform
H	Hermitian transposition operator
T	transposition operator
$\bar{X}$	complex conjugate of X
$\langle . \rangle$	time average

1 INTRODUCTION

Sound plays a very important role in our lives. We use it to communicate, it can alarm us to dangerous situations, and we listen to music. And, although we cannot hear it most of the time, sound also plays a significant role underwater. Marine mammals use sound to communicate, navigate, and orientate themselves.[1] A wide spectrum from 10 Hz to 200 kHz is used by different marine animals, whereas humans can only hear sound in the frequency range of about 20 Hz to 20 kHz.[2] Because sound plays such an import role in marine life, human-generated noise will disturb and impact it. One example of this, is the piling noise of wind turbines in the sea. This type of noise can have a significant effect on the population and behaviour of certain marine animals, and strict regulations apply.[3] Also, ship noise is almost omni-present on rivers, and the world's busiest ocean shipping lanes see continuous traffic. Since 1945, the global number of ships has almost quadrupled, and the low-frequency (10 Hz to 100 Hz) ambient noise has increase at rates of up to 3 decibels per decade (10 years).[4]

However, humans themselves are also affected by noise on ships. The crew on a ship is negatively impacted by noise that can be heard inside the vessel.[5] Human error is responsible for about 80%-85% of all accidents on sea.[6] Therefore, it is vital to have the crew perform in the most optimal conditions possible. Ships have many sources of noise, such as engines, pumps, gears, and other machinery. Also, wave-induced vibrations of the hull and propellers contribute to the radiated noise.[7, 8] This work will focus on the noise a vibrating propeller produces.

The dominant noise source for marine propellers is caused by cavitation.[9, 10] Cavitation is the process where some bubbles appear on the blades of the propeller and subsequently collapse. This collapse results in significant noise. However, when vessels are moving quite slowly, the propeller does not cavitate but still generates noise, due to the turbulence surrounding it. If one would like to design a propeller that minimises this noise, it is essential to be able to estimate the noise radiated by different designs. However, it is quite difficult to precisely predict this noise. The propeller is excited by turbulent flow caused by the ship wake field and the turbulent boundary layer around the blades. This turbulent flow is of such a nature, that it is impossible to deterministically predict the pressure fluctuations it causes. Therefore, we should turn towards stochastics: representing the turbulent flow as a random process with certain statistical properties. Doing this allows us to derive (statistical) properties of the radiated noise.

The goal of this work is to provide a pathway to predict the acoustic noise radiated by an object of an arbitrary geometry that is stochastically excited by pressure fluctuations. In Figure 1.1, a rough overview is given of the processes that have to be taken into consideration to predict the noise a marine propeller radiates. The processes can be split into two main categories: the hydroacoustics and the structural acoustics. Hydroacoustics research must characterise the resulting pressure fluctuations caused by the inflow turbulence and

turbulent boundary layer. Even though these pressure fluctuations are the input for our final model of a propeller, this work will not focus much on the exact characteristics of the inflow turbulence and turbulent boundary layers. This thesis is part of an overarching project called PANPA, of which improving upon the existing models of the pressure spectrum (for marine propellers) is also a part. However, it is still difficult to determine their exact characteristics, as they depend on the geometry of the blade, and exact position on the blade.[11, 12] Potential models of the turbulence will be briefly discussed later in the outlook of thesis (Section 8.3).

From the model of these pressure fluctuations we want to calculate the structural response of the blade, and the radiated noise. This corresponds to the last two steps in Figure 1.1. The product of this work, the structural acoustics part, should be independent of the given pressure spectrum. Our model should be able to predict the radiated noise for any given pressure spectrum. We will use a finite element method to predict the linear transfer of the pressure fluctuations to vibrations of the propeller. Because the response is dominated by resonating modes, we can use a modal approach to determine this transfer.

In principle, the results of this work could be used to calculate the noise generated by any time-invariant linear structure stochastically excited by pressure fluctuations. This theory would not only be useful for marine propellers. Other cases where this would also be useful are for example the automotive and aerospace industries, and train, wind turbine, or rocket design.[13–16] The applications are basically endless, as there are many processes governed by random vibrations. Especially for aeroplanes, the turbulent flow is comparable to that on marine propellers. Damping these random vibrations could potentially increase passenger comfort.

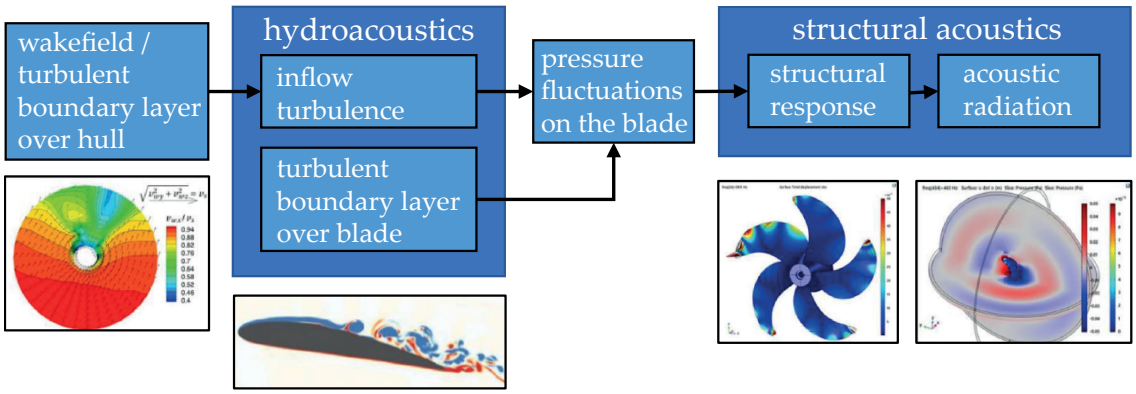

Figure 1.1: An overview of the processes taken into consideration for calculating the radiated noise. This work focusses mostly on the *structural acoustics* block. These are the last two steps, from pressure fluctuations to the structural response, and from there to the acoustic radiation. Image by ir. de Valk, adapted by Dr-Ing. Müller.

1.1 OUTLINE OF THE THESIS

The structure of this thesis will be as follows. Firstly, in Chapter 2 the definitions and mathematical notations used in this thesis are given. In this chapter a first introduction into random vibrations is also provided. In Chapter 3 the theory behind random vibrations of multi-degree-of-freedom systems is discussed. This theory forms the basis of all

calculations done in this thesis and provides some rigorous derivations. The theory behind a multi-degree-of-freedom system is later used in the chapter on finite element systems, as the finite element method also divides the structure into element corresponding to degrees-of-freedom. In Chapter 4 we will look at continuous structures and discuss the possibilities of analytical calculations. This will allow us to verify the results in Chapter 5, which discusses finite element systems and their usefulness in deriving the vibrational response for arbitrary geometries. In Figure 1.1 this is the step of finding the structural response. This finite element method is a very practical and versatile approach, which is useful for many applications. Chapter 6 discusses the coupling between fluid and structure using a finite element model. These coupled structures are needed to determine the radiated noise. This combines the steps of finding the structural response and calculating the radiated noise in Figure 1.1. The conclusions and an outlook into further research are provided in Chapter 7 and Chapter 8. In Chapter 8, an expression for the turbulent boundary layer pressure fluctuations is given, which could be an input for our model, as shown as 'pressure fluctuations on the blade' in Figure 1.1. Lastly, in Appendix A some example code and computational notes are given.

2

THEORY OF RANDOM PROCESSES

In this chapter, we will first introduce the mathematical notations and concepts used throughout this thesis. In the second part of this chapter, a first introduction into random vibrations is provided. This theory behind (ergodic) random vibrations forms the basis of the rest of the thesis. Also, the concept of the power spectral density is explained in this chapter, which will be used extensively throughout this work.

2.1 DEFINITIONS

Throughout this document we use several mathematical notations. In general, we use upper case, blue, bold letters for matrices ($\boldsymbol{X}$) and lower case green letters with an arrow for a vector ($\vec{x}$).

We define $\bar{\boldsymbol{X}}$ as the complex conjugate of a number, vector, or matrix $\boldsymbol{X}$. The transpose of a vector or matrix $\boldsymbol{X}$ is given by $\boldsymbol{X}^{\mathrm{T}}$. The Hermitian transpose of a matrix $\boldsymbol{X}$ is denoted by $\boldsymbol{X}^{\mathrm{H}} \equiv \bar{\boldsymbol{X}}^{\mathrm{T}}$. The inverse of a matrix $\boldsymbol{X}$ is given by $\boldsymbol{X}^{-1}$.

If we want to indicate the r^{th} component of a vector $\vec{x}$, we do that by subscript, i.e. x_r. For a matrix $\boldsymbol{X}$, element (r, s) is written as X_{rs}.

The time derivative of a quantity x is written as $\frac{\mathrm{d}x}{\mathrm{d}t} = \dot{x}$ and the second derivative with respect to time by $\frac{\mathrm{d}^2x}{\mathrm{d}t^2} = \ddot{x}$. The time-average of a signal x is given by $\langle x \rangle$.

The Fourier transform $\mathcal{F}$ of a function $x(t)$ is defined as

$$\mathcal{F}\left[x(t)\right] = x(\omega) = \int_{-\infty}^{\infty} x(t) \mathrm{e}^{-\mathrm{i}\omega t}\, dt\,. \tag{2.1}$$

The inverse Fourier transform $\mathcal{F}^{-1}$ of a function $x(\omega)$ follows from the definition above

$$\mathcal{F}^{-1}\left[x(\omega)\right] = x(t) = \frac{1}{2\pi} \int_{-\infty}^{\infty} x(\omega) \mathrm{e}^{\mathrm{i}\omega t}\, d\omega\,. \tag{2.2}$$

Note that we use the same symbol for both the quantity and its Fourier transform.

We define the unit step function $u(t)$ as

$$u(t) = \begin{cases} 0 & t < 0 \\ 1 & t \geq 0 \end{cases}. \tag{2.3}$$

Lastly, we use the Dirac delta $\delta(x)$ function, which is defined as

$$\int_{-\infty}^{\infty} \delta(x) f(x)\, \mathrm{d}x = f(0), \tag{2.4}$$

where $f(x)$ is any function.

2.2 RANDOM PROCESSES

Processes for which we can determine the values exactly at some time in the future, are *deterministic*. An example of this could be the position of a rock thrown off a building. We know quite well how gravity behaves and the aerodynamics of the rock are of lesser importance, if the rock is large and the tower not too tall. Therefore, at any time t after the rock is thrown, we can calculate and predict its position. In the case of vibrations, if one knows how the structure is excited, by for example a sinusoidal force, then this excitation is called deterministic. The response to such a deterministic excitation is also deterministic. It can of course still be difficult to exactly calculate the response, but in principle one can describe the response of the system as a function of time.

Some physical phenomena however, are less suitable for such a deterministic description. These *non-deterministic* processes are called *random* or *stochastic*. We will use these terms interchangeably throughout this thesis. For example, the shape of the waves on sea at a certain position is affected by many factors, e.g. storms, temperature, etc. It is basically impossible to deterministically predict what the shape of a wave at a certain position in the sea will be at a given time. An example of a vibrational problem that is non-deterministic would be a car on a rocky road. On such a rocky road, we do not exactly know what the surface profile of the road is, and therefore do not know how the car is excited. But is there really nothing we can say or predict about these random phenomena? The answer is no. Most of the time, these processes do have certain statistical properties which can be determined. For example, the rocks on the road do have an average size, or else it would not look like a road at all. Those properties are something we can work with to predict, albeit in stochastic properties, the vibrations of the car.

In Figure 2.1 some example functions are shown. For a) and b), these are deterministic functions, respectively a sine wave and a fifth-degree polynomial. One can easily predict through extrapolation what the value at some time t will be, given these functions. Subplots c) and d) were both created using random sampling. However, they look very different because the underlying statistical process is different. Subplot c) allows some predictability on small timescales. For Subplot d), there is no telling what the next number is going to be. A point at time t_1 and a point a bit later in time at t_2 have no relation whatsoever, they are independent. This is distinctly different from the process in Subplot c).

How a random signal behaves as a function of time is characterised by the *autocorrelation function*. This function is defined in the following way for discrete signals

$$R_x(j) = \lim_{n\to\infty} \frac{1}{n} \sum_{k=1}^{n} x(k)x(k+j) \tag{2.5}$$

and in the continuous case

$$R_x(\tau) = \lim_{T\to\infty} \frac{1}{T} \int_{-T/2}^{T/2} x(t)x(t+\tau)\,\mathrm{d}t\,. \tag{2.6}$$

In the case of Figure 2.1, Subplots c) and d) will have very different autocorrelation functions. The autocorrelation for the truly random signal in d) will be zero for every time delay $\tau > 0$. For the other case in Subplot c) this will not be the case, because the value at t and $t+\tau$ show some degree of correlation for small τ. Now, in practice we cannot collect signals for an infinite amount of time. If however we take a large enough sample

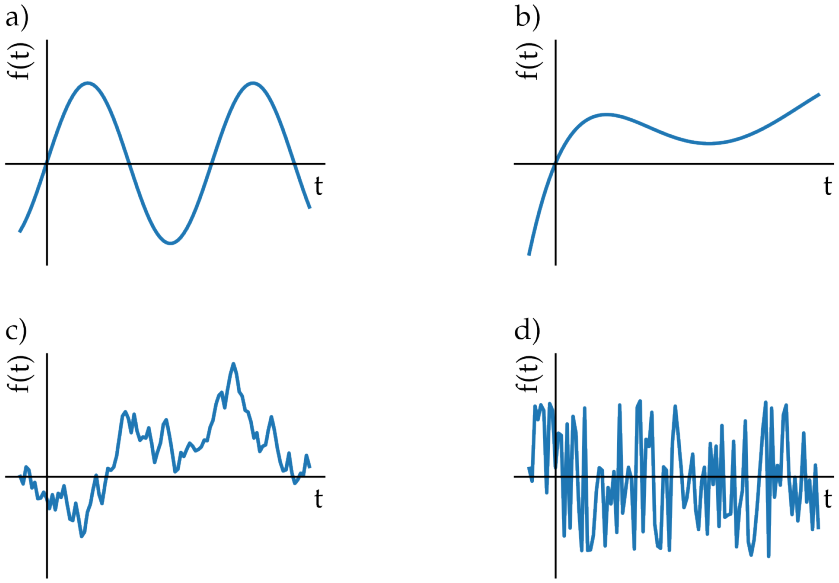

Figure 2.1: Four examples of deterministic and random functions. a) A deterministic function, the sine. b) Another deterministic function, a fifth-degree polynomial. c) A random function with correlated values, generated by adding a random number to the previous value. d) A random signal, where each data point is a randomly chosen number.

we should be able to approximate the autocorrelation function. If the autocorrelation function and the mean value do not change depending on the time at which we take this sample, the statistical process is said to be *stationary*. In this work however, we assume the processes to be *ergodic*. Ergodicity also implies that the whole sample space is visited during an infinite measurement. The takeaway from this assumption for our work is that the underlying statistics never change.

We assume this ergodicity holds for the turbulence on a marine propeller. We assume the statistical properties of the inflow do not depend on time at the relevant timescale. The effect of the sailing speed and the manoeuvring of the ship, the weather, or the specific water composition of the ocean can have an influence on the turbulence, but we will assume these occur on a larger timescale, and thus we view the turbulence as ergodic. Of course, the rotation of the propeller has an impact as well, but we will ignore this, to not complicate things further.

2.2.1 *Statistical properties of stochastic processes*

We can also extract some statistical properties from the autocorrelation function, which is interesting in the case that signal is not known, but only its autocorrelation. For one, we can extract the mean square value of the signal

$$\langle x^2 \rangle = \lim_{T \to \infty} \frac{1}{T} \int_{-T/2}^{T/2} x^2(t)\, \mathrm{d}t = R_x(0). \tag{2.7}$$

For a given signal we can also calculate the standard deviation given by

$$\sigma_x = \sqrt{\langle x^2 \rangle - \langle x \rangle^2}. \tag{2.8}$$

Now, in our case of ergodic physical vibrations, we have a constant mean. For a constant force, we will also have a constant response in a linear system. Therefore, in linear systems such as those we will be dealing with, we can ignore the mean value of the signal, and set $\langle x \rangle \to 0$. This means that the standard deviation is simply given by

$$\sigma_x = \sqrt{\langle x^2 \rangle} = \sqrt{R_x(0)}. \tag{2.9}$$

One can imagine that even with random signals, we can say something about how two random processes are related to each other. For example, in Figure 2.2 you see schematically a 1-dimensional representation of waves rolling into the shore (or over a propeller blade for that matter) from left to right at a constant speed. We can imagine that the exact shape of the waves is random. However, once a wave a passed point p_1 we can imagine that the time between it passing p_1 and p_2 is constant, and we will see the same wave at p_2. The correlation function of the height of the wave at p_1 given by $x(t)$ and p_2 given by $x_2(t)$ are related. If the waves do not decay in height, the amplitude of $x_1(t)$ and $x_2(t)$ would be exactly, but there is a time difference. This can be incorporated into the *cross-correlation function*. In general, the cross-correlation function $R_{x_1x_2}$ between two functions $x_1(t)$ and $x_2(t)$ is defined as

$$R_{x_1x_2}(\tau) = \lim_{T\to\infty} \frac{1}{T} \int_{-T/2}^{T/2} x_1(t)x_2(t+\tau)\,\mathrm{d}t\,. \tag{2.10}$$

This cross-correlation is very important when we look at the spectrum on a propeller blade. It will allow us to characterise the size of the vortices in the turbulence and the speed at which the flow moves over the blade.

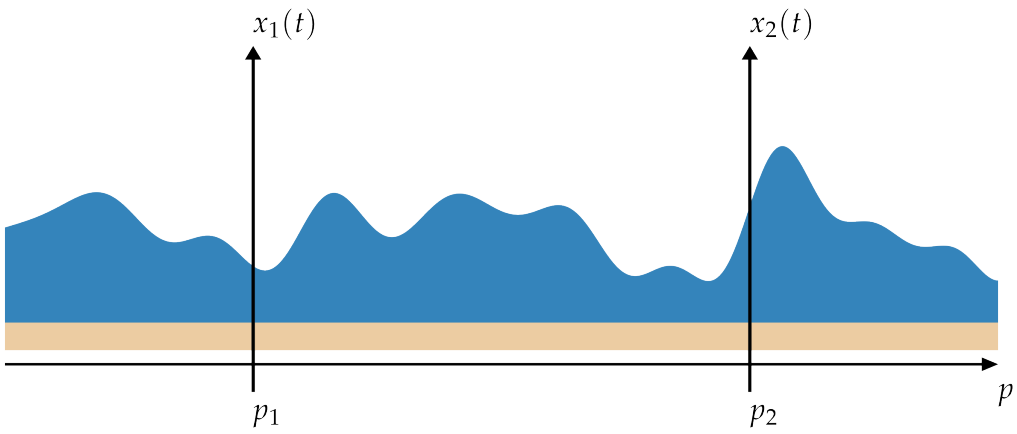

Figure 2.2: Schematic still image of waves on the sea. The functions $x_1(t)$ and $x_2(t)$ describe the height of the wave over time at positions p_1 and p_2 respectively.

2.2.2 *Power spectral density*

Sometimes, it is more convenient to work in the frequency domain than in the time domain. Especially for random processes, time signals are very difficult to interpret. Going to the frequency domain will give us more intuitive information about a signal. For example, sound is made up of signals at different frequencies, allowing us to hear different

tones. In the case of vibrating marine propellers we see peaks at certain frequencies and anti-resonances at others.

The autocorrelation function provides us with information about the signal in the time domain. However, there is also a frequency domain counterpart, the *power spectral density* (PSD). For ergodic processes, this PSD contains the same information as the correlation function, but can sometimes (as mentioned previously) be more practical. The relation between the power spectral density $S_x(\omega)$ and the autocorrelation function R_x is given by

$$S_x(\omega) = \int_{-\infty}^{\infty} R_x(\tau) \mathrm{e}^{-\mathrm{i}\omega\tau} \,\mathrm{d}\tau = \mathcal{F}\left[R_x(\tau)\right], \tag{2.11}$$

and, of course, the autocorrelation function can be obtained by taking the inverse Fourier transform of the power spectral density function. This implies that the mean square value is given by

$$\langle x^2 \rangle = R_x(0) = \frac{1}{2\pi} \int_{-\infty}^{\infty} S_x(\omega) \,\mathrm{d}\omega \,. \tag{2.12}$$

The reason $S_x(\omega)$ is called a power spectral density, is because $S_x \,\mathrm{d}\omega$ represents the power of the signal contained in an infinitesimal frequency band $[\omega, \omega + \mathrm{d}\omega]$ divided by the width of the band $\mathrm{d}\omega$, i.e. the power spectral density scales with the power contained in a signal. If the signal were a voltage, the integrated PSD would describe the power dissipated in a $1\,\Omega$ resistor. But in general power spectral densities can also be used for other kinds of phenomena, in which case the units of the PSD will be some quantity that scales with the power per Hertz. We will mostly look at displacement or velocity spectral densities. In these cases the units of the spectral density will be m^2/Hz or $(\mathrm{m}/\mathrm{s}^2)^2/\mathrm{Hz}$.

The *cross-spectral density* $S_{x_1x_2}(\omega)$ is given by the Fourier transform of the cross-correlation function (Equation 2.10). This spectral density, unlike the auto-spectral density can become complex-valued, indicating that there is a phase shift between $x_1(t)$ and $x_2(t)$. In our example of the waves rolling into the shore, the cross-spectral density will certainly have an imaginary component, because there is a clear phase shift between the arrival of the waves at both points.

We will use this theory of ergodic processes and power spectral densities frequently throughout this thesis. The ergodicity assumption is of great importance, because it allows us to obtain our results. Without it, we would not be able to say much about the underlying statistical processes and therefore the statistical response. The power spectral densities allow for a convenient notation in which to calculate and express these results.

3

MULTI-DEGREE-OF-FREEDOM SYSTEMS

As a first look into vibrations and random vibrations in particular, we turn towards multi-degree-of-freedom systems. An example of a multi-degree-of-freedom system is a discrete mass-spring system consisting of point masses connected by weightless springs, which we will treat in this chapter. These kinds of systems are the basis for the finite element calculations performed on systems with irregular geometries and shapes, such as a marine propeller. Multi-degree-of-freedom systems do not yet represent the physical reality of the propeller blade in water, but they are useful as a starting point from which to build our theory. The theory developed here and the derivations done can be transferred almost directly to finite element systems. Therefore, a good understanding of multi-degree-of-freedom systems will be very helpful in understanding the finite element calculations needed for marine propellers.

3.1 UNDAMPED SYSTEMS

Before we go to random excitations, it is helpful to gain a proper understanding of multi-degree-of-freedom systems. Therefore, we first turn towards one of the simplest systems possible: a system with deterministic excitation and no damping.

A multi-degree-of-freedom system consisting of n masses m_1, m_2, ..., m_n without any damping is governed by the following equations of motion

$$\boldsymbol{M}\vec{\ddot{q}}(t) + \boldsymbol{K}\vec{q}(t) = \vec{f}(t), \tag{3.1}$$

when assuming that the force-displacement relation is linear which holds for e.g. most metals when the stresses are too low for plastic deformation. The assumption of linearity is assumed throughout this entire thesis, and is vital for many of the calculations we do. In Equation 3.1 $\boldsymbol{M}$ is the diagonal mass matrix $\text{diag}[m_1, m_2, \ldots, m_n]$, and $\boldsymbol{K}$ is the stiffness matrix. The stiffness matrix contains information about how the springs in the system are connected and their stiffness. Throughout this text, we will call the mass, stiffness and, as we will see later on, damping matrices the *system matrices*. The vector $\vec{q}$ of length n contains the displacements of the n masses relative to their position without a force acting on the system, and $\vec{f}$ is a vector of length n containing the external forces acting on each mass. In Figure 3.1 an example system with three degrees of freedom is shown. In this example, the mass and stiffness matrix would be

$$\boldsymbol{M} = \begin{bmatrix} m_1 & 0 & 0 \\ 0 & m_2 & 0 \\ 0 & 0 & m_3 \end{bmatrix} \qquad \boldsymbol{K} = \begin{bmatrix} k_1 + k_2 & -k_2 & 0 \\ -k_2 & k_2 + k_3 & -k_3 \\ 0 & -k_3 & k_3 \end{bmatrix}. \tag{3.2}$$

We can also see the damping coefficients c_1, c_2, and c_3 in Figure 3.1. For now, we will ignore these. Damping will be dealt with in Section 3.2.

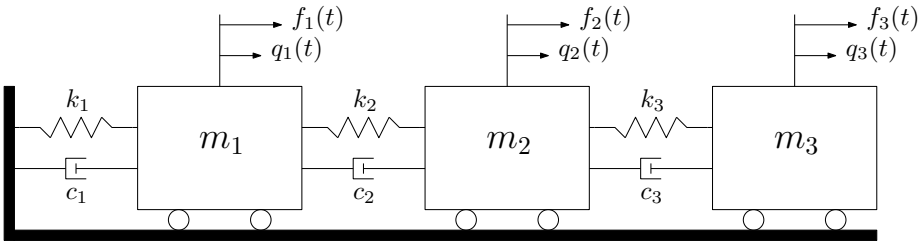

Figure 3.1: A three-degree-of-freedom system. Image adapted from Meirovitch [17].

3.1.1 *Modal analysis*

Equation 3.1 are a set of coupled differential equations that we want to solve. In order to find this solution, it is convenient to look at these equations in modal space. In modal analysis, one uses the fact that we can write the solution as

$$\vec{q}(t) = \sum_{k=1}^{n} \eta_k(t)\vec{u}_k = \boldsymbol{U}\vec{\eta}(t), \tag{3.3}$$

where $\boldsymbol{U} = [\vec{u}_1\ \vec{u}_2\ \dots\ \vec{u}_n]$ denote the so-called eigenmodes, and n is the number of degrees of freedom of the system. η_k is the modal contribution factor of a mode k, and $\vec{\eta}(t)$ is the vector containing all these factors. To put Equation 3.3 into words, every displacement is a linear combination of certain modes, where the size of each individual contribution is contained in $\vec{\eta}(t)$. This modal decomposition is a fundamental concept that we will use not only in discrete systems, but also for continuous systems in Chapter 4, and the finite element method used later on in Chapter 5 and Chapter 6. For multi-degree-of-freedom systems we only need a finite number of modes to describe the entire system (equal to the number of masses). However, for finite element or continuous systems the number of modes can quickly grow very large or even become infinite. This is where we will see the main advantage of a modal approach, as we can only take into account the most important modes, while ignoring the rest. This will result in much faster computations, while still obtaining the desired results.

The eigenmodes $\vec{u}_k$ can be found by solving the following eigenvalue problem

$$\boldsymbol{K}\vec{u}_k = \omega_k^2\boldsymbol{M}\vec{u}_k, \tag{3.4}$$

which has non-trivial solutions if and only if

$$\det\left[\boldsymbol{K} - \omega_k^2\boldsymbol{M}\right] = 0. \tag{3.5}$$

In a system with n degrees of freedom, there will also be n independent solutions to this problem. Each eigenvector $\vec{u}_k$ of the system also has a corresponding eigenvalue ω_k. These eigenvalues are called the natural frequencies or eigenfrequencies of the system. We define the diagonal matrix of the squared eigenfrequencies $\boldsymbol{\Omega}$ as $\operatorname{diag}\left[\omega_1^2, \omega_2^2, \dots, \omega_n^2\right]$.

For further calculations, it is desirable to normalise $\boldsymbol{U}$. In principle, when the eigenvectors are scaled by any factor, they are still eigenvectors of the system. For our calculations, it is most convenient (as we will see later on) to normalise the solution such that

$$\boldsymbol{U}^{\mathrm{T}}\boldsymbol{M}\boldsymbol{U} = \boldsymbol{I} \qquad \boldsymbol{U}^{\mathrm{T}}\boldsymbol{K}\boldsymbol{U} = \boldsymbol{\Omega}, \tag{3.6}$$

where $\boldsymbol{I}$ is the identity matrix and $\boldsymbol{K}$ and $\boldsymbol{M}$ are the stiffness and mass matrix as described earlier. Using Equation 3.3 and Equation 3.6 we can convert Equation 3.1 to modal coordinates. The equation of motion then becomes

$$\ddot{\vec{\eta}}(t) + \boldsymbol{\Omega}\vec{\eta}(t) = \vec{h}(t), \tag{3.7}$$

where $\vec{h}(t)$ is the vector of modal forces given by $\boldsymbol{U}^{\mathrm{T}}\vec{f}(t)$. We see here that the equation is in a very simple form, because of our chosen normalisation. If we assume the system is in rest at $t = 0$, the solution to Equation 3.7 is given by [17]

$$\eta_k(t) = \frac{1}{\omega_k}\int_0^t h_k(t-\tau)\sin(\omega_k\tau)\,\mathrm{d}\tau, \tag{3.8}$$

where $k \in 1, 2, \ldots, n$. As briefly mentioned earlier, each element η_k of $\vec{\eta}$ describes how much mode k contributes to the displacement. For example, if in a three-degree-of-freedom system at a certain time $\vec{\eta} = [1\,0\,0]^{\mathrm{T}}$, then the displacements in the system are those corresponding to the first eigenmode.

If we convert these modal coordinates back to our original coordinate system using Equation 3.3 and convert the modal forces back to our original space through

$$h_k(t) = \vec{u}_k{}^{T}\vec{f}(t), \tag{3.9}$$

we obtain the response vector $\vec{q}(t)$

$$\vec{q}(t) = \sum_{k=1}^{n}\left[\frac{\vec{u}_k{}^{\mathrm{T}}}{\omega_k}\int_0^t \vec{f}(t-\tau)\sin(\omega_k\tau)\,\mathrm{d}\tau\right]\vec{u}_k, \tag{3.10}$$

where $\vec{u}_k$ is the k^{th} column of $\boldsymbol{U}$. This equation gives use a full description of a deterministically excited multi-degree-of-freedom system without damping. Although this result in itself is not very useful for stochastic excitations (with damping), it does show the power of the modal analysis. As we will see later on, we will use many of the normalisations and definitions presented here in the case of random vibrations.

Example 3.1.1. Let us use the three-degree-of-freedom system shown in Figure 3.1 as an example. Because we have not taken into account damping yet, we set all damping coefficients c_1, c_2, and c_3 to 0. For simplicity, we choose $m_1 = m_2 = m_3 = 1\,\mathrm{kg}$, and $k_1 = k_2 = k_3 = 1\,\mathrm{N/m}$. We will now only apply a force to the third mass, such that $f_1(t) = f_2(t) = 0\,\mathrm{N}$ and $f_3(t) = u(t)$. In Figure 3.2 the response for this system is given. As expected, the third mass, which is excited by a constant force, has the largest displacement, because it is connected to the wall via three springs in series and thus moves most easily.

3.2 SYSTEMS WITH PROPORTIONAL DAMPING

The previous analysis did not include any damping. As we are trying to describe a physical system, we should introduce some kind of damping. This will bring us another step closer to a physical propeller, which is of course damped. In a multi-degree-of-freedom system with damping, we have the following equations of motion

$$\boldsymbol{M}\ddot{\vec{q}}(t) + \boldsymbol{C}\dot{\vec{q}}(t) + \boldsymbol{K}\vec{q}(t) = \vec{f}(t). \tag{3.11}$$

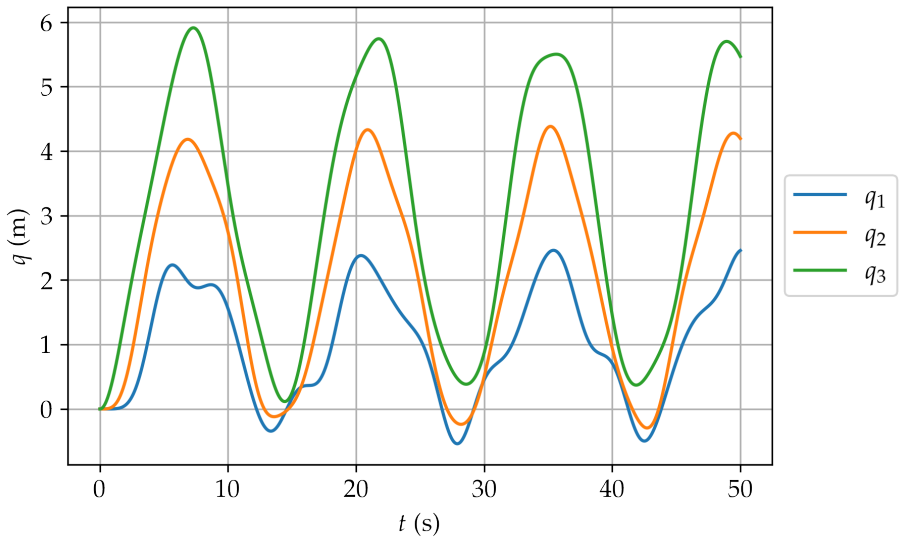

Figure 3.2: The response of the undamped three-degree-of-freedom system given in Figure 3.1, where $f_1(t) = f_2(t) = 0\,\mathrm{N}$, $f_3(t) = u(t)$, $m_1 = m_2 = m_3 = 1\,\mathrm{kg}$, and $k_1 = k_2 = k_3 = 1\,\mathrm{N/m}$.

If we want to solve this system through modal analysis, it is convenient to assume that the damping matrix $\boldsymbol{C}$ is a linear combination of the mass and stiffness matrix. That is,

$$\boldsymbol{C} = \alpha \boldsymbol{M} + \beta \boldsymbol{K}, \tag{3.12}$$

where α and β can be arbitrary constant scalars that are related to the properties of the system. This kind of damping is also known as proportional damping and is often used for modelling internal structural damping.[18] This assumption of proportional damping will make our calculations much simpler, but a downside of this, as we will see in Chapter 6, is that structural-acoustic systems also include some sort of non-proportional damping. From Equation 3.12, recalling Equation 3.6, it follows that

$$\boldsymbol{U}^{\mathrm{T}} \boldsymbol{C} \boldsymbol{U} = \alpha \boldsymbol{I} + \beta \boldsymbol{\Omega}. \tag{3.13}$$

Just as in the undamped case, we can also write the equation of motion in modal coordinates

$$\ddot{\vec{\eta}}(t) + (\alpha \boldsymbol{I} + \beta \boldsymbol{\Omega})\, \dot{\vec{\eta}}(t) + \boldsymbol{\Omega} \vec{\eta}(t) = \vec{h}(t). \tag{3.14}$$

The solution to Equation 3.14 is quite similar to the undamped case, except for an exponential damping component and a damping-related scaling factor in the argument of the sine [17]

$$\eta_k(t) = \frac{1}{\omega_k} \int_0^t h_k(t-\tau) \mathrm{e}^{-\zeta_k \omega_k \tau} \sin\left(\omega_k \tau \sqrt{1-\zeta_k^2}\right) \mathrm{d}\tau, \tag{3.15}$$

where the dimensionless damping factor ζ_k is given by

$$\zeta_k = \frac{\alpha + \beta \omega_k^2}{2\omega_k}, \tag{3.16}$$

and ω_k is the k^{th} natural frequency of the undamped system. We can convert these modal coordinates to our original system through Equation 3.3 and Equation 3.9 giving

$$\vec{q}(t) = \sum_{k=1}^{n} \frac{\vec{u}_k{}^T}{\omega_k} \int_0^t \vec{f}(t-\tau) e^{-\zeta_k \omega_k \tau} \sin\left(\omega_k \tau \sqrt{1-\zeta_k^2}\right) d\tau \, \vec{u}_k. \tag{3.17}$$

This last equation gives a full description of the proportionally damped multi-degree-of-freedom systems, which brings us a step closer to the physical reality. We see that the modal approach still works quite conveniently for proportionally damped systems.

Example 3.2.1. In Figure 3.3 the response for the system in Figure 3.1 with $f_1(t) = f_2(t) = 0$, and $f_3(t) = u(t)$ is given. The system was such that $m_1 = m_2 = m_3 = 1\,\text{kg}$ and $k_1 = k_2 = k_3 = 1\,\text{N/m}$. These are the same masses, spring constants, and forces used in the earlier undamped example. For the damping coefficients we chose $\alpha = 0.2\,\text{s}^{-1}$ and $\beta = 0.01\,\text{s}$.

As we can see, the displacements equilibrate to a certain value. These values are 1 m, 2 m, and 3 m for the masses respectively. This makes sense, because this means that all masses are displaced by 1 m relative to each other, which means that the force on each spring is exactly 1 N. This spring force is exactly balanced by the external force applied on the third mass.

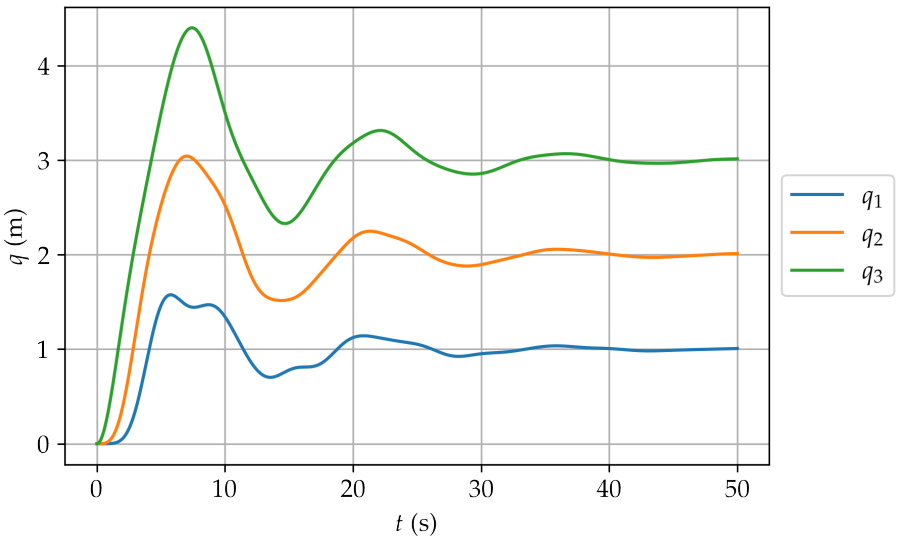

Figure 3.3: The response of the three-degree-of-freedom system with damping given in Figure 3.1, where $f_1(t) = f_2(t) = 0$, $f_3(t) = u(t)$, $m_1 = m_2 = m_3 = 1\,\text{kg}$, $k_1 = k_2 = k_3 = 1\,\text{N/m}$, $\alpha = 0.2\,\text{s}^{-1}$, and $\beta = 0.01\,\text{s}$.

3.3 STOCHASTIC EXCITATION

The goal of this thesis was to be able to deal with random excitations that arise from turbulent boundary layers. Therefore, we now move away from the systems with deterministic excitation, and will allow for stochastic forces. These forces are defined by their

autocorrelation function (and cross-correlation if there are multiple forces) as described in Chapter 2. The correlation function matrix of the excitation $\boldsymbol{R}_f(\tau)$ is given by

$$\boldsymbol{R}_f(\tau) = \lim_{T\to\infty} \frac{1}{T} \int_{-T/2}^{T/2} \vec{f}(t)\vec{f}^{\mathrm{T}}(t+\tau)\,\mathrm{d}t, \tag{3.18}$$

where $\vec{f}(t)$ is the force vector, that has the forces on each mass of the multi-degree-of-freedom system as its components. The off-diagonal elements of this matrix $\boldsymbol{R}_f$ represent the cross-correlation functions, and the diagonal elements the autocorrelation functions. Because the processes we are dealing with in the case of turbulent boundary layers and other physical processes are assumed to be ergodic, it is implied that their autocorrelation function is stationary, and therefore the statistics to not change over time. This allows us to say something about the statistics of the response. In our case, we describe the response of the system in terms of power spectral densities. First we will derive the response in the case of proportional damping, after which we turn towards the more complicated case of non-proportional damping with stochastic excitation. In both cases, we make use of the modal approach seen previously.

3.3.1 *Derivation of the response with stochastic excitation and proportional damping*

As we saw earlier, we could do a modal analysis to find the eigenmodes of the multi-degree-of-freedom system. A similar analysis using the eigenmodes of the system can be done in the case of stochastic excitation. The initial equations of motion for a proportionally damped system in modal space are

$$\ddot{\eta}_k(t) + 2\zeta_k\omega_k\dot{\eta}_k(t) + \omega_k^2\eta_k(t) = h_k(t), \tag{3.19}$$

where we did not use the vector notation as in Equation 3.14, but instead split it up into a set of n equations for $k \in 1, 2, \ldots, n$. Again, ω_k is the k^{th} natural frequency of the undamped system. Also, in this stochastic case we can still find the modal forces using

$$h_k(t) = \vec{u}_k{}^{\mathrm{T}}\vec{f}(t). \tag{3.9}$$

Because we are now dealing with random excitations, it is more convenient to write Equation 3.14 in frequency space as we mentioned earlier in Section 2.2.2. Thus, let us convert Equation 3.14 to the frequency domain instead of the time domain by Fourier transform. Recalling the definition of the Fourier transform from Equation 2.1, we say that

$$\eta_k(\omega) = \mathcal{F}\left[\eta_k(t)\right] = \int_{-\infty}^{\infty} \eta_k(t)\mathrm{e}^{-\mathrm{i}\omega t}\,\mathrm{d}t\,. \tag{3.20}$$

Applying the Fourier transform to both sides transforms Equation 3.19 into

$$\ddot{\eta}_k(\omega) + 2\zeta_k\omega_k\dot{\eta}_k(\omega) + \omega_k^2\eta_k(\omega) = h_k(\omega), \tag{3.21}$$

where $h_k(\omega) = \mathcal{F}\left[h_k(t)\right]$. It can be derived that the first and second derivative with respect to time of the response to a (stochastic) signal in the frequency domain are given by [19]

$$\dot{\eta}_k(\omega) = \mathrm{i}\omega\eta_k(\omega) \qquad\qquad \ddot{\eta}_k(\omega) = -\omega^2\eta_k(\omega). \tag{3.22}$$

Inserting this into Equation 3.21 gives us

$$(-\omega^2 + \mathrm{i}2\zeta_k\omega\omega_k + \omega_k^2)\eta_k(\omega) = h_k(\omega). \tag{3.23}$$

We can simply obtain the solution to Equation 3.23 by dividing by the prefactor giving

$$\eta_k(\omega) = G_k(\omega)h_k(\omega), \tag{3.24}$$

where

$$G_k(\omega) = \frac{1}{-\omega^2 + 2\mathrm{i}\zeta_k\omega\omega_k + \omega_k^2}. \tag{3.25}$$

G_k is called the frequency response function. The subscript k indicates that it is associated with mode k. This frequency response function is the Fourier transform of the impulse response function g_k, which tells you how the system reacts to a (deterministic) unit impulse. This will be useful in deriving the response spectral density, as will be shown in the following derivation. It also shows that there is a direct relationship between excitation and response in the frequency domain.

Our goal is to find the response spectral density matrix $\boldsymbol{S_q}(\omega)$. $\boldsymbol{S_q}(\omega)$ contains all information we can extract from the system. This will characterise the response, and show us which modes are dominant. The spectral density matrix is related to the response correlation matrix $\boldsymbol{R_q}(\tau)$ as

$$\boldsymbol{R_q}(\tau) = \frac{1}{2\pi}\int_{-\infty}^{\infty} \boldsymbol{S_q}(\omega)\mathrm{e}^{\mathrm{i}\omega\tau}\,\mathrm{d}\omega, \tag{3.26}$$

which is simply the inverse Fourier transform of $\boldsymbol{S_q}$. As stated in Section 2.2, the correlation matrix tells us something about the relation between two events in time, either within one signal, or between two signals. Also, at $\tau = 0$ it is equal to the mean square value of the signal, as shown in Equation 2.7. This mean square value can also be found by integrating $\boldsymbol{S_q}$ over all frequencies (see Equation 2.12). The response correlation matrix is given by

$$\begin{aligned}\boldsymbol{R_q}(\tau) &= \lim_{T\to\infty}\frac{1}{T}\int_{-T/2}^{T/2} \vec{q}(t)\vec{q}^{\mathrm{T}}(t+\tau)\,\mathrm{d}t \\ &= \lim_{T\to\infty}\frac{1}{T}\int_{-T/2}^{T/2} \boldsymbol{U}\vec{\eta}(t)\vec{\eta}^{\mathrm{T}}(t+\tau)\boldsymbol{U}^{\mathrm{T}}\,\mathrm{d}t \\ &= \boldsymbol{U}\boldsymbol{R_\eta}(\tau)\boldsymbol{U}^{\mathrm{T}}.\end{aligned} \tag{3.27}$$

To rewrite this into spectral densities we must first take a look at the modal correlation function $\boldsymbol{R_\eta}$ and how it is related to the spectral density of the excitation. The modal correlation function between modes k and l (i.e. element (k,l) of the matrix $\boldsymbol{R_\eta}$) is given by

$$R_{\eta_{kl}}(\tau) = \lim_{T\to\infty}\frac{1}{T}\int_{-T/2}^{T/2} \eta_k(t)\eta_l(t+\tau)\,\mathrm{d}t\,. \tag{3.28}$$

For linear systems, Equation 3.25 and the properties of the Fourier transform allow us to rewrite the modal response through a convolution integral of the impulse response function and the modal forces

$$\eta_k(t) = \int_{-\infty}^{\infty} g_k(\mu_k)h_k(t-\mu_k)\mathrm{d}\mu_k, \tag{3.29}$$

where g_k is the impulse response function and μ_k a dummy variable. Introducing this into Equation 3.28 and swapping the integrals and limit gives

$$R_{\eta_{kl}}(\tau) = \int_{-\infty}^{\infty}\int_{-\infty}^{\infty} g_k(\mu_k)g_l(\mu_l)\left[\lim_{T\to\infty}\frac{1}{T}\int_{-T/2}^{T/2} h_k(t-\mu_k)h_l(t+\tau-\mu_l)\,\mathrm{d}t\right]\mathrm{d}\mu_k\mathrm{d}\mu_l. \quad (3.30)$$

The part in the square brackets can be recognised as a cross-correlation of the modal forces. The ergodic nature of our system allows us to replace $t \to t+\mu_k$, and obtain

$$R_{\eta_{kl}}(\tau) = \int_{-\infty}^{\infty}\int_{-\infty}^{\infty} g_k(\mu_k)g_l(\mu_l)R_{hkl}(\tau+\mu_k-\mu_l)\,\mathrm{d}\mu_k\,\mathrm{d}\mu_l\,. \quad (3.31)$$

Let us now use the following relation between the spectral density and correlation function

$$R_{hkl}(\tau+\mu_k-\mu_l) = \frac{1}{2\pi}\int_{-\infty}^{\infty} S_{hkl}(\omega)\mathrm{e}^{\mathrm{i}\omega(\tau+\mu_k-\mu_l)}\,\mathrm{d}\omega, \quad (3.32)$$

which we can plug into Equation 3.31

$$\begin{aligned} R_{\eta_{kl}}(\tau) &= \int_{-\infty}^{\infty}\int_{-\infty}^{\infty} g_k(\mu_k)g_l(\mu_l)\left[\frac{1}{2\pi}\int_{-\infty}^{\infty} S_{hkl}(\omega)\mathrm{e}^{\mathrm{i}\omega(\tau+\mu_k-\mu_l)}\,\mathrm{d}\omega\right]\mathrm{d}\mu_k\,\mathrm{d}\mu_l \\ &= \frac{1}{2\pi}\int_{-\infty}^{\infty} S_{hkl}(\omega)\left(\int_{-\infty}^{\infty} g_k(\mu_k)\mathrm{e}^{\mathrm{i}\omega\mu_k}\,\mathrm{d}\mu_k\right)\left[\int_{-\infty}^{\infty} g_l(\mu_l)\mathrm{e}^{-\mathrm{i}\omega\mu_l}\,\mathrm{d}\mu_l\right]\mathrm{e}^{\mathrm{i}\omega\tau}\,\mathrm{d}\omega \quad (3.33) \\ &= \frac{1}{2\pi}\int_{-\infty}^{\infty} S_{hkl}(\omega)\bar{G}_k(\omega)G_l(\omega)\mathrm{e}^{\mathrm{i}\omega\tau}\,\mathrm{d}\omega, \end{aligned}$$

where G_k is the Fourier transform of the impulse response g_k. G_k is the frequency response function given in Equation 3.25. Thus, we can now obtain the expression for $\boldsymbol{R_q}(\tau)$ by combining Equation 3.27 and Equation 3.33

$$\boldsymbol{R_q}(\tau) = \frac{1}{2\pi}\int_{-\infty}^{\infty} \boldsymbol{U}\bar{\boldsymbol{G}}(\omega)\boldsymbol{S_h}(\omega)\boldsymbol{G}(\omega)\mathrm{e}^{\mathrm{i}\omega\tau}\boldsymbol{U}^{\mathrm{T}}\,\mathrm{d}\omega, \quad (3.34)$$

where $\boldsymbol{G}$ is diag$[G_1, G_2, \ldots, G_n]$. $\boldsymbol{S_h}$ is the excitation spectral density matrix in modal coordinates, which can be obtained from our initial coordinates through

$$\boldsymbol{S_h}(\omega) = \boldsymbol{U}^{\mathrm{T}}\boldsymbol{S_f}(\omega)\boldsymbol{U}. \quad (3.35)$$

Here, $\boldsymbol{S_f}(\omega)$ is the excitation spectral density in the initial coordinates, which relates to the correlation matrix of the input forces through

$$\boldsymbol{S_f}(\omega) = \int_{-\infty}^{\infty} \boldsymbol{R_f}(\tau)\mathrm{e}^{\mathrm{i}\omega\tau}\,\mathrm{d}\tau, \quad (3.36)$$

where

$$\boldsymbol{R_f}(\tau) = \lim_{T\to\infty}\frac{1}{T}\int_{-T/2}^{T/2}\vec{f}(t)\vec{f}^{\mathrm{T}}(t+\tau)\,\mathrm{d}t\,. \quad (3.37)$$

Finally, we can describe the correlation function matrix of the response by plugging Equation 3.35 into Equation 3.34

$$\boldsymbol{R_q}(\tau) = \frac{1}{2\pi}\int_{-\infty}^{\infty} \boldsymbol{U}\bar{\boldsymbol{G}}(\omega)\boldsymbol{U}^{\mathrm{T}}\boldsymbol{S_f}(\omega)\boldsymbol{U}\boldsymbol{G}(\omega)\mathrm{e}^{\mathrm{i}\omega\tau}\boldsymbol{U}^{\mathrm{T}}\,\mathrm{d}\omega, \quad (3.38)$$

To obtain the response spectral density S_q, we can apply the Fourier transform on both sides of Equation 3.38, giving

$$\boldsymbol{S_q}(\omega) = \boldsymbol{U}\bar{\boldsymbol{G}}(\omega)\boldsymbol{U}^{\mathrm{T}}\boldsymbol{S_f}(\omega)\boldsymbol{U}\boldsymbol{G}(\omega)\boldsymbol{U}^{\mathrm{T}}. \tag{3.39}$$

The response spectral density $\boldsymbol{S_q}$ is a matrix of dimension $n \times n$, which functions similarly to the excitation spectral density matrix $\boldsymbol{S_f}$, with the auto-spectral density on the diagonal, and the cross-spectral density between two masses k and l given by $S_{q_{kl}}$. This result completely describes our system in terms of (cross) power spectral densities, which was what we set out to do. Equation 3.39 is one of the most important results in this chapter. It allows for a complete description of a multi-degree-of-freedom system with proportional damping and random excitation. This same result can directly be translated to finite element systems, which will allow us to incorporate the desired geometry of a propeller.

Furthermore, we can also obtain the velocity and acceleration spectra quite easily. We can use Equation 3.22 to describe the velocity and acceleration, which we can use to obtain the spectral densities, respectively $\boldsymbol{S_v}$ and $\boldsymbol{S_a}$ through

$$\boldsymbol{S_v}(\omega) = \omega^2\boldsymbol{S_q}(\omega) \qquad \boldsymbol{S_a} = \omega^4\boldsymbol{S_q}(\omega). \tag{3.40}$$

Note that the prefactor is squared, because of the squared units in the power spectral density. The velocity spectrum will eventually be useful for calculation of the radiated noise, but in principle these spectra do not contain any information not already described by the displacement power spectral density.

Example 3.3.1. For this example, we use mostly the same system as the earlier examples, but now with stochastic excitation. The difference between this system and the previous one in Example 3.2.1 is the damping coefficients α and β. In this case we chose $\alpha = 0.01\,\mathrm{s}^{-1}$ and $\beta = 0.01\,\mathrm{s}$, in order to enhance the characteristic features of the response. Secondly, instead of a constant force on the third mass, we use a constant power spectral density, also known as white noise. That is

$$S_{f_{11}}(\omega) = S_{f_{22}}(\omega) = 0\,\mathrm{N}^2/\mathrm{Hz} \qquad S_{f_{33}}(\omega) = 1\,\mathrm{N}^2/\mathrm{Hz},$$

where $S_{f_{ii}}$ is the excitation auto-spectral density on mass i. All excitation cross-correlations (e.g. $S_{f_{12}}$) are zero, as we only apply a random force to the third mass. In Figure 3.4, the response of the three-degree-of-freedom system excited randomly on the third mass is shown. The natural frequencies we obtain from the eigenvalue problem given in Equation 3.4 are

$$\omega_1 = 0.445\,\mathrm{rad/s} \qquad \omega_2 = 1.247\,\mathrm{rad/s} \qquad \omega_3 = 1.802\,\mathrm{rad/s}.$$

Peaks at these natural frequencies can clearly be seen in the response spectrum.

If we want to know more about the natural modes occurring in the system, we can also look at the cross-spectral densities. In Figure 3.5 the real parts of the cross-spectral densities are displayed for this system. We can clearly see that in the first mode, all masses move in the same direction, as all cross-spectra are positively correlated. For the second mode, we see that mass 1 and 2 are positively correlated, while masses 1 and 2 are negatively correlated with mass 3. This suggests that masses 1 and 2 move in the same direction, while mass 3 moves in the opposite direction. Lastly, for the third mode, $S_{q_{12}}$ and $S_{q_{23}}$ are negative while $S_{q_{13}}$ is positive. This suggests that masses 1 and 3 behave similarly, while mass 2 moves in the opposite direction.

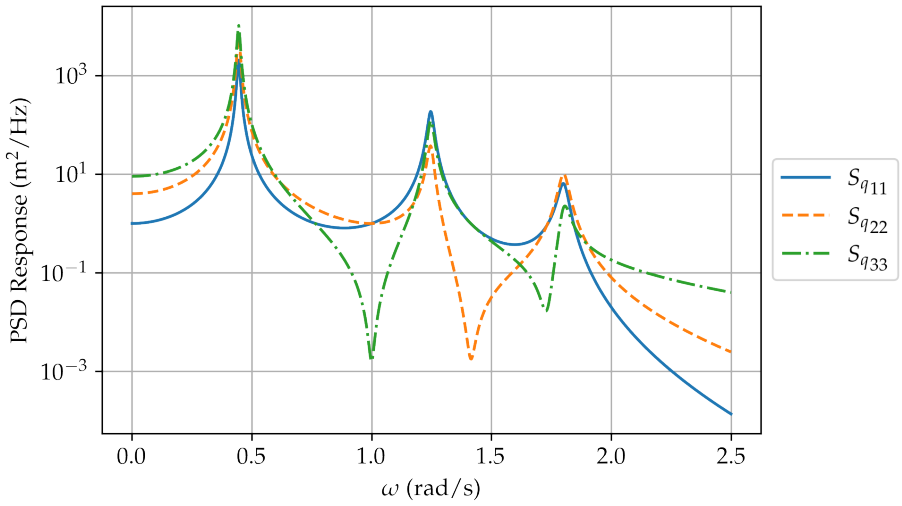

Figure 3.4: The power spectral density of the response of the three-degree-of-freedom system with damping. A white noise spectrum was applied to the third mass. The damping factors were $\alpha = 0.01\,\mathrm{s}^{-1}$ and $\beta = 0.01\,\mathrm{s}$. The masses and spring constants were equal to those in Example 3.2.1.

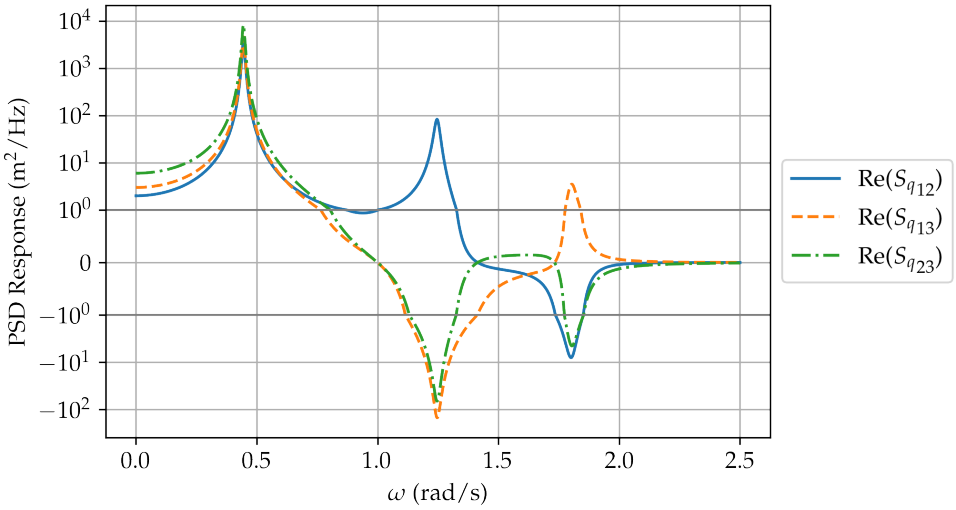

Figure 3.5: The real part of the cross-spectral density of the response of the three-degree-of-freedom system with damping. A white noise spectrum was applied to the third mass. The damping factors were $\alpha = 0.01\,\mathrm{s}^{-1}$ and $\beta = 0.01\,\mathrm{s}$. The masses and spring constants were equal to those in Example 3.2.1. The scale used on the y-axis is linear between -1 and 1. Outside this region it becomes symmetrically logarithmic.

3.4 NON-PROPORTIONAL DAMPING AND STOCHASTIC EXCITATION

We have seen that we can calculate the response to stochastic excitation for proportionally damped systems. However, there are cases in which this proportional damping is not enough to describe the system. This is especially important in structural-acoustic coupled problems, as they never have a proportional damping matrix (see Chapter 6). Eventually we want to move towards such systems, to calculate the radiated noise of a propeller. Therefore, we would also like to be able to describe systems with arbitrary damping.

If we recall the equation of motion given in Equation 3.11

$$\boldsymbol{M}\ddot{\vec{q}}(t) + \boldsymbol{C}\dot{\vec{q}}(t) + \boldsymbol{K}\vec{q}(t) = \vec{f}(t), \tag{3.11}$$

we can see that if $\boldsymbol{C}$ is no longer diagonalised by the same eigenvectors as $\boldsymbol{M}$ and $\boldsymbol{K}$, in case $\boldsymbol{C}$ is not proportional to the damping and stiffness matrix. This means it is not possible to decouple the system. Therefore, the modal analysis with a single eigenmode matrix will no longer give us the proper results. In order to overcome these limitations, we will still use modal analysis. This time however, we use a *state-space* description of the problem. The state vector $\vec{x}(t)$ of the system is defined as

$$\vec{x}(t) = \begin{bmatrix} \vec{q}(t) \\ \dot{\vec{q}}(t) \end{bmatrix}. \tag{3.41}$$

This state vector will allow us to diagonalise the equation of motion, even if the damping matrix is not proportional to the mass and stiffness matrices. As we want to use modal analysis, we should first find the (state-space) modes of this system.

3.4.1 *Eigenmodes*

The equation of motion given in Equation 3.11 can be rewritten in the following way

$$\ddot{\vec{q}}(t) = -\boldsymbol{M}^{-1}\boldsymbol{C}\dot{\vec{q}} - \boldsymbol{M}^{-1}\boldsymbol{K}\vec{q} + \boldsymbol{M}^{-1}\vec{f}(t), \tag{3.42}$$

which allows us to write the following system of equations

$$\begin{bmatrix} \dot{\vec{q}}(t) \\ \ddot{\vec{q}}(t) \end{bmatrix} = \begin{bmatrix} \dot{\vec{q}}(t) \\ -\boldsymbol{M}^{-1}\boldsymbol{C}\dot{\vec{q}} - \boldsymbol{M}^{-1}\boldsymbol{K}\vec{q} + \boldsymbol{M}^{-1}\vec{f}(t) \end{bmatrix}. \tag{3.43}$$

Now, we can introduce the state-space notation used in Equation 3.41 to write Equation 3.43 as

$$\dot{\vec{x}}(t) = \boldsymbol{A}\vec{x}(t) + \boldsymbol{B}\vec{f}(t), \tag{3.44}$$

where

$$\boldsymbol{A} = \begin{bmatrix} \boldsymbol{0} & \boldsymbol{I} \\ -\boldsymbol{M}^{-1}\boldsymbol{C} & -\boldsymbol{M}^{-1}\boldsymbol{K} \end{bmatrix} \qquad \boldsymbol{B} = \begin{bmatrix} \boldsymbol{0} \\ \boldsymbol{M}^{-1} \end{bmatrix}. \tag{3.45}$$

One can now obtain the state-space eigenmodes by setting $\vec{f}(t) = 0$ and solving

$$\dot{\vec{x}}(t) = \boldsymbol{A}\vec{x}(t). \tag{3.46}$$

This is a simple differential equation with constant coefficients, thus the solution has the form

$$\vec{x}(t) = \mathrm{e}^{\lambda t}\vec{x}, \tag{3.47}$$

where λ and $\vec{x}$ are a constant scalar and vector respectively. We can obtain the eigenvalue problem by inserting Equation 3.47 into Equation 3.46 and dividing by $\mathrm{e}^{\lambda t}$

$$\boldsymbol{A}\vec{x}_k = \lambda_k\vec{x}_k, \tag{3.48}$$

which we can solve to obtain the eigenvectors $\vec{x}_k$ and their corresponding eigenvalues λ_k for $k \in 1, 2, \ldots, 2n$. However, because $\boldsymbol{A}$ is no longer symmetric, we do not have our desirable property of orthogonality of the eigenvectors, which is needed to decouple the system. This means we can no longer diagonalise this problem with only one eigenvector matrix. This was to be expected because the damping is non-proportional.

To solve this problem, we can look to find a different (left) eigenmode, which might be able to help with this problem. Because $\boldsymbol{A}$ is real, $\boldsymbol{A}$ and $\boldsymbol{A}^{\mathrm{T}}$ have the same eigenvalues, but not the same eigenvectors. Therefore, we can additionally consider the eigenvalue problem of the transposed matrix $\boldsymbol{A}^{\mathrm{T}}$

$$\boldsymbol{A}^{\mathrm{T}}\vec{y}_l = \lambda_l \vec{y}_l, \tag{3.49}$$

or when we apply the Hermitian transpose

$$\vec{y}_l{}^{\mathrm{H}}\boldsymbol{A} = \lambda_l \vec{y}_l{}^{\mathrm{H}}. \tag{3.50}$$

This is the so-called left eigenvector problem, for obvious reasons. We will call $\vec{x}$ the right eigenvectors, and $\vec{y}$ the left eigenvectors. We used the Hermitian transpose for the eigenvector, because the state-space eigenvectors are no longer necessarily real.

Solving Equation 3.48 and Equation 3.50 will give us $2n$ unique right eigenvectors and $2n$ left eigenvectors. We also obtain $2n$ eigenvalues, which are the same for both the left and right eigenvalue problem. To show that we now have our desired 'orthogonality', we can pre-multiply Equation 3.48 with $\vec{y}_l{}^{\mathrm{H}}$, giving

$$\vec{y}_l{}^{\mathrm{H}}\boldsymbol{A}\vec{x}_k = \lambda_k \vec{y}_l{}^{\mathrm{H}}\vec{x}_k, \tag{3.51}$$

and post-multiplying Equation 3.50 with $\vec{x}_k$ to obtain

$$\vec{y}_l{}^{\mathrm{H}}\boldsymbol{A}\vec{x}_k = \lambda_l \vec{y}_l{}^{\mathrm{H}}\vec{x}_k. \tag{3.52}$$

Subtracting these two equations gives

$$(\lambda_l - \lambda_k)\vec{y}_l{}^{\mathrm{H}}\vec{x}_k = 0 \text{ for } k \neq l. \tag{3.53}$$

Because $\lambda_l \neq \lambda_k$ for $l \neq k$ (as the left and right eigenvector have the same eigenvalues), we can see that it must be so that

$$\vec{y}_l{}^{\mathrm{H}}\vec{x}_k = 0 \text{ for } k \neq l, \tag{3.54}$$

and

$$\vec{y}_l{}^{\mathrm{H}}\boldsymbol{A}\vec{x}_k = 0 \text{ for } k \neq l. \tag{3.55}$$

This is a kind of orthogonality known as *bi-orthogonality*. We can use this for decoupling the equation of motion. For the normalisation of the eigenvectors, we normalise them such that

$$\vec{y}_l{}^{\mathrm{H}}\vec{x}_k = 1 \text{ for } k = l. \tag{3.56}$$

Let us for sake of clarity write the matrix of right eigenvectors as $\boldsymbol{X} = [\vec{x}_1\ \vec{x}_2\ \ldots\ \vec{x}_{2n}]$ and the left eigenvectors as $\boldsymbol{Y} = [\vec{y}_1\ \vec{y}_2\ \ldots\ \vec{y}_{2n}]$ and the diagonal matrix of eigenvalues as $\boldsymbol{\Lambda} =$

diag $[\lambda_1, \lambda_2, \ldots, \lambda_{2n}]$. One can derive the following properties according to Meirovitch [17]

$$\boldsymbol{A}\boldsymbol{X} = \boldsymbol{X}\boldsymbol{\Lambda} \qquad \boldsymbol{A}^{\mathrm{H}}\boldsymbol{Y} = \boldsymbol{Y}\boldsymbol{\Lambda} \qquad \boldsymbol{Y}^{\mathrm{H}}\boldsymbol{X} = \boldsymbol{I} \qquad \boldsymbol{Y}^{\mathrm{H}}\boldsymbol{A}\boldsymbol{X} = \boldsymbol{\Lambda} \qquad \boldsymbol{Y}^{\mathrm{H}} = \boldsymbol{X}^{-1}. \tag{3.57}$$

Of these properties, the last one is a very useful one for computational reasons. Taking the inverse of $\boldsymbol{X}$ is computationally much faster than calculating all eigenvectors of the transposed matrix $\boldsymbol{A}^{\mathrm{T}}$ to find $\boldsymbol{Y}$. Now that we have obtained some sort of orthogonality, we return to our modal decomposition. We can write our state vector as a linear combination of right eigenmodes

$$\vec{x}(t) = \sum_{k=1}^{2n} \xi_k(t)\vec{x}_k = \boldsymbol{X}\vec{\xi}(t). \tag{3.58}$$

If we insert this into Equation 3.44 and pre-multiply with $\boldsymbol{Y}^{\mathrm{H}}$ we obtain

$$\boldsymbol{Y}^{\mathrm{H}}\boldsymbol{X}\dot{\vec{\xi}}(t) = \boldsymbol{Y}^{\mathrm{H}}\boldsymbol{A}\boldsymbol{X}\vec{\xi}(t) + \boldsymbol{Y}^{\mathrm{H}}\boldsymbol{B}\vec{f}(t). \tag{3.59}$$

Now we can see why we needed the bi-orthogonality property, as we can use it to obtain

$$\dot{\vec{\xi}}(t) = \boldsymbol{\Lambda}\vec{\xi}(t) + \vec{v}(t), \tag{3.60}$$

where $\vec{v}(t)$ is the modal force given by

$$\vec{v}(t) = \boldsymbol{Y}^{\mathrm{H}}\boldsymbol{B}\vec{f}(t). \tag{3.61}$$

We see that we can now write both our excitation force (Equation 3.61) and displacement (Equation 3.58) in modal space. This is necessary for our (stochastic) modal derivation of the response.

3.4.2 *Deriving the response*

This thesis is focusses on stochastically excited structures, as we want to find the response of an excitation by a turbulent boundary layer. To find the response of non-proportionally damped systems to stochastic excitations, we can do a similar analysis as we did earlier for the proportionally damped systems. What we want to know is the spectral density matrix of the response $\boldsymbol{S}_{\boldsymbol{x}}(\omega)$. To arrive at this result, we first start, just as in the previous derivation in Section 3.3.1, with the correlation matrix $\boldsymbol{R}_{\boldsymbol{x}}(\tau)$

$$\begin{aligned}
\boldsymbol{R}_{\boldsymbol{x}}(\tau) &= \lim_{T\to\infty} \frac{1}{T} \int_{-T/2}^{T/2} \vec{x}(t)\vec{x}^{\mathrm{H}}(t+\tau)\,\mathrm{d}t \\
&= \lim_{T\to\infty} \frac{1}{T} \int_{-T/2}^{T/2} \boldsymbol{X}\vec{\xi}(t)\vec{\xi}^{\mathrm{H}}(t+\tau)\boldsymbol{X}^{\mathrm{H}}\,\mathrm{d}t \\
&= \boldsymbol{X}\boldsymbol{R}_{\vec{\xi}}(\tau)\boldsymbol{X}^{\mathrm{H}}.
\end{aligned} \tag{3.62}$$

A difference we see here compared to Section 3.3 is that the eigenmodes can now be complex-valued. Therefore, we take the Hermitian transpose, instead of just the transpose.

We saw earlier that the modal correlation function was given by

$$\boldsymbol{R}_{\vec{\xi}}(\tau) = \frac{1}{2\pi} \int_{-\infty}^{\infty} \bar{\boldsymbol{G}}(\omega)\boldsymbol{S}_{\nu}(\omega)\boldsymbol{G}(\omega)\mathrm{e}^{\mathrm{i}\omega\tau}\,\mathrm{d}\omega, \tag{3.63}$$

where $\boldsymbol{S}_v(\omega)$ is the modal excitation spectral density matrix. To find the transfer function $\boldsymbol{G}(\omega)$ we can look towards the solution of the equation of motion for harmonic excitation $\vec{f}(t) = \vec{f}_0 \mathrm{e}^{\mathrm{i}\omega t}$. In this case, the solution to Equation 3.44 is given by [17, p. 351]

$$\vec{x}(t) = \sum_{k=1}^{2n} \frac{\vec{y}_k{}^{\mathrm{H}} \boldsymbol{B} \vec{f}_0}{i\omega - \lambda_k} \vec{x}_k \mathrm{e}^{\mathrm{i}\omega t}, \tag{3.64}$$

from which we can extract the k^{th} transfer function

$$G_k(\omega) = \frac{1}{\mathrm{i}\omega - \lambda_k}, \tag{3.65}$$

and $\boldsymbol{G} = \operatorname{diag}[G_1, G_2, \ldots, G_{2n}]$. Combining the results from Equation 3.62 and Equation 3.63 gives us for the correlation function of the elements of the state vector

$$\boldsymbol{R}_x(\tau) = \frac{1}{2\pi} \int_{-\infty}^{\infty} \boldsymbol{X} \bar{\boldsymbol{G}}(\omega) \boldsymbol{S}_v(\omega) \boldsymbol{G}(\omega) \mathrm{e}^{\mathrm{i}\omega\tau} \boldsymbol{X}^{\mathrm{H}} \, \mathrm{d}\omega \,. \tag{3.66}$$

All that is left is to derive the modal force spectral density $\boldsymbol{S}_v(\omega)$. We can simply fill in the real space representation of the modal force vectors as shown in Equation 3.61

$$\begin{aligned}
\boldsymbol{S}_v(\omega) &= \int_{-\infty}^{\infty} \boldsymbol{R}_v(\tau) \mathrm{e}^{\mathrm{i}\omega\tau} \, \mathrm{d}\tau \\
&= \int_{-\infty}^{\infty} \lim_{T\to\infty} \frac{1}{T} \int_{-T/2}^{T/2} \vec{v}(t) \vec{v}^{\mathrm{H}}(t+\tau) \, \mathrm{d}t \; \mathrm{e}^{\mathrm{i}\omega\tau} \, \mathrm{d}\tau \\
&= \int_{-\infty}^{\infty} \lim_{T\to\infty} \frac{1}{T} \int_{-T/2}^{T/2} \boldsymbol{Y}^{\mathrm{H}} \boldsymbol{B} \vec{f}(t) \vec{f}^{\mathrm{H}}(t+\tau) \boldsymbol{B}^{\mathrm{H}} \boldsymbol{Y} \, \mathrm{d}t \, \mathrm{e}^{\mathrm{i}\omega\tau} \, \mathrm{d}\tau \\
&= \int_{-\infty}^{\infty} \boldsymbol{Y}^{\mathrm{H}} \boldsymbol{B} \boldsymbol{R}_f(\omega) \boldsymbol{B}^{\mathrm{H}} \boldsymbol{Y} \mathrm{e}^{\mathrm{i}\omega\tau} \, \mathrm{d}\tau \\
&= \boldsymbol{Y}^{\mathrm{H}} \boldsymbol{B} \boldsymbol{S}_f(\omega) \boldsymbol{B}^{\mathrm{H}} \boldsymbol{Y}.
\end{aligned} \tag{3.67}$$

Finally, the response spectral density matrix is easily obtained by taking the Fourier transform of both sides in Equation 3.66, and inserting the modal force spectral density from Equation 3.67 giving

$$\boldsymbol{S}_x(\omega) = \boldsymbol{X} \bar{\boldsymbol{G}}(\omega) \boldsymbol{Y}^{\mathrm{H}} \boldsymbol{B} \boldsymbol{S}_f(\omega) \boldsymbol{B}^{\mathrm{H}} \boldsymbol{Y} \boldsymbol{G}(\omega) \boldsymbol{X}^{\mathrm{H}}. \tag{3.68}$$

This newly developed theory, culminating in Equation 3.68, will allow us to calculate the response of systems that do not have proportional damping. This is very useful as we will see later on in Chapter 6, because structural-acoustic coupled systems we are working towards do not have a proportional damping matrix.

Example 3.4.1. As an application of the state-vector approach, let us redo Example 3.3.1. This allows us to verify that this new theory indeed produces the same results as the non state-space method that could only deal with proportional damping. We again apply white noise to the third mass in the three-degree-of-freedom system. To calculate the response, we use the state-space approach given in this section. In Figure 3.6, the response for the first mass in the system is given twice. The blue line corresponds to the power spectral density response calculated with the state-space approach, and the dashed orange line was calculated using the 'normal' approach for proportional damping systems given in Section 3.3. As one can see, these lines are identical, suggesting that our newly developed approach is consistent with the previous one.

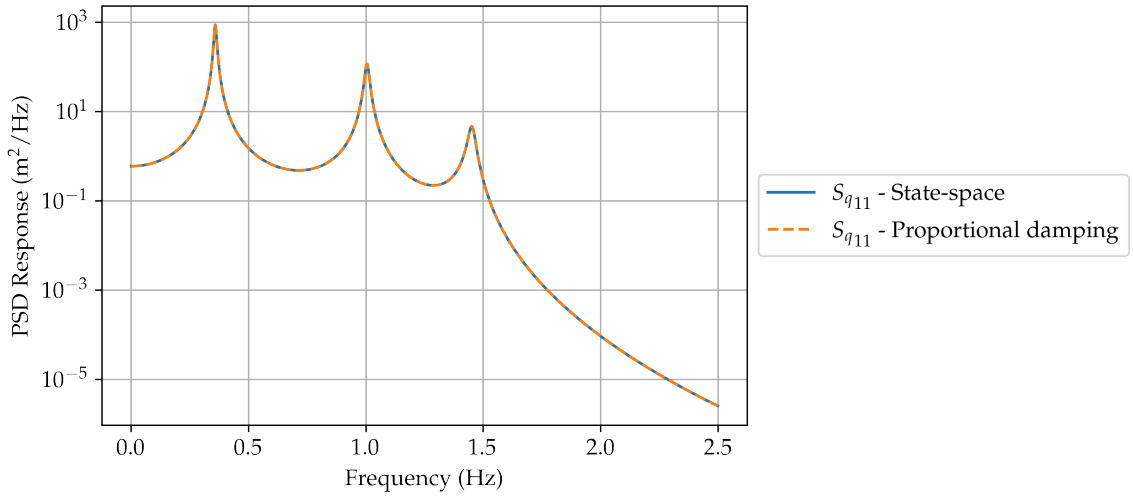

Figure 3.6: PSD response of the first mass of the three-degree-of-freedom system shown in Figure 3.1 using the damping and excitation of Example 3.3.1. The blue line was calculated using the state-space method given in Section 3.4, and the orange line using the derivation done in Section 3.3.

To confirm this, let us check if the cross-responses are also in agreement. In Figure 3.7 the magnitude (top) and phase (bottom) of the cross-spectral density between the displacement of masses 1 and 2 is shown. We indeed see an exact match for both the magnitude and the phase of the spectral densities.

Finally, we check that the relationship between the velocity and displacement still holds true. The velocity spectrum S_v should be given by $S_v = \omega^2 S_q$. Indeed, if we look at Figure 3.8, we see the velocity spectrum calculated using the relation between velocity and displacement (the displacement was obtained using the state-space approach) in blue and the velocity component of the state-space vector in orange. The spectra are identical. This suggests that our approach is indeed correct.

3.5 CONCLUSION

In conclusion, we have now developed various ways of dealing with both proportional and non-proportional damping in this chapter. We used a modal approach, which will make for faster calculations in the finite element system we will see later on. Finite element systems can be used to directly model a marine propeller. Although proportional damping is not used in the physical system of a propeller, it can still sometimes be useful for simple models. However, the state-space approach is of great importance, because it allows us to deal with structural-acoustic coupled problems (Chapter 6), which are vital in calculating the radiated noise. Besides, it also allows us to solve purely structural problems that cannot be approximated in a meaningful way by proportional damping, such as an added-mass system we will discuss in Chapter 5.

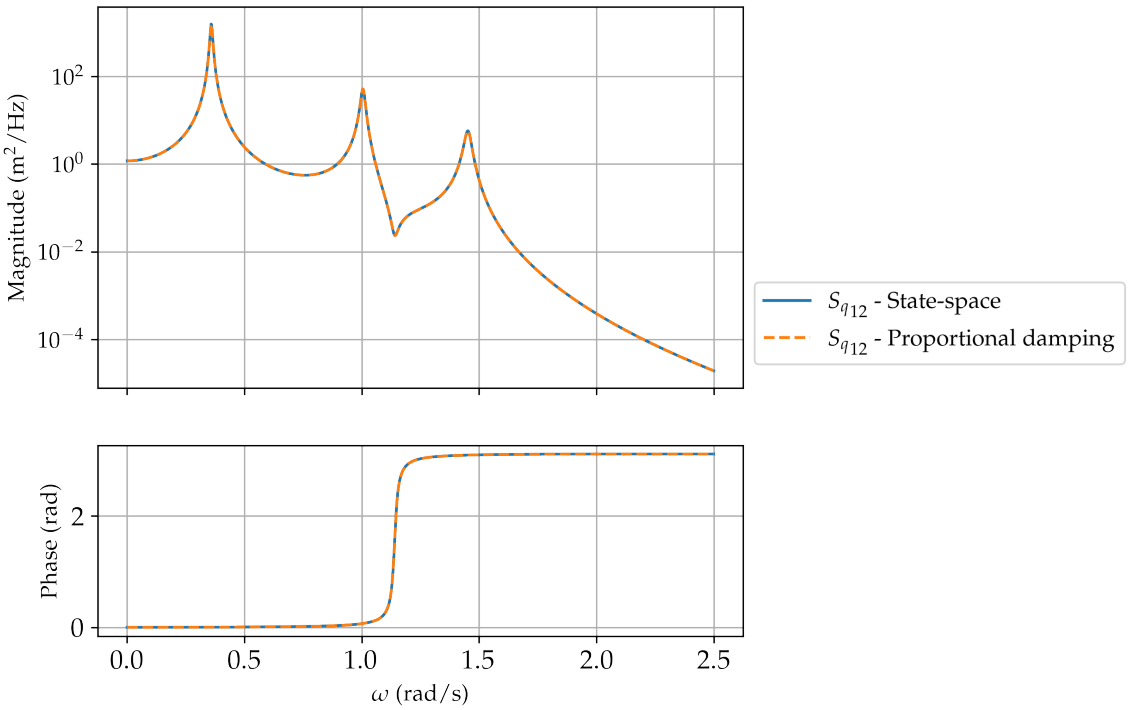

Figure 3.7: Magnitude (top) and phase (bottom) of the cross-spectral density of the first and second mass of the three-degree-of-freedom system shown in Figure 3.1 using the damping and excitation of Example 3.3.1. The blue line was calculated using the state-space method given in Section 3.4, and the dashed orange line using the derivation done in Section 3.3.

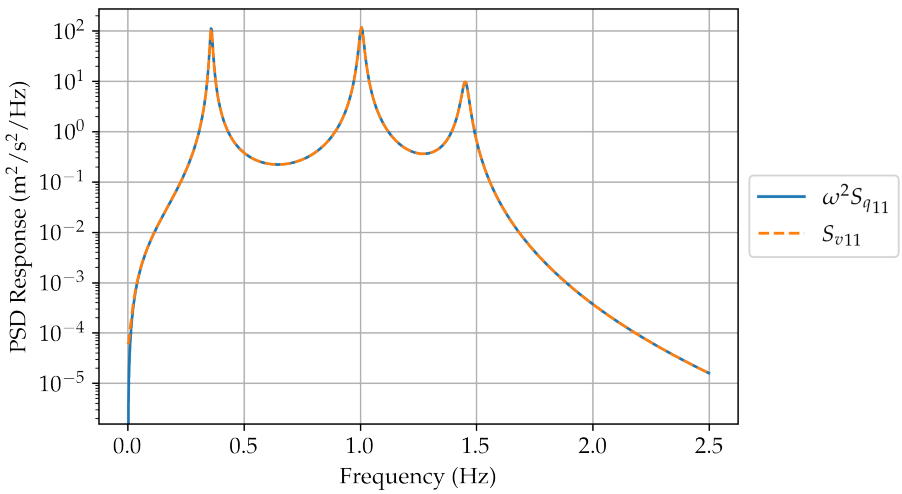

Figure 3.8: The velocity spectrum calculated using the relation between displacement and velocity for harmonic motion $S_v = \omega^2 S_q$ in blue and the velocity component of the state-space vector in orange.

4

CONTINUOUS SYSTEMS

So far we have seen that we can describe both deterministically and stochastically excited multi-degree-of-freedom systems. However, these discrete systems are not our final goal. We would like to be able to accommodate for continuous real geometries instead of only artificial discrete systems of point masses and springs. As opposed to a discrete multi-degree-of-freedom system, a continuous system does not assume the masses are point-like and connected with spring and dampers. Instead, the mass is distributed continuously as a function of position. We are interested in these continuous systems because they allow for analytical response calculations of simple structures, such as plates and rods. These analytical calculations can later be used to verify the response calculated using a finite element model, which we will use to model the propeller blades (for which no analytical mode shapes exist).

For these continuous systems, we can use an approach similar to the one for discrete systems. We again turn towards modal analysis. A challenge for continuous systems is finding the eigenmodes of the system. We restrict our analysis to systems for which the analytical solutions are known. We first look at 1-dimensional (1D) systems, because these are easiest to understand and visualise. For this 1D case we will look at a beam in axial vibration. The calculation is almost analogous for the 2- and 3-dimensional case, as we will see later on. As an example of this, we will look at a rectangular plate vibrating out of plane.

4.1 1D CONTINUOUS SYSTEMS WITH DETERMINISTIC EXCITATION

Just as in the case of the multi-degree-of-freedom system, we will first try to understand deterministically excited systems to obtain a better grasp of continuous systems. To find the solution to the equation of motion, we can simply re-use Equation 3.8. The modal solution to the equation of motion was given by

$$\eta_k(t) = \frac{1}{\omega_k} \int_0^t h_k(t-\tau) \sin(\omega_k \tau)\, \mathrm{d}\tau, \tag{4.1}$$

where in this case [17]

$$h_k(t) = \int_{\mathscr{L}} \psi_k(x) f(x,t)\, \mathrm{d}x\,. \tag{4.2}$$

Here ψ_k is the k^{th} continuous mode shape of the system as a function of the position x, and $f(t,x)$ is the force at time t at position x. We have to integrate over the entire one-dimensional system $\mathscr{L}$. The mode shapes $\psi_k(x)$ can be found by formulating the relevant equation of motion together with the correct boundary conditions, which leads

to an eigenvalue problem by setting the force to zero. An example of such an eigenvalue problem would be

$$-\frac{\mathrm{d}}{\mathrm{d}x}\left[EA(x)\frac{\mathrm{d}\psi_k(x)}{\mathrm{d}x}\right] = \omega_k^2 m(x)\psi_k(x), \tag{4.3}$$

which is used to calculate the mode shapes for a rod in axial vibration, ignoring any stresses in the transverse direction or rotational effects. In Equation 4.3 E is the Young's modulus of elasticity, A is the cross-sectional area, and m is the mass per unit length. The rod is fixed at one end, and free at the other. This rod in axial vibration will be used in Example 4.2.1 to calculate the response for random excitation. We will not focus on how to obtain these mode shapes, as we assume that they are known from now on. Also, for our purpose, the modes shapes can be determined using the finite element method, as we will see in the next chapter.

To convert the solution from Equation 4.1 to the original coordinate system we can use the following relationship

$$q(x,t) = \sum_{k=1}^{\infty} \psi_k(x)\eta_k(t), \tag{4.4}$$

where $q(x,t)$ is the displacement of the system at time t and position x. In Equation 4.4, one would need to sum over all modes, of which there are infinitely many for a continuous system. We only consider the first n eigenmodes, because shear contraction can no longer be ignored when the system becomes heavily distorted from its original shape, as our rod will no longer represent a 1-dimensional system well.[17] This would mean that the equation of motion (and thus our mode shapes) is no longer valid. Another reason to not use all eigenmodes is of a computational nature. Especially for higher dimensional systems, the computational cost increases significantly per added mode. Therefore, one would like to use the minimum number of modes necessary to adequately describe the system in the desired frequency range.

Combining Equation 4.2 and Equation 4.4, we obtain the final solution for the response to a deterministic force [17]

$$q(x,t) = \sum_{k=1}^{n} \frac{\psi_k(x)}{\omega_k} \int_0^t h_k(t-\tau)\sin(\omega_k\tau)\,\mathrm{d}\tau, \tag{4.5}$$

where only the first n modes contribute to the solution. Just as in the discrete case, we normalise the modes on the density such that

$$\int_{\mathscr{L}} m(x)\psi_k^2(x)\,\mathrm{d}x = 1, \tag{4.6}$$

where $m(x)$ is the mass per unit length. We will use this same normalisation on density for all continuous modes from now on.

4.2 1D CONTINUOUS SYSTEMS WITH RANDOM EXCITATION

Now that we know how a continuous system with deterministic excitations behaves, we can move on to continuous systems with random excitations. We would be able to

completely describe the stochastic response of a marine propeller, if we had analytical mode shapes. Of course, we do not have access to those for a propeller. However, in other cases, such as vibrating plates or rods, we can calculate the response analytically. Doing this stochastic calculation on simple systems, will also allow us to analytically verify the response of such systems calculated using the finite element method presented in the next chapter. That in turn will lend credibility of the proposed method to more geometrically complicated structures.

This analytical calculation with stochastic excitation is again done through modal analysis. The response cross-correlation of the displacement $q(x,t)$ between points x and x' can be written as

$$R_q(x,x',\tau) = \lim_{T\to\infty} \frac{1}{T} \int_{-T/2}^{T/2} q(x,t)q(x',t+\tau)\,\mathrm{d}t\,. \tag{4.7}$$

Combining this expression with Equation 4.4, we obtain

$$\begin{aligned} R_q(x,x',\tau) &= \lim_{T\to\infty} \frac{1}{T} \int_{-T/2}^{T/2} \sum_{k=1}^{n} \psi_k(x)\eta_k(t) \sum_{l=1}^{n} \psi_l(x')\eta_l(t+\tau)\,\mathrm{d}t \\ &= \sum_{k=1}^{n}\sum_{l=1}^{n} \psi_k(x)\psi_l(x')R_{\eta,kl}(\tau), \end{aligned} \tag{4.8}$$

where in the last step, we moved the sums out of the integral and recognise the modal cross-correlation integral. We saw earlier that this modal correlation function $R_{\eta,kl}$ between two modes k and l is related to the excitation cross-spectral density $S_{h,kl}$ in modal space through

$$R_{\eta,kl} = \frac{1}{2\pi} \int_{-\infty}^{\infty} \bar{G}_k(\omega)G_l(\omega)S_{h,kl}(\omega)\mathrm{e}^{\mathrm{i}\omega\tau}\,\mathrm{d}\omega\,. \tag{4.9}$$

This equation still holds in the continuous case, because both the discrete and continuous system behave the same in modal space. The only difference is the way the forces and displacements are converted from real space to modal space (summation versus integration).

Combining Equation 4.8 and Equation 4.9 and dropping the Fourier transform, gives us an expression for output spectral density

$$S_q\left(x,x',\omega\right) = \sum_{k=1}^{n}\sum_{l=1}^{n} \psi_k(x)\psi_l(x')\bar{G}_k(\omega)G_l(\omega)S_{h,kl}\left(\omega\right), \tag{4.10}$$

where $S_q\left(x,x',\omega\right)$ is the output cross-spectral density between the points x and x'. In the case that $x = x'$ we obtain the auto-spectral density at the point x. G_k is the transfer function we saw earlier (Equation 3.25), and ψ_k is the k^{th} mode of the system.

It should be noted here that the excitation cross-spectral density is given in modal space. In order to convert the excitation cross-spectral density in real space to modal space we apply the following operation

$$S_{h,kl}\left(\omega\right) = \int_{\mathscr{L}}\int_{\mathscr{L}} \psi_k(x)\psi_l(x')S_f\left(x,x',\omega\right)\,\mathrm{d}x\,\mathrm{d}x', \tag{4.11}$$

where x and x' are just dummy variables for the integration. S_f is the cross-spectral density of the forces acting on positions x and x'. Of course, for $x = x'$ this reduces to the

auto-spectral density at position x. The discrete version of the conversion of the real space to modal space force spectral density was given in Equation 3.35.

The final expression for the response of the system, including the modal force conversion is given by

$$S_q\left(x,x',\omega\right) = \sum_{k=1}^{n}\sum_{l=1}^{n}\psi_k(x)\psi_l(x')\bar{G}_k(\omega)G_l(\omega)\int_{\mathscr{L}}\int_{\mathscr{L}}\psi_k(\mu)\psi_l(\mu')S_f\left(\mu,\mu',\omega\right)\mathrm{d}\mu\,\mathrm{d}\mu', \tag{4.12}$$

where we introduced μ and μ' as dummy variables for the spatial integration of the force spectral density. We will see in Example 4.2.1, that we have a modal displacement in the x-direction, and thus also response in this direction (axial vibration). However, in the case of 1-dimensional transversely vibrating beams, the displacement (and mode shape) are in the direction perpendicular to the x-axis. The direction of the response is completely determined by the mode shapes and can be in any direction.

Equation 4.12 is the continuous 1D equivalent of the discrete case in Equation 3.39. This 1-dimensional description is already closer to the physical reality, but the real world is obviously three-dimensional. After an example of a 1D rod, we will therefore move on to 2- and 3-dimensional continuous systems.

Example 4.2.1. As an example, let us find the response of a rod in axial vibration. A rod in axial vibration stretches along its long axis. This particular rod is fixed at one end ($x = 0$) and free at the other ($x = L$). The rod is excited randomly at the free end with white noise. In Figure 4.1 a graphical representation of the rod is shown. The white noise excitation is marked with S_f, which is also pointed along the axis in which the rod vibrates. In this example, we are dealing with 1-dimensional modes, but the physical rod represented by the 1-D system still has an area corresponding to certain coordinates along the x-axis. This area determines the mass distribution along the rod. In this particular example, a uniform mass distribution is chosen.

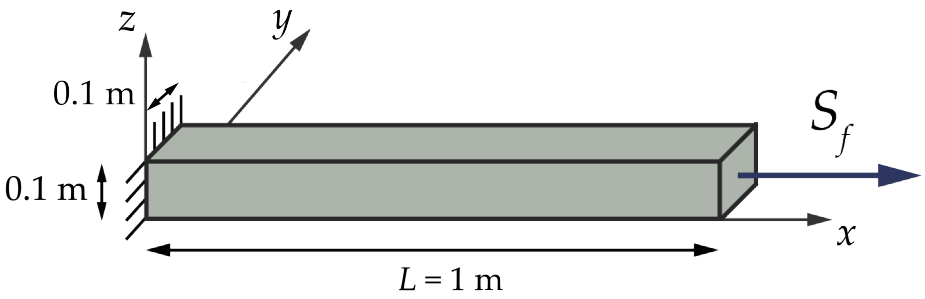

Figure 4.1: The rod used in Example 4.2.1, where the response of the system is calculated. The rod is fixed on the side at $x = 0$, as indicated by the lines (ɛ). The rod is rectangular with dimensions 1 m × 0.1 m × 0.1 m.

According to Meirovitch [20, p. 395], we can find the eigenfrequencies of this system through

$$\omega_k = \frac{(2k-1)\,\pi}{2}\sqrt{\frac{EA}{mL^2}}, \tag{4.13}$$

and the eigenmodes are given by

$$\psi_k(x) = \sqrt{\frac{2}{mL}} \sin\left(\frac{(2k-1)\pi x}{2L}\right), \tag{4.14}$$

where E is the modulus of elasticity, A the cross-sectional area, $m = A\rho$ the (constant) mass per unit length, and L the length of the rod. In our example, we will use a rod of structural steel. The properties of structural steel and the rod are shown in Table 4.1.

L	A	E	ρ
1 m	0.01 m^2	200 GPa	7850 kg/m^3

Table 4.1: The properties of the rod used in Example 4.2.1.

Using these values, we can obtain the eigenfrequencies of the system. The lowest seven are shown in Table 4.2. We will use these seven eigenfrequencies and their corresponding mode shapes to calculate the response of the system. The number of eigenfrequencies is of course arbitrary. The reason we chose seven in this case will become apparent in Example 5.1.1. The damping factor ζ was 0.05 for each mode.

	ω_1	ω_2	ω_3	ω_4	ω_5	ω_6	ω_7
Freq. (rad/s)	7929	23786	39643	55501	71358	87215	103072
Freq. (Hz)	1262	3786	6309	8833	11357	13881	16405

Table 4.2: The first seven eigenfrequencies of the structural steel rod used in Example 4.2.1 in rad/s and Hz.

We can now apply a stochastic load at the free end of the rod. We use a white noise spectrum with a constant value of 1 N^2/Hz. Because it is a boundary load, we will have to represent S_f as a delta function [17]

$$S_f(x, x', \omega) = \begin{cases} \delta(x - L) & x = x' \\ 0 & x \neq x' \end{cases}. \tag{4.15}$$

In Figure 4.2 the response of the rod at $x = L$ in the axial direction to a boundary load at the tip is shown in blue. One can clearly observe peaks at the eigenfrequencies of the rod. If we go to even higher frequencies than shown in the figure, we will not see a significant response. This is because we only used the first seven eigenmodes.

Instead of a boundary load, we can also apply a fully correlated body load. A fully correlated load means that the behaviour of the forces is exactly the same in all places along the rod, i.e. there is no difference in phase or strength anywhere. It can be seen as one single force acting everywhere on the rod. Applying this fully correlated body load is mathematically done by setting

$$S_f(x, x', \omega) = 1\,(\mathrm{N/m})^2/\mathrm{Hz}, \tag{4.16}$$

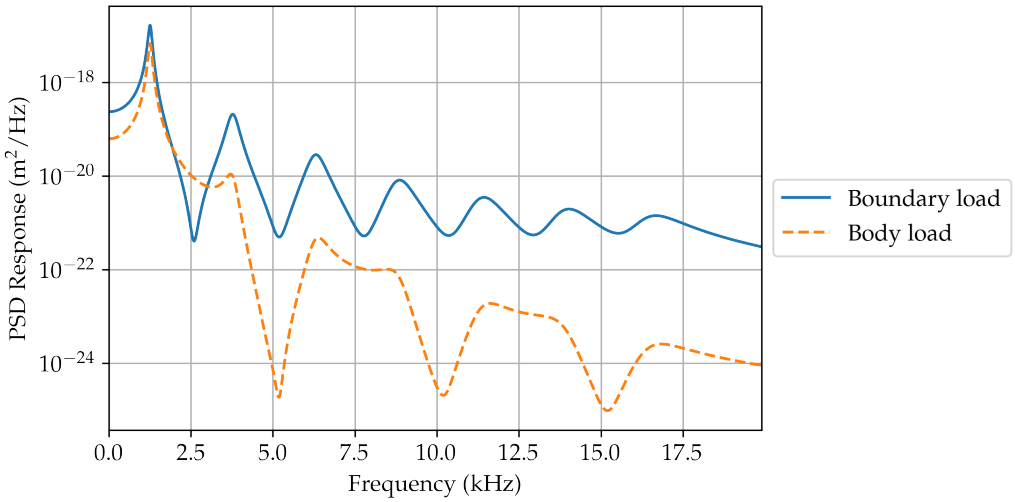

Figure 4.2: The power spectral density of the displacement at $x = L$ of a steel rod in axial vibration with dimensions $1\,\mathrm{m} \times 0.1\,\mathrm{m} \times 0.1\,\mathrm{m}$ to white noise excitation of $1\,\mathrm{N}^2/\mathrm{Hz}$ at the free end of the rod in blue, and to fully correlated white noise body excitation of $1\,(\mathrm{N/m})^2/\mathrm{Hz}$ in orange. The properties of the rod are found in Table 4.1.

for all x, x' and ω. In Figure 4.2, the results are plotted in orange. Again, peaks are visible at the same eigenfrequencies, because the eigenfrequencies are independent of the applied force. However, the behaviour between these peaks has changed. That is because the modal force no longer only takes into account the mode shape at the end of the rod, but instead along the entire rod. Therefore, it is quite logical that the first mode is most present, because this mode only extends the rod in one direction (as can be seen in Figure 5.2, where we show the same modes of this system, but calculated with the finite element method), which means the fully correlated force does not contract the rod in some place and extends it in others. This is the case for modes of higher order than the first, and therefore the response is not as high compared to the boundary load case. They have at least one node which causes the force at to work against mode excitation in some ranges.

4.3 2D CONTINUOUS SYSTEMS WITH RANDOM EXCITATION

We will now continue with a 2-dimensional problem. 2-dimensional problems often have real-world applications, such as outer panels on an aircraft or ship that are excited by a turbulent boundary layer. Therefore, the analytical calculation can be interesting for comparison between experiment and theory in these systems. For a 2-dimensional system, we can easily adapt Equation 4.10 and Equation 4.11. We can simply integrate the 2D modes over the entire area $\mathscr{A}$ in both the x and y-direction to obtain the excitation modal spectrum

$$S_{h,kl}(\omega) = \int_{\mathscr{A}} \int_{\mathscr{A}} \psi_k(x,y)\psi_l(x',y') S_f(x,x',y,y',\omega)\,\mathrm{d}x\,\mathrm{d}y\,\mathrm{d}x'\,\mathrm{d}y'\,. \tag{4.17}$$

Now all that is needed to obtain the output spectrum is sum the forces multiplied with their modes and transfer functions

$$S_q(x,x',y,y',\omega) = \sum_{k=1}^{\infty}\sum_{l=1}^{\infty} \psi_k(x,y)\psi_l(x',y')\bar{G}_k(\omega)G_l(\omega)S_{h,kl}(\omega)\,. \tag{4.18}$$

This time, our modes need to be normalised such that

$$\int_{\mathscr{A}} \rho(x,y)\psi_k^2(x,y)\,\mathrm{d}x\,\mathrm{d}y = 1, \tag{4.19}$$

where ρ is the density of the material in $\mathrm{kg/m^2}$. As we can see, these calculations are indeed very similar to the 1-dimensional case. However, they are much more computationally intensive, because one has to integrate over the area, instead of the length of the system.

Example 4.3.1. Let us look at an example of a rectangular plate that is stochastically excited. This example is largely based on work by De Rosa and Franco [21]. For this example we will use a plate that is simply supported along the edges. This means that the edges are free to move in-plane, but no displacement is allowed out-of-plane, i.e. fixed in the z-direction. In Figure 4.3 a graphical representation of the system is shown. The dashed lines indicate the simply supported edges. The arrows indicate the direction of the excitation.

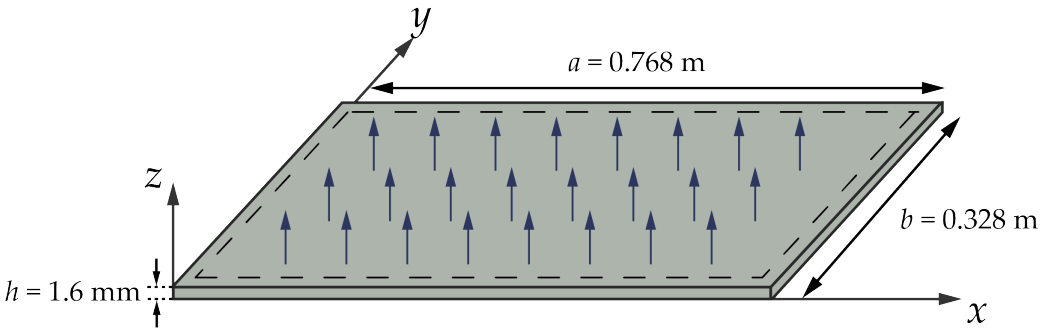

Figure 4.3: The plate used to calculate the PSD response of the system. The plate is simply supported, i.e. restrained in the z-direction on all sides, as indicated by the dashed lines (⬚). The direction of the equally distributed white noise body excitation is indicated with arrows.

Because we are doing a modal analysis, we will need to find the eigenfrequencies and modes. Eigenfrequencies and mode shapes of many types of plates were described by Leissa.[22] For a simply supported plate used here the eigenfrequencies are [22, p. 44]

$$\omega_k = \sqrt{\frac{Eh^2}{12\rho(1-\nu^2)}}\left[\left(\frac{j_x\pi}{a}\right)^2 + \left(\frac{j_y\pi}{b}\right)^2\right]. \tag{4.20}$$

Here E is again the modulus of elasticity, ν is the Poisson's ratio, h is the (uniform) thickness of the plate, and a and b are the lengths of the plate in the x and y-directions respectively. j_x and j_y are integers that can be varied separately from each other to obtain the different eigenfrequencies. In Table 4.3 the properties of the plate used in this example are given.

a	b	h	E	ν	ρ
0.768 m	0.328 m	0.0016 m	70 GPa	0.33	$11.2\,\mathrm{kg/m^2}$

Table 4.3: The properties of the simply supported plate used in Example 4.3.1.

We order the eigenfrequencies by value. That means that the eigenfrequencies with $j_x = 2$, $j_y = 1$ is not necessarily ω_2. This will depend on the value a and b. In Table 4.4, the lowest ten eigenfrequencies with their corresponding j_x and j_y are given. The damping factor ζ was 0.01 for each eigenmode. The eigenmodes, giving the displacement out of plane, i.e. in the z-direction, normalised as shown in Equation 4.19, are [22]

$$\psi_k = \frac{2}{\sqrt{ab\rho}} \sin\left(\frac{j_x \pi x}{a}\right) \sin\left(\frac{j_y \pi y}{b}\right). \tag{4.21}$$

	ω_1	ω_2	ω_3	ω_4	ω_5	ω_6	ω_7	ω_8	ω_9	ω_{10}
Freq. (rad/s)	270	395	604	896	956	1081	1271	1289	1581	1729
Freq. (Hz)	43	63	96	143	152	172	202	205	252	275
(j_x, j_y)	(1, 1)	(2, 1)	(3, 1)	(4, 1)	(1, 2)	(2, 2)	(5, 1)	(3, 2)	(4, 2)	(6, 1)

Table 4.4: The lowest ten eigenfrequencies of the plate in both rad/s and Hz. The corresponding j_x and j_y are also given.

We use a fully correlated body load of $1\,\mathrm{Pa}^2/\mathrm{Hz}$ as excitation in this case. That is

$$S_f(x, y, x', y') = 1\,\mathrm{Pa}^2/\mathrm{Hz} \tag{4.22}$$

for all x, x', y, and y'. In this calculation, the 20 eigenmodes with the lowest eigenfrequencies were taken into consideration. In Figure 4.4 the response in the z-direction is given at $x = a/2$, $y = b/2$. We do not see a response at every eigenfrequency. This is caused by the fact that some modes will have zero displacement in the middle of the plate. Therefore, one will not see these modes in the response. Also, because of the body loading, antisymmetric modes will not be excited, and therefore will not be visible in the response. The antisymmetric modes also cannot have any displacement in the middle of the plate, thus are not visible for both reasons.

4.4 3D SYSTEMS

For completeness, the formula for the response of a 3-dimensional system is also provided

$$\begin{aligned} S_q\left(x, x', y, y', z, z', \omega\right) = &\sum_{k=1}^{n} \sum_{l=1}^{n} \psi_k(x, y, z) \psi_l(x', y', z') \bar{G}_k(\omega) G_l(\omega) \\ &\int_{\mathscr{V}} \int_{\mathscr{V}} \psi_k(\chi, \kappa, \mu) \psi_l(\chi', \kappa', \mu') S_f\left(\chi, \kappa, \mu, \chi', \kappa', \mu', \omega\right) \mathrm{d}\chi \, \mathrm{d}\chi' \, \mathrm{d}\kappa \, \mathrm{d}\kappa' \, \mathrm{d}\mu \, \mathrm{d}\mu' . \end{aligned} \tag{4.23}$$

Here we have to integrate over the entire domain $\mathscr{V}$. The dummy variables χ, κ, and μ are used for calculating the modal force.

4.5 CONCLUSION

In principle, we can now calculate the response for any system for which we know the analytical mode shapes. However, calculating these analytical mode shapes is often not

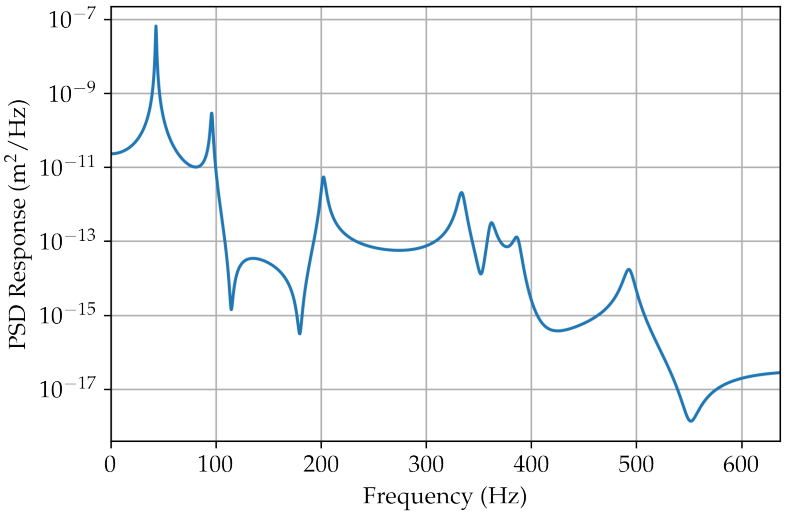

Figure 4.4: The response of a steel plate of dimensions 0.768 m × 0.328 m × 0.0016 m in out-of-plane vibration at $x = 0.384$, $y = 0.164$ to a white noise body load of $1\,N^2/Hz$. The properties of the plate can be found in Table 4.3.

possible for complicated geometries with specific boundary conditions. Therefore, we will now turn towards finite element methods which are able to reasonably approximate any geometry. This will bring us significantly closer to the geometry of a propeller. The analytical calculations in this chapter will however still be useful in verifying the finite element theory for simple systems.

5

FINITE ELEMENT SYSTEMS

We have shown in Chapter 4 that we can calculate the response for any continuous system for which we know the analytically defined modes. In most cases however, the modes are not known analytically. That is why we turn to the finite element method. In a finite element calculation, a structure is divided into small elements, which are used to calculate the eigenmodes. There are many books that give a detailed explanation of the finite element method, such as the ones by Ottosen and Petersson [23], or Fish and Belytschko [24]. Therefore, we will not go in depth into the exact calculations of the finite element method here. In this chapter, we will compare the analytical solutions of the beam in axial vibration to the one using the finite element method. Apart from this, we will look at the more complicated structure of an elliptical flat plate, which has no analytical modes.

Although it is possible to calculate a stochastic response using the commercial software package COMSOL Multiphysics, it is unable to deal with position-dependent excitation spectra as in the case of a marine propeller. Therefore, we would like to be able to calculate the response ourselves, and allow for a position dependency of the excitation. First, we turn towards position-independent spectra, to verify our calculations using the analytical methods from Chapter 4 and COMSOL Multiphysics' own output. Afterwards, we also use the analytical method to verify the response to position-dependent excitations. A more in-depth look at a possible excitation spectrum for a marine propeller is provided in Chapter 8.

5.1 PROPORTIONAL DAMPING

COMSOL Multiphysics calculates the response of a stochastically excited system with a finite element modal analysis, as we are trying to do here. Within COMSOL Multiphysics there is the capability to extract the value of the eigenmodes at the nodes of a finite element system. In Appendix A some example code of how to do this is given. In this way, we can construct a matrix of eigenmode vectors $\boldsymbol{U}$. The columns of $\boldsymbol{U}$ represent the eigenvectors, with each row corresponding to a certain degree of freedom. The eigenmodes should be real in the case of proportional damping, although in COMSOL Multiphysics they sometimes contain a negligibly small imaginary component. These eigenmodes are normalised in the same way as we saw in Equation 3.6 such that

$$\boldsymbol{U}^{\mathrm{T}}\boldsymbol{M}\boldsymbol{U} = \boldsymbol{I}. \tag{5.1}$$

We can also extract the eigenfrequencies from COMSOL Multiphysics. Thus, we have all ingredients required to calculate the response power spectral density. Using the matrix of eigenmodes $\boldsymbol{U}$ and the eigenfrequencies we can calculate the response spectral density matrix $\boldsymbol{S}_q$ using the expression

$$\boldsymbol{S}_q(\omega) = \boldsymbol{U}\bar{\boldsymbol{G}}(\omega)\boldsymbol{U}^{\mathrm{T}}\boldsymbol{S}_f(\omega)\boldsymbol{U}\boldsymbol{G}(\omega)\boldsymbol{U}^{\mathrm{T}}, \tag{3.39}$$

which we derived earlier in Section 3.3. This direct transfer from multi-degree-of-freedom systems shows why our calculations in Chapter 3 were very useful, even if they did not yet represent a physical system. For now, we can only calculate the response at the nodes, which is where we know the value of the eigenmode. If we also want to determine the response between these points, we have to do some kind of interpolation which is beyond the scope of this thesis. Also, this approach will in general only work for proportional damping as we saw in Section 3.2 or if mode-specific damping factors are provided, because the eigenmodes are not given in state-space. This means we do not have a left and right eigenmode that can diagonalise the state-space matrix of the system.

5.1.1 *Comparing the results of the analytical and finite element method*

In this section we will compare the response calculated with three methods. The first is the analytical method derived in Chapter 4 for continuous systems, the second is the one provided in this section for the finite element method, where we extract the eigenvector matrix U from COMSOL Multiphysics. Lastly, we will compare these to the results that COMSOL Multiphysics can produce within its own user interface. Because our analytical method only works for systems for which we have an analytical mode shape, we use very simple systems at first. Once we have used such systems to prove that our finite element method provides correct results, we move on towards more propeller-like geometries, such as an elliptical flat plate.

Example 5.1.1. As example of our FEM calculations, let us find the response of the rod used in Example 4.2.1 excited by a white noise boundary load. We have to model the rod in COMSOL Multiphysics in such a way that only axial modes are found. This can be done by restraining the system in the proper way. The way we have chosen here, is to implement a symmetry condition along two sides of the beam. This means that two sides of the rod always have the exact same displacement, as if they were connected. If one uses this kind of symmetry conditions, it suffices to only model one fourth of the rod in the yz-plane to get the complete results. In Figure 5.1 a graphical representation of the rod and its boundary conditions are shown. Note from the dimensions that we only modelled one fourth of the rod, as the initial dimensions were $1\,\text{m} \times 0.1\,\text{m} \times 0.1\,\text{m}$ and now $1\,\text{m} \times 0.05\,\text{m} \times 0.05\,\text{m}$.

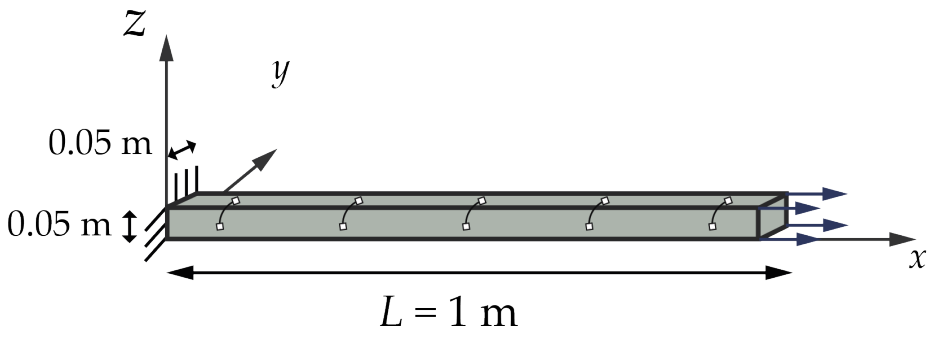

Figure 5.1: The rod modelled in COMSOL Multiphysics. The symmetry condition (⊏⊐) on two sides is marked as well as the fixed end (E). A boundary load, as used in Example 5.1.1 is also indicated, with the four arrows corresponding to the four nodes at the end of the rod.

The eigenmodes that were calculated by COMSOL Multiphysics, together with the mesh used to model the rod are shown in Figure 5.2. For these eigenmodes, we have plotted the displacement in the axial direction. The darker the colour, the larger the displacement in the axial direction. The shape of the rod is the true mode shape, therefore we also see some displacement in the yz-plane for higher modes, because the contraction of the rod caused the rod to broaden in certain other areas. One can clearly see that these are axial modes. This was also the reason only seven eigenmodes were chosen in Example 4.2.1. For higher modes, we could no longer visually confirm that they were indeed axial eigenmodes in COMSOL Multiphysics. Also, for these higher modes the non-axial component increases in importance, and the 1-dimensional approximation, which requires the rod to be slender compared to the wave length, is no longer valid.

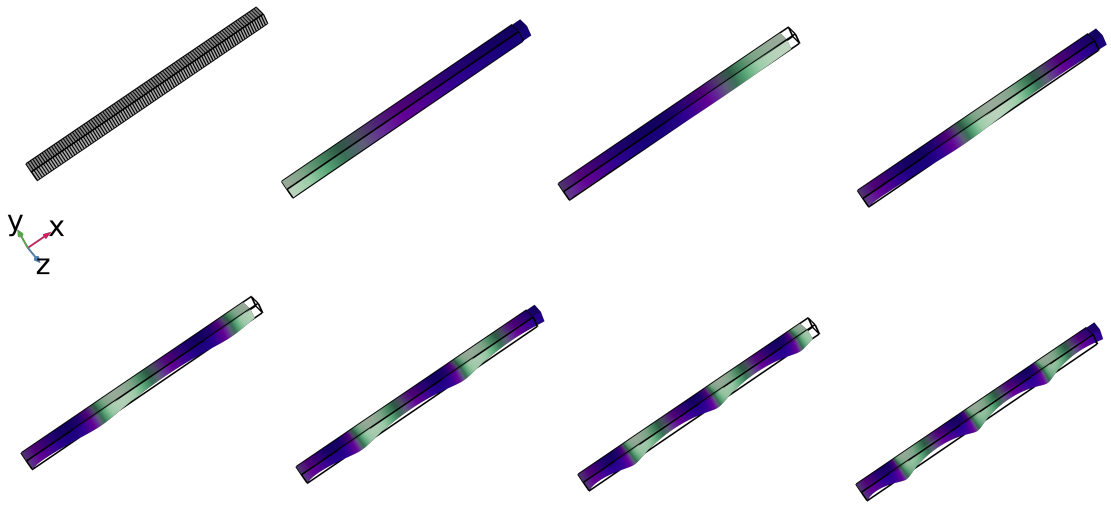

Figure 5.2: In the top left the mesh used to calculate the mode shapes is shown. The other seven images are the first seven eigenmodes of the system. The color represents the displacement in the x-direction for the eigenmodes of the rod as calculated by COMSOL Multiphysics. The darker the colour, the larger the displacement in the axial direction (x-direction). The shape of the rod represents the actual displacement.

The next step in finding the response, is generating the excitation spectral density matrix S_f from Equation 3.39. The matrix will look like

$$S_f = \begin{bmatrix} S_{xx} & S_{xy} & S_{xz} \\ S_{yx} & S_{yy} & S_{yz} \\ S_{zx} & S_{zy} & S_{zz} \end{bmatrix}, \tag{5.2}$$

where the subscripts correspond to the set of degrees of freedom in a certain direction. Our system consists of 100 elements (which can be confirmed by very carefully looking at the top left image in Figure 5.2) and 404 nodes (each vertex in the meshing is a node), which makes for 1212 degrees of freedom. Therefore, S_f will be a 1212×1212 matrix. Because we only have a boundary load in the x-direction, all components will be zero, except for the submatrix S_{xx}. This excitation spectral density matrix in the x-direction will

also contain only zeros, except for the four nodes corresponding to the degrees of freedom at the end of the rod

$$\boldsymbol{S_{xx}} = \begin{bmatrix} 0 & \dots & 0 \\ \vdots & \ddots & \vdots \\ 0 & \dots & \boldsymbol{S_{\text{node}}}^{4\times4} \end{bmatrix}. \tag{5.3}$$

$\boldsymbol{S_{\text{node}}}^{4\times4}$ is a 4×4 matrix (corresponding to the four degrees of freedom at the end of the rod) with all components equal to S_{node}. This converts the 1-dimensional boundary load to a surface loading on the nodal points. S_{node} is the nodal load needed to mimic the white noise boundary load of $1\,\text{N}^2/\text{Hz}$ in the 1-dimensional system. The cross components are also equal to S_{node}, because the boundary load has to be fully correlated to imitate the 1-dimensional case. We can find the value of S_{node} by defining that the total surface loading spectral density $S_{\text{A}}(y,z)$ over the entire end of the rod should be equal to the applied 1-dimensional power spectral density $S_{1\text{D}}$. This gives us the following equality

$$\int_A \int_A S_{\text{A}}(y,z)\,(\text{d}A)^2 = S_{1\text{D}} = 1\,\text{N}^2/\text{Hz}, \tag{5.4}$$

where we used the area of the full rod (of dimensions $0.1\,\text{m} \times 0.1\,\text{m}$) as boundaries for the integral. Solving this equation gives us that $S_{\text{A}}(y,z) = 10\,000\,(\text{N}/\text{m}^2)^2/\text{Hz}$. This force has to be divided equally over the four nodes at the end of the rod. Because each node corresponds to an equal area, each node experiences the same force. The area corresponding to one such node is $A_{\text{node}} = \frac{1}{4} \cdot \frac{1}{4} A = \frac{1}{16} A$. The first factor of one fourth is because we are only modelling one fourth of the rod, the second one because there are four nodes at the end of the rod. This means each node has a corresponding excitation spectral density of

$$S_{\text{node}} = S_{\text{A}} A_{\text{node}}^2 = S_{\text{A}} \left(\frac{A}{16}\right)^2 = 0.0039\,\text{N}^2/\text{Hz}. \tag{5.5}$$

Now we have all ingredients we need to calculate the response, except for the damping factor corresponding to each mode. The damping factors are the same as in the analytical case, which were $\zeta = 0.05$ for each mode.

In Figure 5.3 the response calculated using the FEM-based approach described in this chapter (FEM Method) is shown in blue. In orange, the analytical response calculation from Example 4.2.1 is plotted, and in green the response by COMSOL Multiphysics's software. The results of both the analytical calculation and the FEM method calculation match very well at lower frequencies. However, at higher frequencies the two curves deviate more. This is caused by the fact that the eigenfrequencies are no longer the same for the analytical and FEM method. An explanation for this is that, as mentioned earlier, for higher order modes the 1-dimensional approximation ceases to be valid. The non-axial components are playing a significant role. Note also, that this mismatch starts to appear when the wavelength shrinks closer to the order of magnitude of the diameter of the rod. The speed of sound in steel is approximately $5000\,\text{m/s}$, thus the wavelength is about $0.4\,\text{m}$ at $12.5\,\text{kHz}$.[25] This explanation is confirmed if we make the rod longer. As Figure 5.4 shows, the methods now match for the higher modes as well. If the rod is longer, the non-axial displacement will be lower for higher modes, thus the rod can be described better by the 1-dimensional system.

COMSOL Multiphysics is also capable of calculating the response within its own software, allowing us to skip the steps of extracting the eigenmodes, converting the excitation spectral density, and calculating this response. Instead, COMSOL Multiphysics can directly generate a plot of the response at a certain point, as shown in Figure 5.3. We see that our response and the one provided by COMSOL Multiphysics are indeed practically identical. A major downside to using COMSOL Multiphysics to calculate the response is that it cannot handle coordinate-dependent excitation spectra or cross-correlations as we will see in Section 5.2. This means that it is not suitable for the coordinate-dependent excitation spectra of the propeller blade.

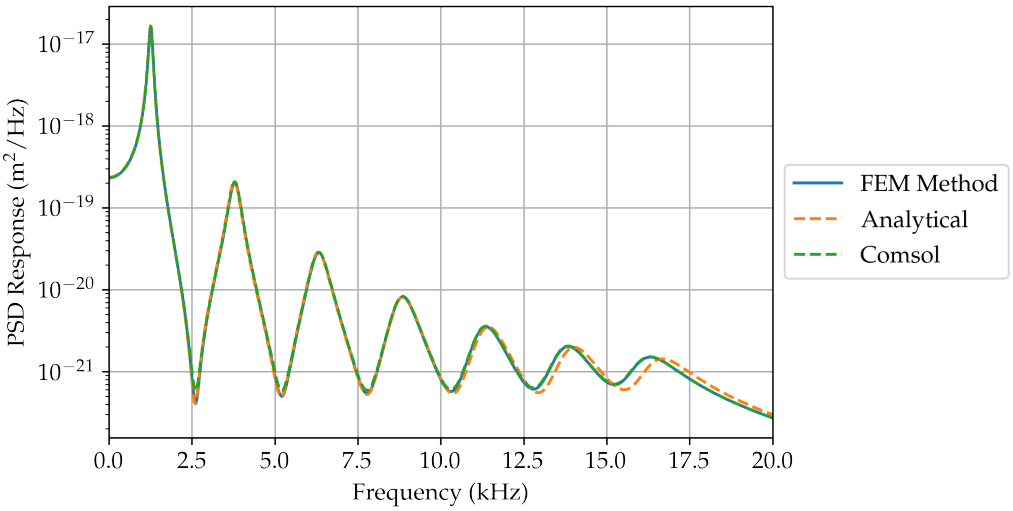

Figure 5.3: The power spectral density of the displacement of the end of a rod in axial vibration of dimensions $1\,\mathrm{m} \times 0.1\,\mathrm{m} \times 0.1\,\mathrm{m}$ to a white noise boundary load of $1\,\mathrm{N}^2/\mathrm{Hz}$ for the FEM method calculation in blue, the analytical method in orange, and COMSOL Multiphysics in green. In the FEM method and COMSOL Multiphysics calculation we used a symmetry condition to ensure only axial modes are present.

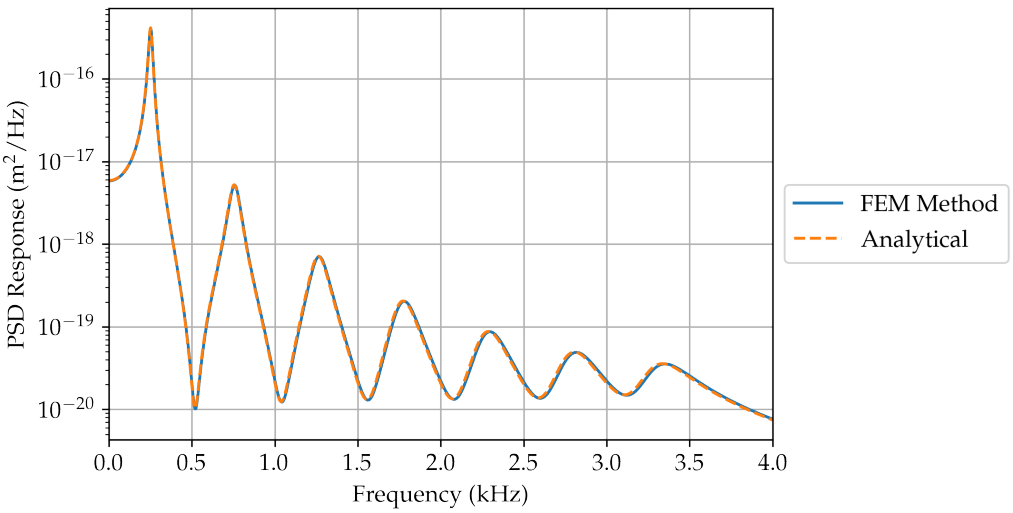

Figure 5.4: The power spectral density of the displacement of the same system as Figure 5.3, but now five times as long, giving the rod dimensions of $5\,\mathrm{m} \times 0.1\,\mathrm{m} \times 0.1\,\mathrm{m}$.

This shows that we can indeed apply boundary loads, and obtain results similar to COMSOL Multiphysics and the analytical calculations, using our own FEM-based method. However, the pressure spectrum applied on a propeller blade will be a load on all sides of the propeller. Therefore, we will now show that we are also able to deal with body loads, which apply a force in all nodes in the system. This has the advantage that it is basically the most complete loading, so that we can apply any shape of pressure loading we would like.

Example 5.1.2. As another example, we can apply a fully correlated body load to the same rod we saw in Example 5.1.1, as depicted in Figure 5.1. To this end, we should first generate the excitation spectral density matrix $\boldsymbol{S}_f$ as seen in Equation 5.2. Just as in the boundary load case, all components of the input spectral density matrix $\boldsymbol{S}_f$ are zero except for the $\boldsymbol{S}_{xx}$ components, because we only have excitation in this direction. However, in this case we have two types of nodes. Those at the two ends of the rod, and those not at the ends, i.e. body nodes. $\boldsymbol{S}_{xx}$ is now given by

$$\boldsymbol{S}_{xx} = \begin{bmatrix} \boldsymbol{S}_{\text{end}}^{4\times4} & \boldsymbol{S}_{\text{cross}}^{4\times396} & \boldsymbol{S}_{\text{cross}}^{4\times4} \\ \boldsymbol{S}_{\text{cross}}^{396\times4} & \boldsymbol{S}_{\text{body}}^{396\times396} & \boldsymbol{S}_{\text{cross}}^{396\times4} \\ \boldsymbol{S}_{\text{cross}}^{4\times4} & \boldsymbol{S}_{\text{cross}}^{4\times396} & \boldsymbol{S}_{\text{end}}^{4\times4} \end{bmatrix}, \tag{5.6}$$

where we split up the two ends of the rod into two submatrices, as this ordering is most intuitive (the first four degrees of freedom correspond to the nodes at $x = 0$ and the last four to those at $x = 1$). We also used a similar notation as earlier to clarify the size of the matrices, for example the submatrix $\boldsymbol{S}_{\text{body}}^{396\times396}$ consists of 396×396 elements with values S_{body}. The cross-correlation spectrum between two nodes is given by

$$S_{\text{cross}} = \sqrt{S_{\text{end}} S_{\text{body}}}, \tag{5.7}$$

which gives us the proper fully correlated cross-spectra.

Now, we have to calculate the equivalent nodal load. This time, we are working with volume forces acting on the entire volume $V = 1\,\text{m} \times 0.1\,\text{m} \times 0.1\,\text{m} = 0.01\,\text{m}^3$ instead of a boundary load. Therefore, we obtain the following equivalence relation

$$\int_V \int_V S_{\text{V}}(y,z)\,(\text{d}V)^2 = S_{\text{1D}} = 1\,\text{N}^2/\text{Hz}. \tag{5.8}$$

Solving this equation gives us that $S_{\text{V}}(y,z) = 10\,000\,(\text{N}/\text{m}^3)^2/\text{Hz}$. This force has to be divided equally over the rod. Therefore, each node experiences a force related to its corresponding volume. This gives us a force at a certain node of

$$S_{\text{node}} = S_{\text{V}} V_{\text{node}}^2. \tag{5.9}$$

Let us first calculate the volume associated with an end node V_{end}. There are 8 nodes connected to one element, and we modelled only one fourth of the beam, thus

$$V_{\text{end}} = \frac{1}{8} \cdot \frac{1}{4} \cdot (V / N_{\text{elements}}) = 3.125 \times 10^{-6}\,\text{m}^3, \tag{5.10}$$

where V is the volume of the rod, and N_{elements} is the number of elements used for the meshing. In this case the number of elements $N_{\text{elements}} = 100$.

Now for the body nodes, they have twice the corresponding volume, because they are connected to two elements. Therefore, the volume associated with these nodes V_{body} is also twice as large as an end node

$$V_{\text{body}} = 2 \cdot \frac{1}{8} \cdot \frac{1}{4} \cdot (V/N_{\text{elements}}) = (V/N_{\text{elements}})/16 = 6.25 \times 10^{-6}\,\text{m}^3. \tag{5.11}$$

This results in an excitation power spectral density applied to an end node with volume V_{end} of

$$S_{\text{end}} = S_V V_{\text{end}}^2 = 9.77 \times 10^{-8}\,\text{N}^2/\text{Hz}. \tag{5.12}$$

For a body node the applied power spectral density is

$$S_{\text{body}} = S_V V_{\text{body}}^2 = 3.91 \times 10^{-7}\,\text{N}^2/\text{Hz}. \tag{5.13}$$

In Figure 5.5, the results are shown for all three methods. We see a perfect match between the FEM method calculation and COMSOL Multiphysics. Again, we see the effect of the mismatch in eigenfrequencies at higher frequencies between the analytical case and the other two. This mismatch happens around the same frequency as the boundary load case. As mentioned in the previous example, this is caused by the fact that the model for the FEM method calculation is not truly a 1-dimensional model, which becomes more apparent for higher order modes.

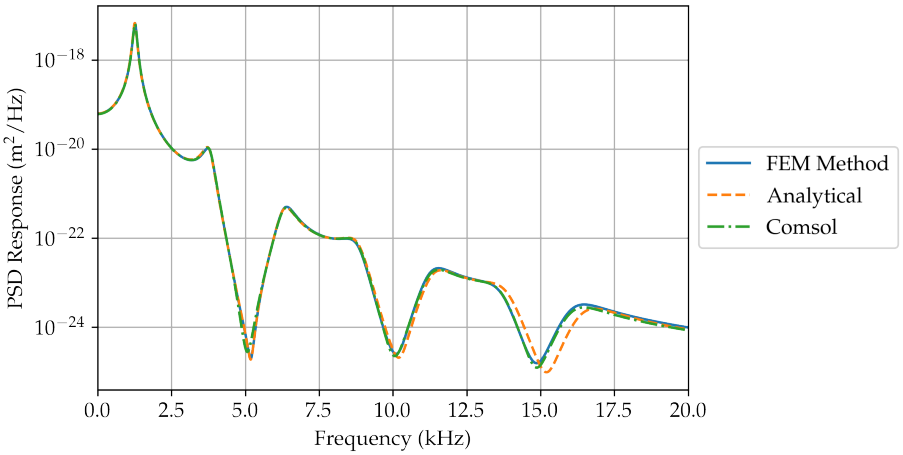

Figure 5.5: The PSD response of a rod of dimensions 1 m × 0.1 m × 0.1 m with symmetry boundary conditions to a white noise body load of 1 N^2/Hz for FEM calculation in blue, the analytical calculation in orange, and COMSOL Multiphysics in green.

5.1.2 *A more complicated geometry: the Burrill plate*

So far, we have only verified our method for simple systems. The interest of this work, a marine propeller, has a more complicated geometry. A marine propeller however is very computationally intensive as it is quite a big system. Therefore, we will use the Burrill plate as an academic substitute of a real propeller. It was first used by Burrill in 1949 for underwater vibration tests.[26] In Figure 5.6 a schematic version of the plate is shown, together with its dimensions. The lines at the left of the plate indicate that it is fixed on

that side. The Burrill plate is also referred to as an elliptical flat plate. In principle, the exact geometry of our system does not matter when it comes to testing our results, as the FEM-based approach is independent of the geometry. Therefore, the results presented in this chapter can directly be used in calculations on a real marine propeller.

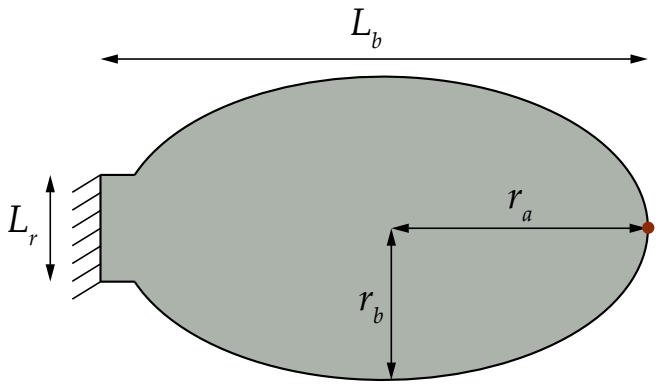

r_a	67.31 mm
r_b	43.05 mm
L_b	131.32 mm
L_r	50.8 mm
Thickness	1.359 mm

Figure 5.6: Top view of the Burrill plate and its dimensions. The lines at the base indicate the plate is fixed there (ɛ). The red dot represents the position of the applied force perpendicular to the plate.

We apply the method described earlier in this chapter to calculate the response. In Figure 5.7 the first five eigenmodes of the plate are shown. We apply a point load of $1\,\mathrm{N}^2/\mathrm{Hz}$ to the tip of the blade (the red dot in Figure 5.6), and calculate the response in the same place. In Figure 5.8 the results of the response calculations are shown. We see that both our own FEM method and COMSOL Multiphysics practically give the same response.

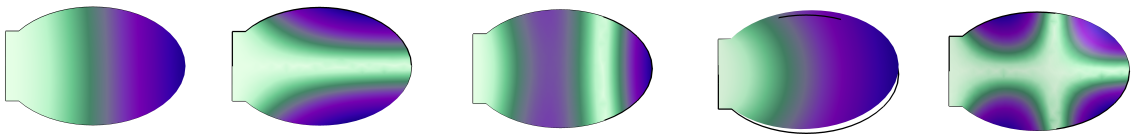

Figure 5.7: The first five eigenmodes and their eigenfrequencies of the Burrill plate. The darker the colour, the larger the overall displacement.

If we zoom in on the results, as shown in Figure 5.9, we see that there is no peak visible for the second and fifth eigenmode. This is because these modes do not have a significant displacement in the z-direction (perpendicular to the plate) in the tip as shown in Figure 5.7. Thus, they are not excited, nor will they be present in the response spectrum at the tip. Also, the fourth eigenmode does not show up, because the displacement of the tip is only in the plane of the plate, and not in the z-direction. The first and third eigenmode do show up, because they do have a displacement of the tip in the z-direction.

Overall, we can state that we can indeed calculate the response for more complicated structures, which is necessary if one wants to calculate the response of a geometrically complicated structured without analytical modes, such as a marine propeller. This section shows that we can calculate the vibrational response to a position-independent excitation

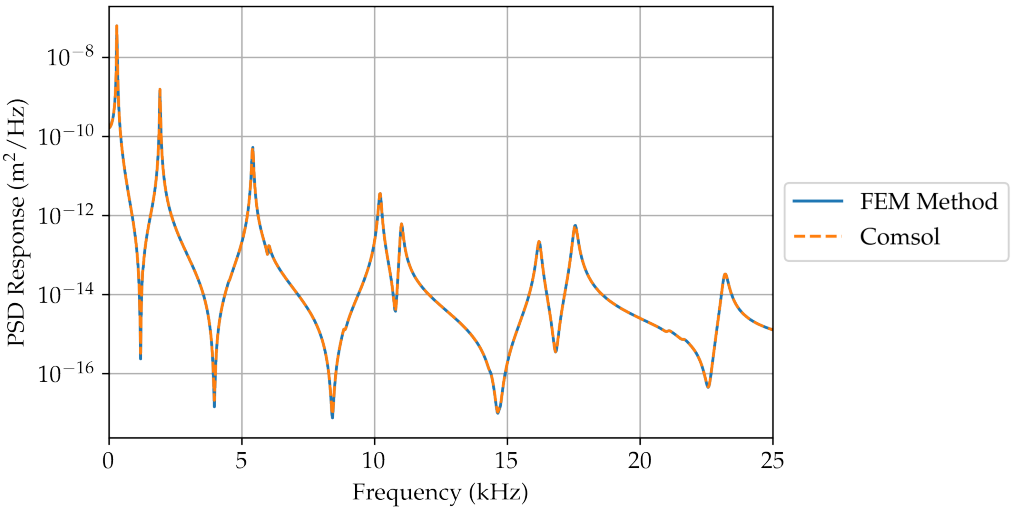

Figure 5.8: The PSD response of the Burrill plate at the tip to a white noise point load of $1\,\mathrm{N}^2/\mathrm{Hz}$ at the tip, for our calculation in blue, and COMSOL Multiphysics in orange.

for an arbitrary geometry, such as a marine propeller. As we will show in the next section, we have also improved upon COMSOL Multiphysics's calculation, as we are capable of dealing with spectra that vary based on the position and cross-spectra that account for the distance between points. This is vital for calculating the noise from marine propellers, as the turbulent boundary layer also depends on position, and has cross-spectra that depend on the position and distance between points.

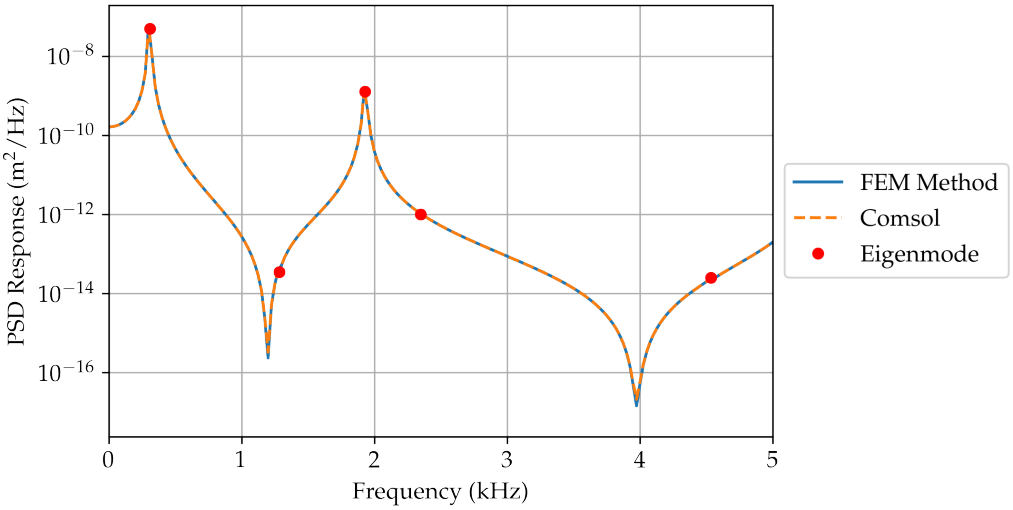

Figure 5.9: The response of the Burrill plate at the tip to a white noise point load of $1\,\mathrm{N}^2/\mathrm{Hz}$ at the tip, for our calculation in blue, and COMSOL Multiphysics in orange. Only the frequency range in which the first five eigenmodes are located is shown. The red dots are placed at the frequencies of these first five eigenmodes.

5.2 COORDINATE-DEPENDENT EXCITATION SPECTRA

As mentioned earlier, the excitation spectrum on the blade of a marine propeller depends on the position, as is often the case in real-life applications. Its cross-spectra also depend on the distance between two points. COMSOL Multiphysics is unable to deal with such position or distance-dependent spectra. Therefore, we have developed our own FEM calculations earlier in this chapter. We can now compare our calculations to the analytical case for cross-spectra that depend on the distance between two points. We can do this for the 1-dimensional rod in axial vibration we saw earlier in this chapter. It was chosen to compare the calculations on the extended rod with a length of 5 m, because this made a better match to the analytical system. The applied spectrum S_f was in the analytical case

$$S_f(x, x', \omega) = x e^{|x-x'|}. \tag{5.14}$$

Of course, we have to convert this to a nodal loading. This was done by assuming that the loading does not change between the nodes. That is, the spectral density of the loading at one node was just multiplied with the volume corresponding to it. The cross-spectrum was then only dependent on the distance between these two nodes. In Figure 5.10 the results are shown. It is indeed confirmed that the results of the FEM method are equal to the analytical method. We can thus state that our method can also deal with distance-dependent cross-spectra, and auto-spectra that depend on position. This is important, because it is essential to our goal of describing a propeller excited by a turbulent boundary, which is dependent on the distance between points and the exact position on the blade.

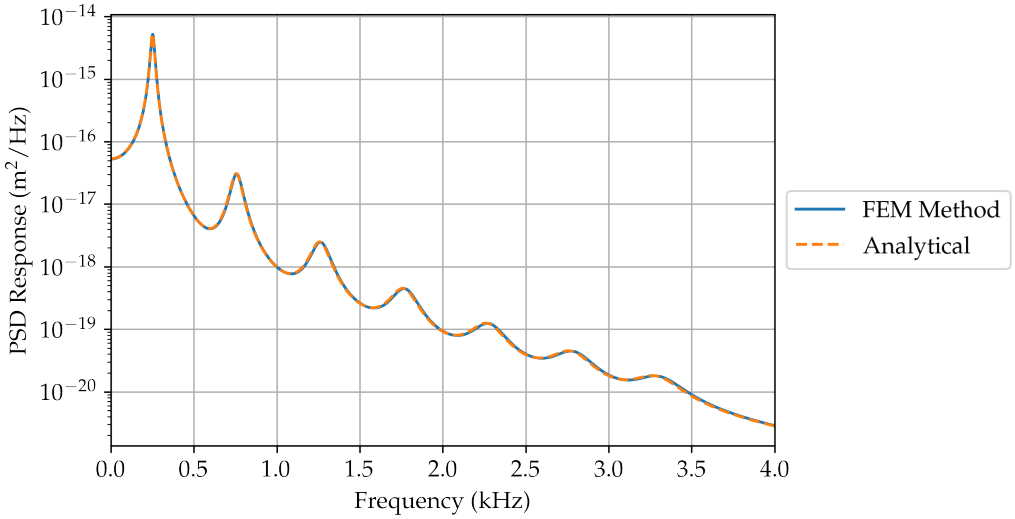

Figure 5.10: The power spectral density of the displacement of the end of a rod in axial vibration of dimensions 5 m × 0.1 m × 0.1 m to a body load with a cross-correlation that depends on the position as shown in Equation 5.14 for the FEM method calculation in blue and the analytical method in orange. In the FEM method calculation we used a symmetry condition to ensure only axial modes are present.

5.3 ARBITRARY DAMPING

Generally, in the case of acoustic radiation, the system is not described well by proportional damping. One very important case we will see in the next chapter, is that of coupled

systems. Coupled systems are needed for calculating the radiated noise from a propeller, and never have proportional damping matrices. In such cases, we would like to be able to use arbitrary damping. To this end, we can use the state-space description derived in Section 3.4, which gave us the solution

$$\boldsymbol{S}_x(\omega) = \boldsymbol{X}\bar{\boldsymbol{G}}(\omega)\boldsymbol{Y}^{\mathrm{H}}\boldsymbol{B}\boldsymbol{S}_f(\omega)\boldsymbol{B}^{\mathrm{H}}\boldsymbol{Y}\boldsymbol{G}(\omega)\boldsymbol{X}^{\mathrm{H}}. \tag{3.68}$$

We do however have to calculate our own state-space eigenmodes, because COMSOL Multiphysics does not provide them. We can extract the mass, damping, and stiffness matrix from COMSOL Multiphysics, and calculate the eigenmodes through the state-space matrix as shown earlier in Equation 3.44. The rows and columns of the matrices corresponding to those degrees of freedom that are fixed have already been removed by COMSOL Multiphysics. This allows us to calculate modes that adhere to the imposed constraints. This however also restricts us. Only the fixed constraints are directly applied. We cannot directly extract system matrices with symmetry or other types of boundary conditions already applied from COMSOL Multiphysics. We can however, constrain the system matrices ourselves by removing certain rows and columns. Many boundary conditions can be written as such constraints, and can therefore be implemented by ourselves.

Example 5.3.1. Let us do a calculation using the state-space method, where we compare our results with COMSOL Multiphysics. In this case, we calculate the response to a body load of $1\,(\mathrm{N/m^3})^2/\mathrm{Hz}$, applied to a flat plate. This plate is fixed on all sides, in all directions. The dimensions of the plate are $1\,\mathrm{m} \times 1.4\,\mathrm{m} \times 0.01\,\mathrm{m}$. In Figure 5.11 a schematic of the plate is shown.

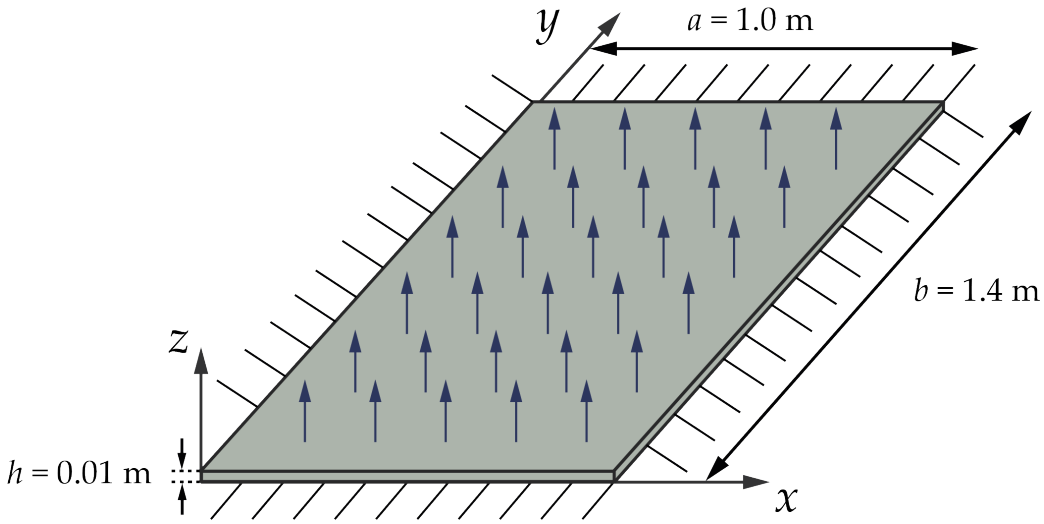

Figure 5.11: The plate used to calculate the PSD response of the system with the state-space method. The plate is fully fixed on all sides as indicated by the lines (⋿). The arrows signify the body loading on the plate.

For our response calculation, we use all possible modes, which is the same number of modes as the number of unconstrained degrees of freedom, giving us twice as many eigenvectors in state-space. We used proportional damping with coefficients $\alpha = 10^{-6}\,\mathrm{s}^{-1}$ and $\beta = 10^{-8}\,\mathrm{s}$. The response was measured at point $[0.4, 0.4, 0]$. As we can see in Figure 5.12, the responses calculated using the state-space FEM method (in blue) and

COMSOL Multiphysics (in orange) match very well. This suggests that our state-space method is indeed valid for this type of system.

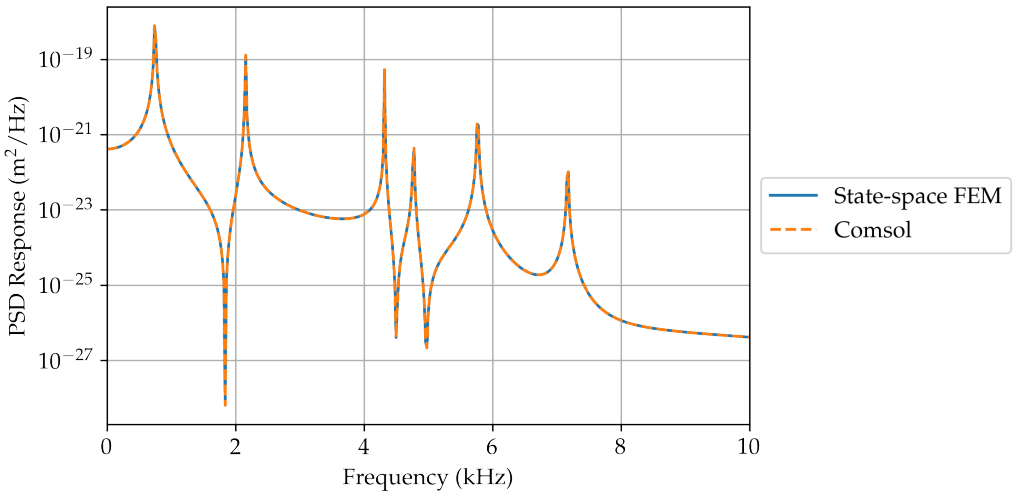

Figure 5.12: The response of a rectangular plate with dimensions 1 m × 1.4 m × 0.01 m as shown in Figure 5.11 to a white noise body load of 1 $(\mathrm{N/m^3})^2/\mathrm{Hz}$ for the state-space calculation in blue and Comsol in orange.

One of the advantages of the modal calculation, is that for larger systems one can remove certain unimportant modes to speed up the computation. This is also possible for state-space calculations. If one would like to get rid of a mode, one can remove the two columns corresponding to that eigenvalue in the right eigenvector matrix $\boldsymbol{X}$. The left eigenvector matrix $\boldsymbol{Y}$ can then easily be calculated by using the fact that they are each other's inverse (see Equation 3.57). In Figure 5.13, an example of this is shown. This is the response at the tip of the Burrill plate to a white noise body load. In this case, only ten modes were taken into account. The response still matches the response given by COMSOL Multiphysics very well.

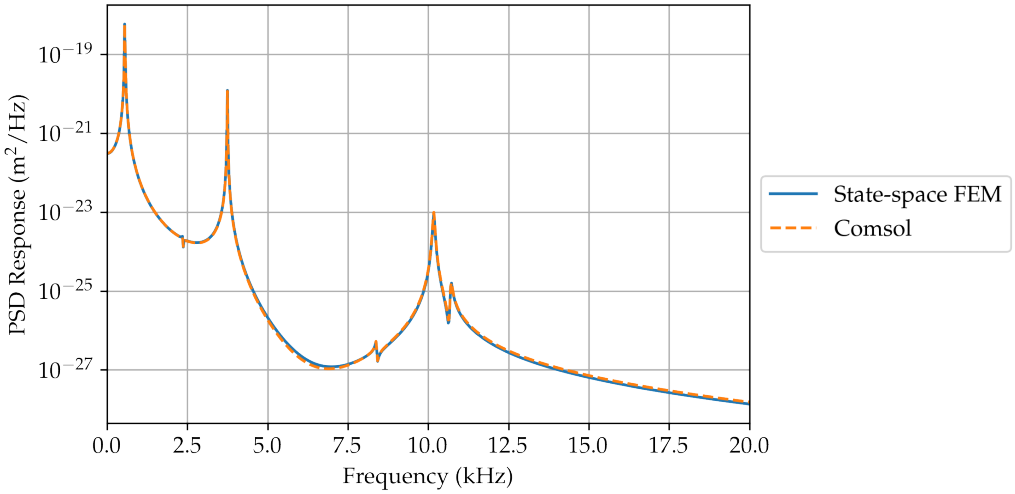

Figure 5.13: The response of the Burrill plate at the tip to a white noise body load of 1 $(\mathrm{N/m^3})^2/\mathrm{Hz}$ for our calculation using state-space in blue and COMSOL Multiphysics in orange.

5.3.1 *Added mass of water*

To simulate the effect of water on the structure, but mainly as an example of non-proportional damping, one can add an extra term to the mass matrix. This term represents the incompressible water surrounding the structure. More information on this can be found in several books, such as the one by Zienkiewicz and Taylor [27]. Of course, incompressible water is not physical, but it allows us to calculate mode shapes and responses for structures that interact with fluids without having to simulate the entire fluid domain. In this case however, the damping matrix will never be proportional to the mass and stiffness matrix, because for proportional damping ($\boldsymbol{C} = \alpha\boldsymbol{M} + \beta\boldsymbol{K}$) the original matrices without the added water mass are used. This is where the state-space method is essential for calculating the response. As we will see in Chapter 6, the state-space method can also be used to calculate the response of an object in a fluid in a more neat way, where the water is not represented as an incompressible fluid, but instead fully simulated with finite elements.

In Figure 5.14 the response for a plate as shown in Figure 5.11 with added mass is given. For this calculation we used 25 eigenmodes. The added mass had a density of 997 $\mathrm{kg/m^3}$, which corresponds approximately to that of water.[28] Although the density of (sea)water can vary, the exact value is not relevant for this example calculation. Our response and the one calculated by COMSOL Multiphysics are in agreement, which indicates that this state-space description is indeed able to deal with non-proportional damping matrices, as will be needed for coupled systems.

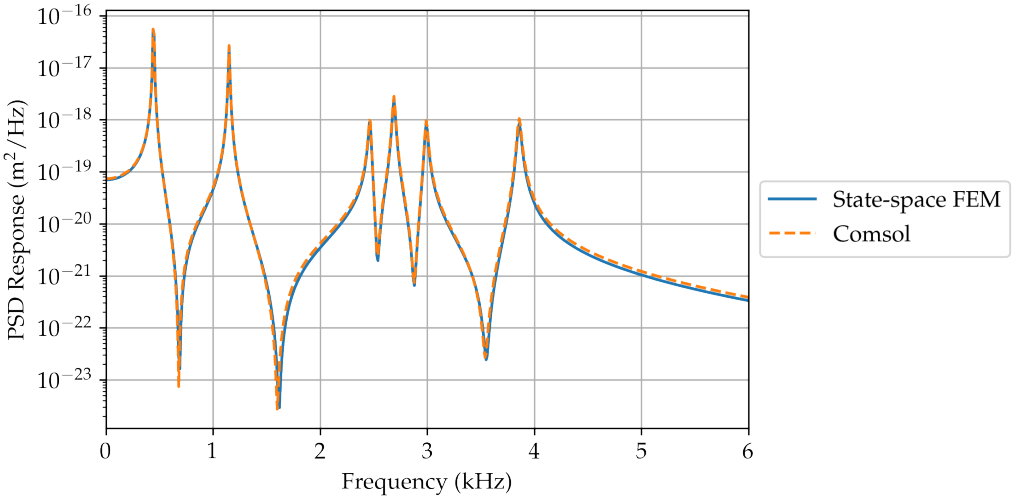

Figure 5.14: The response of the rectangular plate as shown in Figure 5.11 with added mass and dimensions 1 m × 1.4 m × 0.01 m to a white noise body load of 1 $(\mathrm{N/m^3})^2/\mathrm{Hz}$ for the state-space calculation in blue and Comsol in orange.

5.3.2 *Limitations of the state-space approach*

Unfortunately, there are several limitations with the state-space approach. The first one seems to be the rigid body modes. Rigid body modes are modes at zero frequency, where the structure as a whole is translated or rotated. There are six of such modes, three rotations and three translations. COMSOL Multiphysics and our calculation do not give

the same answer when taking into account rigid body modes. This could be caused by the fact that either our solver or the one COMSOL Multiphysics uses, becomes inaccurate for modes with eigenvalue zero, as is the case for rigid body modes. In principle, these rigid body modes are not relevant in the situations in which these random vibrations are applied. Marine propellers are always connected to a rigid hub and thus do not display rigid body modes, because the coordinate systems translates according to the movement of this hub, thus invalidating these rigid modes.

Another limitation of the state-space method is the fact that in state-space using modes calculated by ourselves, a point load does not seem to give the expected results. In Figure 5.15, we can see the response of the plate used in Example 5.3.1 to a white noise point load at position $[0.4, 0.4, 0]$. As we can see, the response using our calculation and COMSOL Multiphysics are only a partial match. The peaks are at the right frequency, but especially the antiresonances are very different. The response also does not match at zero frequency and the high-frequency side.

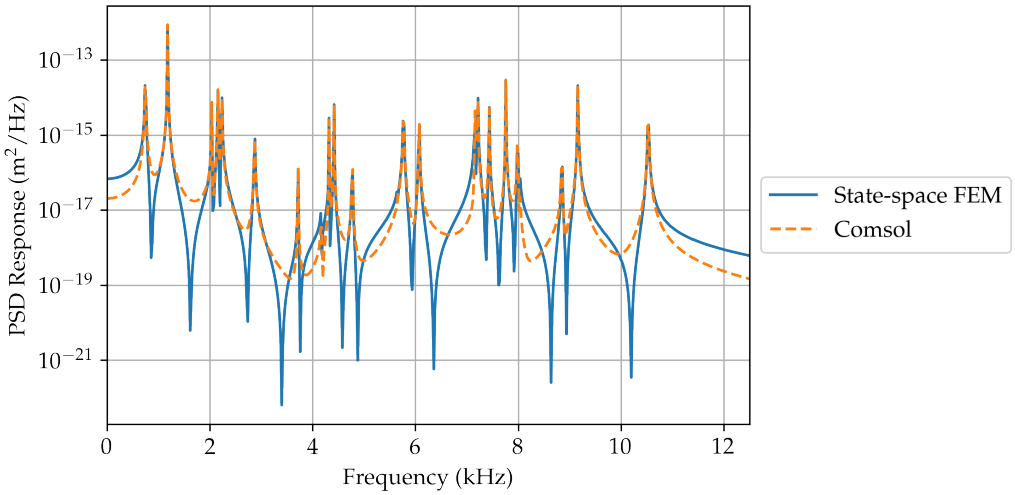

Figure 5.15: The response spectrum of the rectangular plate with dimensions $1\,\mathrm{m} \times 1.4\,\mathrm{m} \times 0.01\,\mathrm{m}$ at position $[0.4, 0.4, 0]$ to a white noise point load at position $[0.4, 0.4, 0]$ of $1\,\mathrm{N}^2/\mathrm{Hz}$ for the calculation using state-space in blue and Comsol in orange.

An explanation for this difference could be that it is caused by the fact that a load on a single node is not the same as a point load in COMSOL Multiphysics. However, if this were the true cause of the difference, using a finer mesh should decrease the difference between our calculation and the one from COMSOL Multiphysics, but this does not seem to be the case.

An alternative explanation, which we believe to be the more likely one, could be that the modes are not calculated correctly by us in state-space. The fact that for the proportional finite element method as discussed in Section 5.1, where we directly extracted the modes from COMSOL Multiphysics, we could implement a point load and obtain similar results to COMSOL Multiphysics, indicates that this could be the case. This could be a consequence of not understanding exactly what kind of system matrices COMSOL Multiphysics provides, as we will also see in Chapter 6.

There are also some similarities. We see in Figure 5.15 that the height and position of the resonances are comparable in both cases. As often most energy is contained in the resonances, the differences in antiresonances is of lesser importance. Apart from this, in real-life situations, the excitations are never point-like. In most cases, such as a marine propeller in turbulent flow, the excitation will be distributed over the whole object. Therefore, these differences may be of little importance.

5.4 CONCLUSION

In conclusion, it seems that we can now describe the vibrational response of non-proportionally damped systems of arbitrary geometries. We have also improved upon COMSOL Multiphysics' software, by allowing for position-dependent spectra. In principle, these possibilities together allow us to calculate the vibrational response of a marine propeller, where we could mimic the effect of the water loading through added mass. Although there are some differences between our approach and COMSOL Multiphysics, they will vanish in most practical applications. However, we cannot yet calculate the radiated noise. As we will see in the next chapter, the radiated noise can be approximated using coupled modes, which makes for a non-proportional damping matrix in all cases.

6

COUPLED SYSTEMS

Being able to calculate the response of a structural system for any given excitation is only the first step, as shown in Figure 1.1. Our goal was to calculate the radiated noise, for which we obviously need a medium to radiate into. For marine propellers, the surrounding environment of the propeller blade is not a vacuum, but water which has a mass that cannot be neglected compared to that of the propeller. As shown before, we can use the added-mass method to calculate the vibration of a structure in water. However, from there we would still need to calculate the radiated noise, and the added-mass method does not take into account the interaction between fluid and structure (apart from the extra mass). An even more convenient and accurate approach would therefore be to use coupled modes. In this chapter we will discuss how one can use coupled modes to calculate the radiated intensity of the noise. This will conclude the work done in this thesis.

6.1 DERIVATION OF THE RESPONSE AND RADIATED NOISE

For a coupled system, we still have a similar equation of motion as in the purely structural case. Now however, the matrices also include components that couple the structural and acoustic part. The equation of motion becomes the following [29]

$$\begin{bmatrix} \boldsymbol{M}_{ss} & \mathbf{0} \\ \boldsymbol{M}_{fs} & \boldsymbol{M}_{ff} \end{bmatrix} \begin{Bmatrix} \ddot{\vec{q}} \\ \ddot{\vec{p}} \end{Bmatrix} + \begin{bmatrix} \boldsymbol{C}_{ss} & \mathbf{0} \\ \mathbf{0} & \boldsymbol{C}_{ff} \end{bmatrix} \begin{Bmatrix} \dot{\vec{q}} \\ \dot{\vec{p}} \end{Bmatrix} + \begin{bmatrix} \boldsymbol{K}_{ss} & \boldsymbol{K}_{sf} \\ \mathbf{0} & \boldsymbol{K}_{ff} \end{bmatrix} \begin{Bmatrix} \vec{q} \\ \vec{p} \end{Bmatrix} = \begin{Bmatrix} \vec{f}_{\text{tbl}} \\ \vec{0} \end{Bmatrix}, \tag{6.1}$$

where we split the complete mass matrix $\boldsymbol{M}$ into its components: the structural mass matrix $\boldsymbol{M}_{ss}$, the fluid mass matrix $\boldsymbol{M}_{ff}$, and the coupling matrix $\boldsymbol{M}_{sf}$. A similar deconstruction was done for the damping and stiffness matrix, where the subscript $\boldsymbol{s}$ indicates the structural domain and $\boldsymbol{f}$ the fluid domain. We can directly extract these system matrices from COMSOL Multiphysics. The vector $\vec{q}$ contains the nodal displacements of the structural domain, while the vector $\vec{p}$ contains the nodal pressure in the fluid domain. The right side of the equation contains the loading. For the structural domain, this is the turbulent boundary layer pressure fluctuations p_{tbl} which cause a nodal loading $\vec{f}_{\text{tbl}}$. As shown in Figure 1.1, this turbulent boundary layer is generated through multiple processes. In Section 8.3 a model for this turbulent boundary layer is given for completeness, although the characterisation of the turbulent boundary layer is beyond the scope of this thesis. Dos Santos is working on this within the overarching project.[30] This turbulent boundary will still need to be converted to nodal loadings, as mentioned in Chapter 5. If the mesh is fine enough, this can be done similarly to Section 5.2, where you only take into account the pressure at a node multiplied with its area. The fluid domain is not excited by any external forces.[31]

In Equation 6.1 the damping matrix is no longer a linear combination of the mass and stiffness matrix. This means that we should use the state-space method to calculate

the eigenmodes and eigenvalues. The eigenvalues and vectors are calculated from the following matrix $\boldsymbol{A}$

$$\boldsymbol{A} = \begin{bmatrix} \boldsymbol{0} & \boldsymbol{I} \\ -\begin{bmatrix} \boldsymbol{M}_{ss} & \boldsymbol{0} \\ \boldsymbol{M}_{fs} & \boldsymbol{M}_{ff} \end{bmatrix}^{-1} \begin{bmatrix} \boldsymbol{C}_{ss} & \boldsymbol{0} \\ \boldsymbol{0} & \boldsymbol{C}_{ff} \end{bmatrix} & -\begin{bmatrix} \boldsymbol{M}_{ss} & \boldsymbol{0} \\ \boldsymbol{M}_{fs} & \boldsymbol{M}_{ff} \end{bmatrix}^{-1} \begin{bmatrix} \boldsymbol{K}_{ss} & \boldsymbol{K}_{sf} \\ \boldsymbol{0} & \boldsymbol{K}_{ff} \end{bmatrix} \end{bmatrix}. \tag{6.2}$$

This will give us a set of eigenvectors that consist of a structural part and a pressure part. The other matrix $\boldsymbol{B}$ that we need to calculate the spectrum of the solution is given by

$$\boldsymbol{B} = \begin{bmatrix} \boldsymbol{0} \\ \begin{bmatrix} \boldsymbol{M}_{ss} & \boldsymbol{0} \\ \boldsymbol{M}_{fs} & \boldsymbol{M}_{ff} \end{bmatrix}^{-1} \end{bmatrix}. \tag{6.3}$$

This now allows us to calculate the response spectral density matrix $\boldsymbol{S}_q$ as we saw earlier in Section 5.3

$$\boldsymbol{S}(\omega) = \boldsymbol{X}\bar{\boldsymbol{G}}(\omega)\boldsymbol{Y}^{\mathrm{H}}\boldsymbol{B}\boldsymbol{S}_f(\omega)\boldsymbol{B}^{\mathrm{H}}\boldsymbol{Y}\boldsymbol{G}(\omega)\boldsymbol{X}^{\mathrm{H}}. \tag{3.68}$$

This matrix consists of four submatrices

$$\boldsymbol{S} = \begin{bmatrix} \boldsymbol{S}_{qq} & \boldsymbol{S}_{pq} \\ \boldsymbol{S}_{qp} & \boldsymbol{S}_{pp} \end{bmatrix}. \tag{6.4}$$

The structural response is given by $\boldsymbol{S}_{qq}$ and the response of the pressure in the fluid domain by $\boldsymbol{S}_{pp}$. These however, are not the most interesting quantities for calculating the radiated noise. Instead, the submatrix $\boldsymbol{S}_{pq}$ gives the pressure times the displacement at the interface. This is interesting, because the sound intensity $I(\vec{r}, \omega)$ at a position $\vec{r}$ on the surface of the object is given by pressure times complex conjugate of velocity in the following way [32]

$$I(\vec{r}, \omega) = \frac{1}{2} \operatorname{Re}\left\{ p(\omega) \bar{v}_{\perp}(\vec{r}, \omega) \right\}, \tag{6.5}$$

where $\bar{v}_{\perp}(\vec{r}, \omega)$ is the velocity perpendicular to the surface at position $\vec{r}$. The quantity $\boldsymbol{S}_{pq}$ can easily be converted to the desired pressure-velocity spectrum $\boldsymbol{S}_{pv}$ as we saw in Equation 3.40 through

$$\boldsymbol{S}_{pv} = \mathrm{i}\omega \boldsymbol{S}_{pq}. \tag{6.6}$$

Of course, the sound intensity $I(\omega)$ is only defined at the surface of the structure. Therefore, the only relevant elements in $\boldsymbol{S}_{pv}$ are the ones that are the cross spectrum between a structural node and a pressure node at the surface. Let us define the matrix of cross-spectra between a pressure and structural node at the interface as $\boldsymbol{S}_{pv_{\perp}}(\omega)$. If we integrate this quantity over the entire surface of the vibrating object Γ we obtain the radiated sound power $P_{\mathrm{rad}}(\omega)$ in the form of a spectral density [31, 32]

$$P_{\mathrm{rad}}(\omega) = \frac{1}{2} \int_{\Gamma} \operatorname{Re}\left\{ S_{pv_{\perp}}(\vec{r}, \omega) \right\} \mathrm{d}\Gamma, \tag{6.7}$$

where $S_{pv_{\perp}}(\vec{r}, \omega)$ is the cross-spectrum normal to the surface at positions $\vec{r}$. It is needed to make a suitable conversion from the value of $\boldsymbol{S}_{pv_{\perp}}(\omega)$ at discrete node points to a

continuous quantity used for integration. The most simple approximation would be the same method as for the initial conversion of the pressure spectrum to nodal loadings, where the nodal response is divided equally over its area. This would mean that the integral in Equation 6.7 turns into a summation over all elements. An alternative could be that $S_{pv_\perp}$ is interpolated linearly between two nodes. Other more complicated schemes are of course also possible, such as a quadratic interpolation between the nodes.

In theory this now allows us to calculate the spectral density of the total radiated sound power of any system that can be modelled using the finite element method, such as a marine propeller in water. Apart from this, it would also be possible to calculate the far-field radiated noise using the Helmholtz-Kirchhoff integral, which only depends on the pressure and the velocity at the surface.[33]

Note here, that especially for marine propellers in a large body of water, a large piece of the fluid domain has to be modelled as well. This means that the modal approach used here will be vital in reducing the computational cost, by only using those modes that are needed to describe the behaviour of the propeller in the frequency regime you are interested in.

Example 6.1.1. As an example of such a coupled system, we will use a very simple one, to save on computational cost. A plate with the edges fixed in all directions (density $\rho = 2700\,\mathrm{kg\,m^{-3}}$, Poisson's ratio $\nu = 0.33$ and Young's modulus $E = 70\,\mathrm{GPa}$) of dimensions $0.49\,\mathrm{m} \times 0.244\,\mathrm{m} \times 0.001\,\mathrm{m}$ on top of a tank filled with water (density $\rho = 997\,\mathrm{kg\,m^{-3}}$, and speed of sound $c = 1481\,\mathrm{m\,s^{-1}}$) of dimensions $0.49\,\mathrm{m} \times 0.244\,\mathrm{m} \times 0.06\,\mathrm{m}$. In Figure 6.1 a schematic of the system is shown. The origin of the coordinate system lies in the bottom corner of the fluid domain. In this case, we used 30 eigenmodes with frequencies between 464 Hz and 9985 Hz. The excitation was a white noise body load of $1\,(\mathrm{N/m^3})^2/\mathrm{Hz}$ in the structural domain.

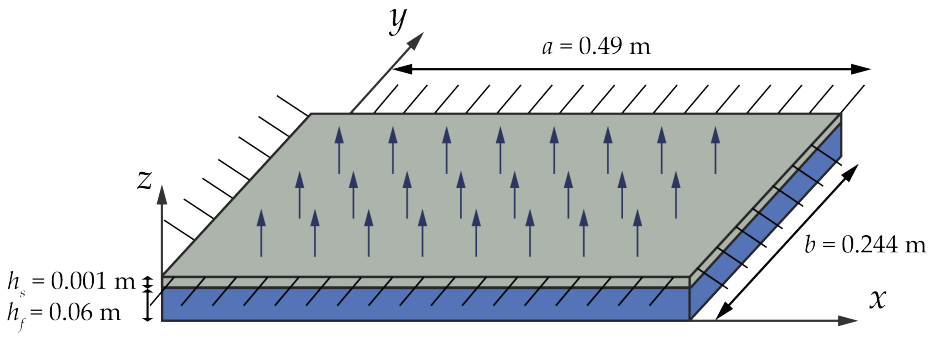

Figure 6.1: The mesh of the plate and water system that was used as an example of a coupled system. The density of the fluid domain is $\rho = 997\,\mathrm{kg/m^3}$, and the speed of sound $c = 1481\,\mathrm{m\,s^{-1}}$. The structural domain had a density of $\rho = 2700\,\mathrm{kg\,m^{-3}}$, Poisson's ratio $\nu = 0.33$ and a Young's modulus of $E = 70\,\mathrm{GPa}$. The structural domain is indicated in blue. The structural domain was fixed on all sides as indicated (Ɛ).

In Figure 6.2 and Figure 6.3 the results for the calculation of respectively the vibrational response of the structural domain and pressure response of the fluid domain are shown. The displacement power spectral density in the structural domain was calculated at $[0.07, 0.061, 0.061]$, while the pressure spectral density in the fluid domain was evaluated in $[0, 0, 0]$. In order to be able to show both our results and the one produced by COMSOL

Multiphysics in the same figure, we had to scale our result with a factor of 10^{-24}. We can conclude that there is no match between the two methods. Apart from some peaks at a similar eigenfrequency there are no real similarities for either the structural or fluid domain response.

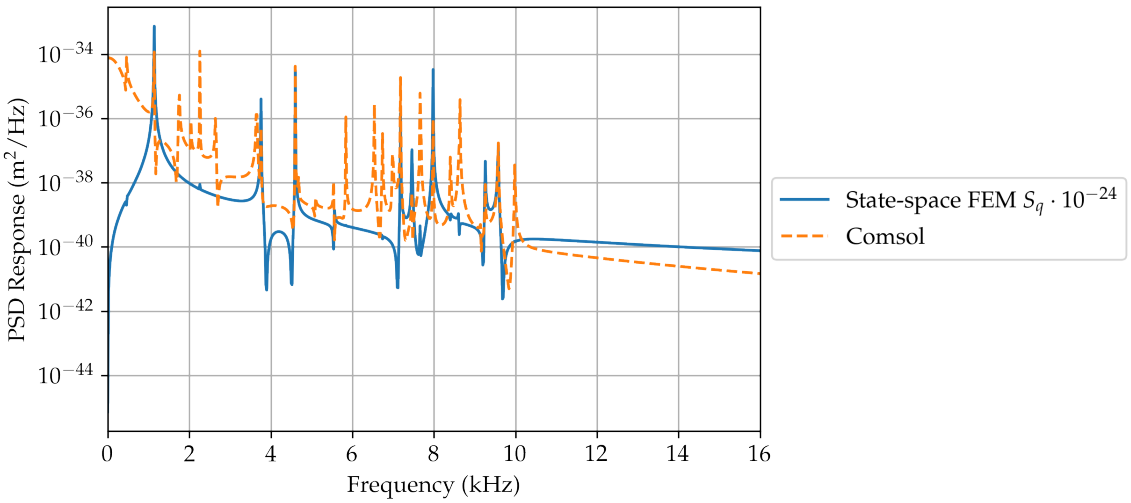

Figure 6.2: The power spectral density of the displacement at [0.07, 0.061, 0.061] to a white noise body load of $1\,(\mathrm{N/m^3})^2/\mathrm{Hz}$ in the structural domain for our calculation in blue and COMSOL Multiphysics in orange. The properties of the structural system were $\rho = 2700\,\mathrm{kg\,m^{-3}}$, $\nu = 0.33$, $E = 70\,\mathrm{GPa}$, and of the fluid domain $\rho = 997\,\mathrm{kg\,m^{-3}}$, $c = 1481\,\mathrm{m\,s^{-1}}$.

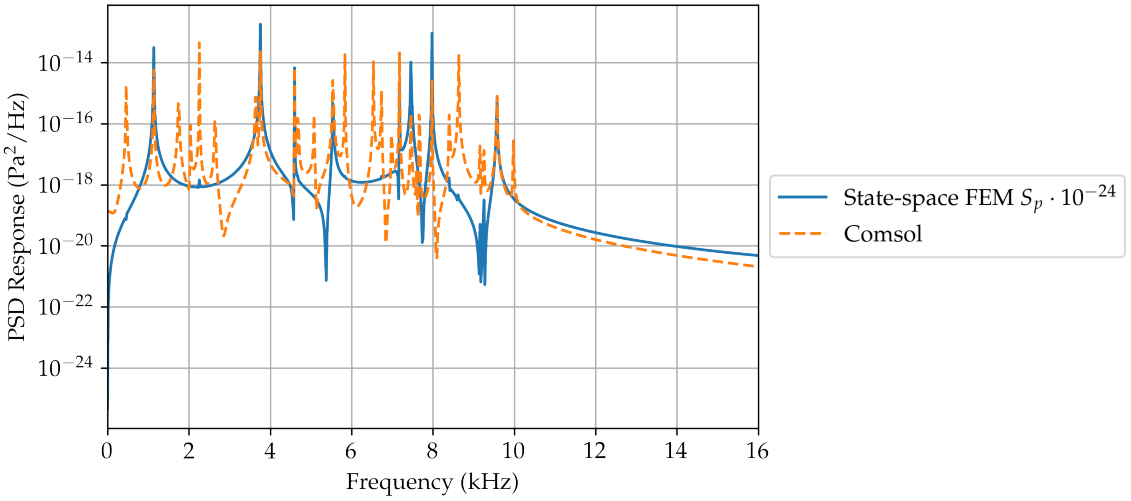

Figure 6.3: The power spectral density of the pressure in the fluid domain at [0, 0, 0] to a white noise body load of $1\,(\mathrm{N/m^3})^2/\mathrm{Hz}$ in the structural domain for our calculation in blue and COMSOL Multiphysics in orange. The properties of the structural system are the same as in Figure 6.2.

In order to investigate these differences, we also calculate the same properties using the same excitation, but now the water has been replaced by a very low density (fictional) fluid. The fluid domain consists of a fluid with density $\rho = 1 \times 10^{-10}\,\mathrm{kg\,m^{-3}}$, and a speed of

sound $c = 1\,\mathrm{m\,s^{-1}}$. For the calculations we used 14 eigenmodes with frequencies between 3595 Hz and 15 550 Hz.

In Figure 6.4 and Figure 6.5 the results are shown for respectively the structural and fluid domain. As we can see, the results for the structural domain are a near perfect match. Apart from a few features in the high frequency domain, the results are very similar. The pressure domain calculations are again very different. The peaks at the correct eigenfrequencies arise, but are not equal in shape or magnitude.

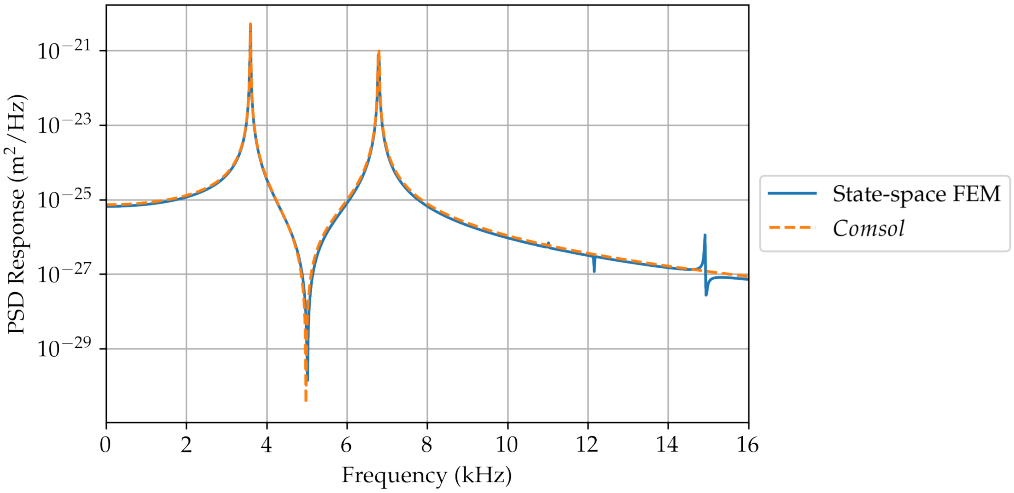

Figure 6.4: The power spectral density of the displacement in the structural domain at $[0.07, 0.061, 0.061]$ for our calculation in blue and COMSOL Multiphysics in orange. The properties of the structural system were $\rho = 2700\,\mathrm{kg\,m^{-3}}$, $\nu = 0.33$ $E = 70\,\mathrm{GPa}$, and of the fluid domain $\rho = 1 \times 10^{-10}\,\mathrm{kg\,m^{-3}}$, $c = 1\,\mathrm{m\,s^{-1}}$.

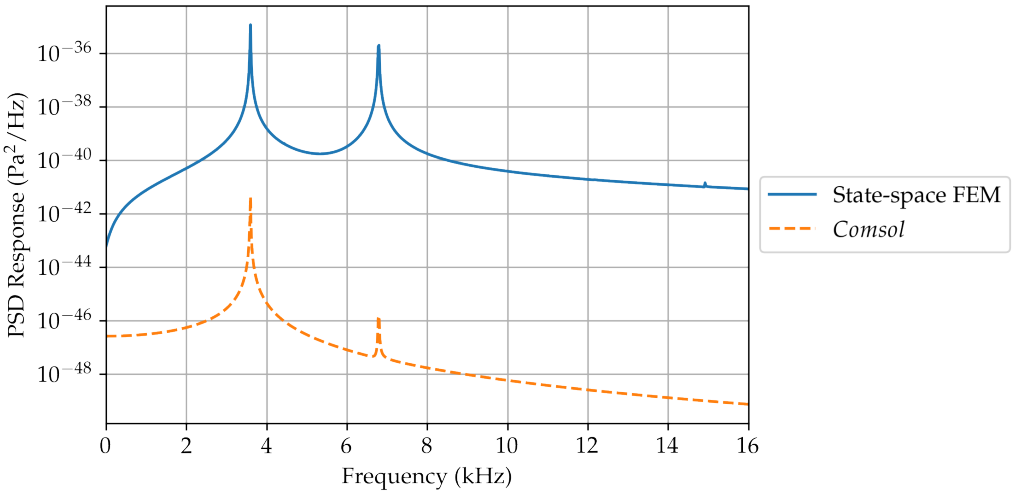

Figure 6.5: The power spectral density of the pressure in the fluid domain at $[0, 0, 0]$ for our calculation in blue and COMSOL Multiphysics in orange. The properties of the structural system were $\rho = 2700\,\mathrm{kg\,m^{-3}}$, $\nu = 0.33$ $E = 70\,\mathrm{GPa}$, and of the fluid domain $\rho = 1 \times 10^{-10}\,\mathrm{kg\,m^{-3}}$, $c = 1\,\mathrm{m\,s^{-1}}$.

We can now conclude that our method and the calculation by COMSOL Multiphysics are not the same. There seems to be a problem with the fluid part of the modes, as can

be derived from the fact that the structural domain gives similar results in the case of a near vacuum. We believe there is some scaling in the fluid part of the mass matrix that causes this mismatch between the modes. This can also explain the larger difference for the water-like fluid calculations. The fluid domain has a major impact on all modes. If these modes are then not calculated correctly, the whole system will be distorted.

Another argument that supports the theory that we do not yet understand what COMSOL Multiphysics exactly provides, is the fact that the mass matrix does not stay the same upon applying constraints. Within COMSOL Multiphysics it is possible to extract both the original mass matrix, and the mass matrix where constraints have already been built in, i.e. those rows and columns removed that correspond to restricted degrees of freedom. However, in the case of a coupled system, all mass matrix elements that correspond to the structural domain also get scaled inversely with some factor times the fluid density. This suggests that somehow the mass or fluid domain are not in the proper units before applying the constraints.

Lastly, within COMSOL Multiphysics it is not possible to obtain the cross-spectral density at the interface between the fluid and structural domains, or anywhere else for that matter. Therefore, it is not possible to use COMSOL Multiphysics to extract $\boldsymbol{S}_{pq}$. Also, it seems that COMSOL Multiphysics cannot even calculate the displacement spectral density of the structural part at the interface.

6.2 CONCLUSION

In conclusion, the theory developed in this chapter for coupled modes should be able to calculate the intensity of the radiated noise for any system that can be modelled using finite elements. This should combine both of the structural acoustics steps in Figure 1.1, and directly give us the intensity of the radiated noise from the pressure fluctuations. Note here, that the domain that is modelled using FEM is not infinitely large, as is the common approximation for marine propeller in the sea. However, using a big enough fluid domain (several times the longest wavelength of interest) could probably suffice.

However, it seems that the system matrices extracted from COMSOL Multiphysics are not exactly what we think they are. Therefore, a mismatch arises between our calculations and the one from COMSOL Multiphysics. COMSOL Multiphysics itself is also not capable of calculating any spectra at the interface, and can therefore not be used as a replacement for our own calculation. Also, COMSOL Multiphysics cannot deal with position-dependent excitation spectra (with arbitrary coherence), as mentioned earlier, which is vital for doing calculations concerning the turbulent boundary layer.

As a way forward, we would recommend using some open source software, such as Elmer [34], to obtain the system matrices, so that one can more easily find out what is going on. However, an even greater insight could be gained by calculating the system matrices oneself, and comparing it to both the system matrices generated by COMSOL Multiphysics and some other open source software package. An in-depth explanation of how to construct these system matrices can be for example found in a paper by Liang et al. on the numerical simulation of the fluid added mass effect for a Francis turbine in water.[35]

7

CONCLUSIONS

The goal of this work was to calculate the noise radiated by randomly excited structures. We wanted to achieve this through coupled modes calculated with a finite element method. This would allow for arbitrary geometries of the structural and fluid domain. However, we first had to look towards simple system multi-degree-of-freedom systems to develop the necessary theory and use analytical systems to verify our calculations.

We started with a look into multi-degree-of-freedom systems in Chapter 3 and saw that we could describe the vibrations of these systems through power spectral densities. With a modal analysis it was possible to calculate the response of the entire system through a simple formula. The modal analysis was used frequently throughout this thesis, because it can significantly reduce the complexity of the system when we can select only the relevant modes for a specific purpose. For a marine propeller we can select only the modes that are present in our desired frequency range, and therefore this is a viable strategy for simplifying the calculations.

However, the modal approach was only possible for proportional damping matrices. In order to allow non-proportional damping it was necessary to develop our own theory using state-space. In state-space we used a solution vector consisting of a displacement and velocity part. Using this new theory it was also possible to describe the response of non-proportionally damped systems, which was later on needed for structural-acoustic coupled systems. We verified the correctness of this theory by comparing it to the approach that only worked for proportionally damped systems. The two approaches indeed gave the exact same outcome. It was also found that the displacement and velocity part of the solution vector were internally consistent. These multi-degree-of-freedom calculations (both the proportional and non-proportional approach) are the basis on which the rest of this work was built. The finite element calculations, which are used to calculate the radiated noise, use the exact same theoretical basis.

In Chapter 4, we continued with continuous systems. These kinds of systems describe the response of a vibrating object analytically. We used these analytical systems to verify our calculations in Chapter 5 using the finite element method. We saw that we could calculate the response for 1D, 2D, and 3D-systems using a modal approach. The downside of using such a system is that it is necessary that one knows the mode shapes analytically. This is mostly possible for very simple geometries, such as rods and plates. Analytical expressions for the mode shapes depend on assumptions and approximations that are only valid for the lower-frequency range. For a geometrically-complicated system such as a propeller, it is not possible to find analytical mode shapes.

Because the analytical method was only applicable in specific circumstances, we had to use a different method for more complicated geometries, such as a propeller. Therefore, we turned towards finite element calculations in Chapter 5. The finite element method can in principle describe any geometry. The finite element method gives mode shapes

that can be used to calculate the response of systems, through the same methods we used for multi-degree-of-freedom systems. This is also where we see a strength of the modal approach. Usually, finite element systems consist of very many elements, say (tens of) thousands. The behaviour of such a finite element system can be described in the time or frequency domain, but we need very many time steps or many closely sampled frequencies to describe the response adequately, and still we can miss peaks easily. Therefore, the modal approach can significantly reduce the complexity of the system and improve accuracy, because the response is dominated and describe reliably by, say tens of these resonances. We saw that we could indeed use this approach to calculate the response of certain systems, for which the damping matrix was proportional to the mass and stiffness matrix. After using a finite element software to give us mode shapes, we verified that the response obtained for a proportionally damped rod in axial vibration matched the analytical calculations. We also verified that we could implement position and distance-vector-dependent (cross) spectra as excitation. This was not possible within the finite element software package (COMSOL Multiphysics) we used, but can be implemented in our own calculations. These position-dependent calculations were also verified using an analytical calculation, which indeed turned out to be a perfect match.

After it turned out we could describe proportionally damped systems using modes extracted from a finite element software, we moved on to non-proportionally damped systems. Unfortunately, within this specific finite element package (COMSOL Multiphysics), it was not possible to extract state-space eigenmodes. Therefore, we had to calculate them ourselves. It turned out that it was very much possible to use the state-space method for body loads. It was also possible to calculate the response of systems which had an added mass component to simulate the effect of water loading on the structure. However, in the case of point loads, the state-space approach did not seem give the same results as those obtained through the finite element software. There are two possible explanations for this. The first is that a point load should not be implemented at a single node, but instead be spread out to mimic the effect of a true point load. However, increasing the density of the nodes did not reduce the difference between the two methods, which would be expected in the case of a badly mimicked point loading. A different explanation, that we therefore find more likely, is that the modes are not calculated correctly. It could be that certain strains and stresses are not incorporated into the mass, stiffness, and damping matrix, but should be applied later. This hypothesis is strengthened by the fact that we could calculate proportionally damped systems for which we extracted the mode shapes directly from the finite element software.

The most important reason we developed the state-space approach, was to be able to deal with coupled systems. In coupled systems there is an acoustic domain coupled to the structural domain. We saw that the response of our calculation and the one given by the FE software package did not match. We investigated this difference by modelling the acoustic domain as a near vacuum. It turned out that in this case, the structural response did match, whereas the pressure response still did not. We believe this mismatch is caused by the incorrectness of the acoustic part of the mode shapes. This belief is strengthened by looking at the system matrices extracted from the finite element software. We saw that the constrained mass matrix was quite different from the unconstrained mass matrix in the structural domain. That suggests that the original unconstrained mass matrix did not have the fluid and mass part in the correct units.

The reason these coupled modes would be so convenient, is that one can directly integrate the cross spectrum of the pressure in the fluid and the velocity of the structure at the interface to obtain the radiated sound power as shown in Section 6.1. This would be a useful quantity to compare the radiated noise of two concept propellers, to aid in the design phase. The far-field radiated noise can also be determine using the Helmholtz-Kirchhoff integral.[33] To determine these quantities, it is also necessary to develop a proper model for the excitation of the structure. This work is part of the overarching PANPA project, in which this development also takes place.[30] In the outlook a first description of the turbulent boundary layer is provided, together with suggestions for improvements and experiments.

Overall, we do believe we have made significant steps in the development of a method that can calculate the radiated noise. Using this radiated noise, one can turn towards propeller design to minimise the radiated noise. Also, one can look at the spectrum and find out if specific modes are more present than others, and try to remove or lower the intensity of these modes. However, it is necessary to have a complete understanding of the mass, damping, and stiffness matrices produced by a finite element software to be able to properly calculate the response. It remains difficult to exactly understand what calculations are done behind the scenes of a commercial software package. An alternative to this could be to use an open source software package such as Elmer [34], where it is easier to find out how exactly the (constrained) system matrices are generated. Another advantage of open-source software, is that there is no licencing issue, and therefore it is easier to involve multiple parties in a project. For very simple systems, such as the example of a plate and a tank of water underneath, it is also possible to calculate the system matrices oneself. By comparing system matrices, some insight into what is going on behind the scenes in COMSOL Multiphysics could be obtained.

8

OUTLOOK

In this chapter, some suggestions for continuing this research are presented. Apart from this, a potential model for the turbulent boundary layer and its limitations are discussed. This characterisation of the turbulent boundary layer on a marine propeller is the last ingredient needed to properly calculate the radiated noise using coupled modes, as shown in this thesis.

8.1 EXPERIMENTS TO VALIDATE THE THEORY

The first and most essential continuation of this research, would be to conduct an experiment to validate this theoretical framework. This experiment should contain both an exactly verifiable structure such as a plate, and a more complicated geometry such as marine propeller. Within such an experiment, it would be wise to apply both a fully correlated white noise spectrum, and a position (and frequency) dependent spectrum that has a certain coherence spectrum based on the distance vector. In this way it would be possible to calculate the response using the FE software that can only deal with position-independent spectra, but also validate that the position-dependent spectra can be correctly modelled. As part of the PANPA project, a first look into applying specific spectra at certain positions, which is not trivial, has already been conducted by Mijnheer in unpublished work.

8.2 SOLVING THE MISMATCH IN COUPLED SYSTEMS

In order to look further into the mismatch between our approach in state-space and the one provided by the finite element software COMSOL Multiphysics, it is necessary to gain a deeper understanding of the FE software. Especially a better understanding of how exactly the modes and matrices are calculated within this software would greatly increase our chances of finding the error in either of the methods. One could look into the results provided by different commercial finite element packages, such as Actran [36]. Comparing these could give greater insight into what exactly is going on behind the scenes of a certain FE software package. Alternatively, one could look towards open-source packages, such as Elmer [34], where it is, in theory at least, easier to see what is going on. Lastly, calculating the system matrices for a very simple system by oneself would give most insight. This would be the most logical step to proceed with.

8.3 MODELLING THE TURBULENT BOUNDARY LAYER

Apart from experimental verification and resolving issues in our model, a well-developed theory for the turbulent boundary layer over a marine propeller is also essential for describing the radiated noise of a marine propeller. Therefore, to properly model a marine propeller a suitable model should be developed and tested.

There have been many attempts to model the turbulent boundary layer.[37] This research, however, has mostly been focussed on infinitely large flat plates and turbulent boundary layers consisting of air, and not water. For infinitely large plates, the auto and cross-spectra cannot depend on the position, but only on the distance vector, and therefore it does not accurately represent a propeller geometry, where the spectrum does depend on position. Characterising the exact wavenumber-frequency spectrum of the turbulent boundary layer for arbitrary geometries, such as a propeller, is quite difficult, especially when the geometry is hard to describe in the wave number domain. It is not within the scope of this thesis, and would require many years of research on its own, if one succeeds at all. The focus of this thesis was finding the stochastic response to an arbitrary stochastic input pressure field. This section will however, provide some background information about a possible model for the turbulent boundary layer on a propeller blade, as is being researched in the PANPA project.

Both the turbulent boundary layer and the inflow turbulence are geometry-dependent. Over the years, several models have been proposed for the resulting pressure field. In this section we will go a bit more in depth on one such model. A model provided by Amiet [12] for airfoils, which was later adapted by Mish and Devenport [38]. This model however, was not developed for marine propellers. It does not take into account the disturbance generated by the hull of the ship, behind which the propeller operates, although they assume that the incoming flow can include turbulence, which can be described by a model of choice, as we will see in Section 8.3.1.

As mentioned earlier, Amiet's model was originally developed for an airfoil geometry. A cross-sectional view of this geometry in show in Figure 8.1. The Amiet model assumes *zero angle of attack* and isotropic incoming turbulence.[39] The zero angle of attack means that the incoming turbulent flow is coming in parallel to the chord line of the airfoil, i.e., in the x-direction. This is another limitation of this model, as this is generally not the case for a marine propeller.

A propeller geometry can be described using multiple of such airfoils. The way this is done is shown in Figure 8.2. Each of these slices is assumed to be airfoil-like, but with different chord lengths, thickness, etc. One can apply the Amiet spectrum tailored to each slice. Using this model, we would ignore the effects of the orientation of the propeller in the flow. We assume there is no interaction between these slices, and thus the cross-correlation between them is zero. The width of a slice should be larger than the coherence length of the turbulence, to reduce the error of the assumption that the cross-correlation between the slices is zero. Another advantage of larger slices, is that the area at the edges of a slice, where there is no interaction with a different slice becomes relatively smaller. However,

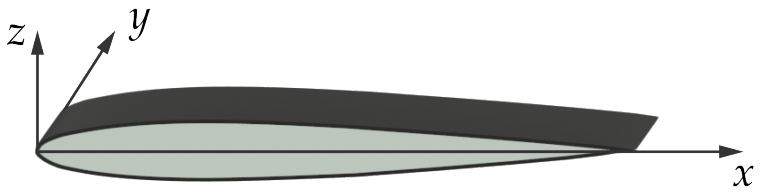

Figure 8.1: A side view of an airfoil geometry, which is symmetric in the xy-plane. In the Amiet model it is assumed this is extended infinitely in the y-direction.

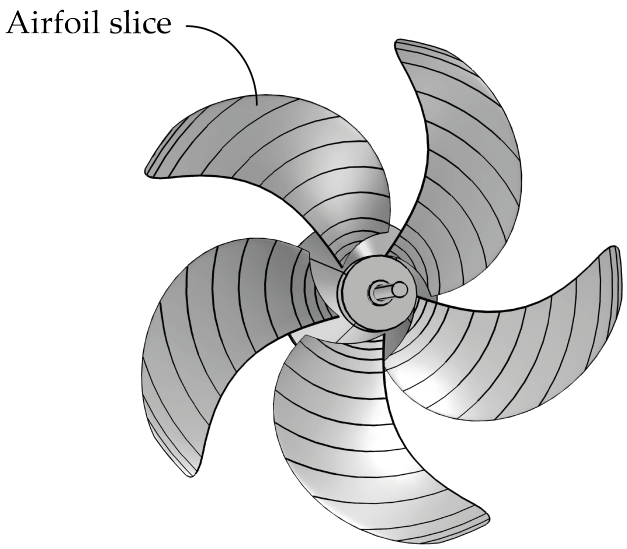

Figure 8.2: A schematic representation of a propeller blade divide up into airfoil-like geometries. The Amiet pressure spectrum can be applied to each slice individually. The Amiet model does not account for the orientation of the blade as shown in this image (it assumes zero angle of attack).

a downside of this is that the leading edge shape becomes less like the real propeller, because of the curvature of the propeller blade that is absent within one airfoil slice. Also, a propeller is not symmetric along the z-axis like an airfoil. The slices in Figure 8.2 do not fully represent the ones that can be used for the Amiet model, as they still need to be simplified further, because the Amiet model also assumes each slice is oriented at a zero angle compared to the flow.

Now, for the individual slices, the spectrum can be given in terms of the pressure jump. The pressure jump is simply the difference in pressure between both sides of the airfoil. A model for the power spectral density of this pressure jump is given by De Santana [39]

$$S(x,x',y,y',\omega) = 8U_\infty \pi^2 \rho^2 \int_0^\infty \bar{\gamma}(x',K_x,k_y)\gamma(x,K_x,k_y)\Phi_{ww}(K_x,k_y)\mathrm{e}^{\mathrm{i}k_y(y-y')}dk_y, \quad (8.1)$$

where U_∞ is the uniform far-field velocity, which in the case of a marine propeller would be influenced by the speed at which the propeller is rotating, and the wakefield of the vessel. ρ is the fluid density, and k_y is the span-wise wave number. K_x is a particular chord-wise wave number given by $K_x = \omega/U_\infty$. Φ_{ww} is given by the two-dimensional turbulence spectrum of the incoming flow.

The other term in the equation, the airfoil response function $\gamma(x,K_x,k_y)$, links the incoming air flow to pressure differences over the airfoil, and is given by Mish [40]

$$\gamma = -\frac{\chi}{\pi\beta}\left(\pi x\left[\left(\frac{k_y^2}{\beta^2}-\mu^2\right)^{1/2}+\mathrm{i}\left(\mu M+k_x\right)\right]\right)^{-1/2}\mathrm{e}^{-x\left(\frac{k_y^2}{\beta^2}-\mu^2\right)^{1/2}+\mathrm{i}(\mu M+k_x)}, \quad (8.2)$$

where $M = U_\infty/c$ is the Mach number, with c the speed of sound in the medium. In the case of marine propellers, this will be a very low number, as the speed of sound, say

1500 m/s, is two orders of magnitude larger than the speed of the flow. The terms β and μ are given by

$$\beta = \sqrt{1 - M^2} \qquad \mu = \frac{M k_x}{\beta^2}. \tag{8.3}$$

Finally, χ is divided up into two cases, for span-wise wave numbers either large or small compared to the chord-wise wave number. χ is given by

$$\chi = \begin{cases} 1 - \left(\frac{x}{2}\right)^{1/2} \left(1 - \operatorname{erf}\left[\left(2\,(2-x)\left(\frac{k_y^2}{\beta^2} - \mu^2\right)^{1/2}\right)^{1/2}\right]\right) & \text{for } k_y \geq (M/\sqrt{1-M^2})k_x \\ 1 - \left(\frac{x}{2}\right)^{1/2} \left(1 - (1-\mathrm{i})\,\mathrm{E}\left[2\mathrm{i}\left(\frac{2-x}{\pi}\left(\mu^2 - \frac{k_y^2}{\beta^2}\right)^{1/2}\right)^{1/2}\right]\right) & \text{for } k_y < (M/\sqrt{1-M^2})k_x \end{cases}. \tag{8.4}$$

Here E[.] is the Fresnel integral function given by

$$\mathrm{E}[x] = \operatorname{erf}[((1-\mathrm{i})\sqrt{x/2})/(1-\mathrm{i})] \tag{8.5}$$

and erf[.] is the error-function given by

$$\operatorname{erf}[z] = \frac{1}{\sqrt{\pi}} \int_0^z \mathrm{e}^{-t^2}\,\mathrm{d}t\,. \tag{8.6}$$

In principle, if a model for the inflow turbulence Φ_{ww} is chosen, the pressure spectrum on the airfoils can directly be applied. In our modelling of the radiated noise, we would need to integrate this pressure over the area surrounding a node, to find the corresponding nodal loading. From there we can calculate the radiate noise as shown in Chapter 6.

8.3.1 *Turbulence spectrum*

Although many models have been formulated for the inflow turbulence Φ_{ww}, the Von Kármán spectrum as given by Paterson and Amiet [41] is most commonly used (for the explicit expression, see the work by Dos Santos et al. [30, Eq. 6]). This Von Kármán turbulence spectrum was optimised for wind gusts in the atmosphere causing turbulence, and thus does not necessarily represent the turbulence generated by the ship wake field and the turbulent boundary layer. Several adaptations of this spectrum have already been proposed, such as modelling the dissipation range by Pope.[30, 42] The latter spectrum was also experimentally verified in a work by Dos Santos et al.[30]. However, exactly classifying this kind of turbulence, and improving the analytical spectrum to better fit experimental data is a study on its own, which is being conducted as a different part of the larger PANPA project (of which this thesis is also a part) at the University of Twente.

Still, Pope's spectrum was also not designed for marine propellers. Also, the experiments being conducted at the University of Twente are done in a wind tunnel. This might still need to be translated to a description of the spectrum of the turbulent flow of a ship wake field, which is a different geometry and medium. Therefore, an experiment validating that this spectrum could indeed also apply for underwater structures would be very useful to conduct.

In the same vein, the model by Amiet for the transfer of the turbulence spectrum to pressures on the airfoil, was mainly meant for airfoil geometries in air. An experiment using an airfoil in water would already be interesting to validate whether this theory is still suitable. The different fluid densities could have an impact on the transfer of the turbulent flow to pressures on the airfoil.

8.4 optimisation of the propeller and other applications

Further research once the theoretical framework has been verified could look into optimising the shape and material of the propeller. Of course the goal is then to minimise the radiated noise. Alternatively, one could look into applying this theory to different parts of a ship, or completely different fields, such as aerospace engineering, car manufacturing, HVAC (heating, ventilation, and air conditioning) or civil engineering to name a few.

A

COMPUTATIONAL NOTES

This appendix provides some computational notes to guide the reader in the reproduction of my work. This includes how to extract the needed matrices and vectors from COMSOL Multiphysics using Matlab, and some recommendations for speeding up the code.

A.1 EXTRACTING VARIABLES FROM COMSOL MULTIPHYSICS

The first step in extracting values from COMSOL Multiphysics through Matlab, is by connecting to the COMSOL Multiphysics server. This is most easily done by using the *COMSOL Multiphysics with Matlab* script for Matlab provided by COMSOL Multiphysics.

Once this is script is run, Matlab will automatically start. The first thing to do is import your COMSOL Multiphysics model in the Matlab code.

```
model = mphopen('model.mph');
```

This model will be used to extract the mass, damping, and stiffness matrices, as well as the eigenvectors and values already calculated by COMSOL Multiphysics.

A.1.1 *System matrices*

Let us first extract the system matrices. This can be done in the following way

```
mass_matrix = mphmatrix(model,'sol1','out',{'E'}).E;
stiff_matrix = mphmatrix(model,'sol1','out',{'K'}).K;
damp_matrix = mphmatrix(model,'sol1','out',{'D'}).D;
```

Here one has to make sure that the eigenfrequency analysis done in within the COMSOL Multiphysics framework is the first solution (`'sol1'`). If this is not the case, this should be changed to whatever solution name is given to the eigenfrequency analysis. Apart from these matrices, we can also extract the constrained matrices. In these matrices, the rows and columns of constrained degrees of freedom are already removed. This can simply be done by changing the name of the variable you want to extract.

```
constrained_mass_matrix = mphmatrix(model,'sol1','out',{'Ec'}).Ec;
constrained_stiff_matrix = mphmatrix(model,'sol1','out',{'Kc'}).Kc;
constrained_damp_matrix = mphmatrix(model,'sol1','out',{'Dc'}).Dc;
```

Now, it is also essential to know which nodes correspond to which row and column in these matrices. The following code snippet allows us to extract all the necessary information.

```
dof_information = mphxmeshinfo(model).nodes.dofs;
nodal_coordinates = mphxmeshinfo(model).nodes.coords;
```

Firstly, the variable `dof_information` is a matrix of which each column corresponds to a node and contains the row/column number (1-based) of each degree of freedom in a system matrix for that specific node. In case that degree of freedom is not present, the value will be `-1`. This will happen in the case of coupled systems, where some nodes have only pressure or structural degrees of freedom. Each row in the matrix corresponds to one specific degree of freedom. Therefore, in a purely structural system, this will have three rows, while in a coupled system there are four. The coordinates of the node to which a certain column corresponds is given by `nodal_coordinates`. This matrix contained in this variable is in the same order as the one in `dof_information`.

In general, a system matrix (mass, stiffness, or damping) is ordered in such a way that the row and columns corresponding to a single node are next to each other, in the order $p \rightarrow x \rightarrow y \rightarrow z$, where constrained (in the case of a constrained matrix) or non-present (in the case of a coupled system) degrees of freedom are deleted. Please note that in the case of constrained matrices, the variables `dof_information` and `nodal_coordinates` are not changed, and will need to be manually filtered if one wants to obtain the list without constrained degrees of freedom.

For calculating the radiated noise, one should be able to extract the surface nodes and their indices from COMSOL Multiphysics. This can be easily done by looking at the `dof_information` variable. If a column does not contain a `-1` for the pressure degree of freedom, and one of the structural degrees of freedom is also not `-1` it is a node on the interface between the acoustic and structural domain.

Lastly, it is also possible to extract the loading on the structure. In the case of random vibration, this loading should be squared to obtain the power spectral density value at each node in the case of white noise. For other spectra, this squared value should be multiplied with the desired spectrum at a certain node.

```
10 load = mphmatrix(model,'sol1','out',{'L'}).L;
11 constrained_load = mphmatrix(model,'sol1','out',{'Lc'}).Lc;
```

A.1.2 *Eigenmodes and eigenvalues*

It is also possible to obtain the eigenmodes generated by COMSOL Multiphysics at certain coordinates. First, one needs to evaluate the eigenmode at the nodal positions.

```
12 eigenmodes = mpheval(model, {'u', 'v', 'w'});
```

The variables `'u'`, `'v'`, and `'w'` correspond respectively to the x, y, and z part of eigenmode displacement. In case that one has a coupled system and would also like to extract the pressure part of the eigenmodes, it can be done with the variable `'p'`.

Once this is done, one can extract the values of the eigenmodes as shown in the following code snippet. One has to import the x, y, and z components separately.

```
13 eigenmodes_x = eigenmodes.d1;
14 eigenmodes_y = eigenmodes.d2;
15 eigenmodes_z = eigenmodes.d3;
```

Again, it is vital to know what you are dealing with here. Therefore, one should also extract the coordinates of the nodes at which you have evaluated the eigenmode.

```
16 node_coords = eigenmodes.p;
```

Please note that this ordering is **not** the same as the one used for the system matrices. When using the extracted values, one should always carefully take stock of what you are dealing with. In order to make a complete eigenvector matrix, one has to combine them by stacking them in a way the user finds convenient, while keeping in mind which rows correspond to which degree of freedom.

It is also possible to extract the eigenfrequencies given by COMSOL Multiphysics. The eigenfrequencies are directly extracted from the eigenfrequency analysis.

```
17 eigenfrequencies = mphsolinfo(model).solvals * 1i;
```

It should be noted here, that to obtain the real and imaginary part (used for damping) of the eigenfrequency correctly, the extracted values from COMSOL Multiphysics should be multiplied with the imaginary unit i. This is another reminder to always check what exactly COMSOL Multiphysics provides as output.

A.1.3 *Exporting data*

These objects can easily be saved as a (very inefficient) text file for later import in some other software of your choice. Of course, there are many other more efficient file formats (such as .mat, imported in Python with SciPy's `loadmat`) to which Matlab can directly export your data. A warning when importing a text file into for example Python is that the imaginary unit in python is `j` whereas in Matlab it will output it as `i`. Apart from this, one should also keep in mind that negative values in complex numbers are exported by Matlab using `a+-bi`. Some programs, such as Python's `numpy.genfromtext` cannot deal with this, and it should be first converted to `a-bi`. As an example of the export function, the following code snippet exports the mass matrix to a path of your choice.

```
18 writematrix(mass_matrix, 'C:\your\path\mass_matrix.txt')
```

For completeness, a function in Python that applies the conversion mentioned earlier to a text file is also provided.

```
1 def convert_plus_minus_i_j(txtfile):
2     with open(txtfile, 'r') as file:
3         filedata = file.read()
4     # Replace the target string
5     filedata = filedata.replace('+-', '-')
6     filedata = filedata.replace('i', 'j')
7     # Write the file with the conversion applied
8     with open(txtfile, 'w') as file:
9         file.write(filedata)
```

A.2 RESPONSE CALCULATIONS

Firstly, we will provide some code that can calculate the response of a system in Python. This code provides the response at all nodes. In this code, `damp_fact_list` is a list containing the damping factors corresponding to each mode. `U` is the matrix of eigenvectors. `w_range` is a list of all frequencies at which the response is calculated. Lastly, `eigenfrequencies` is a list of all eigenfrequencies, and `excitation_spectral_density_matrix` is the matrix of excitation spectral densities at the nodes, which can be a function that depends on frequency.

```
1  def output_spectral_density(w_range, eigenfrequencies, eigenvectors, damp_fact_list,
       excitation_spectral_density_matrix):
2      N = len(eigenfrequencies)
3      P = len(eigenvectors)
4      response = numpy.zeros((len(w_range),P,P), dtype = complex)
5
6      for count, omega in enumerate(w_range):
7          G = numpy.diag(numpy.array([1 / (w_eig**2 - omega**2 + 2j*omega*zeta*w_eig)
8              for w_eig, zeta in zip(eigenfrequencies, damp_fact_list)]))
9
10         temp = eigenvectors @ G.conj()
11         temp = temp @ (eigenvectors.T.conj() @ excitation_spectral_density_matrix(omega)
12             @ eigenvectors)
13         temp = temp @ G @ eigenvectors.T.conj()
14
15         response[count] = temp
16     return response
```

For large systems, this can be very computationally intensive. Another thing that can slow the computation down, is that the response matrix, which has dimensions $n_\omega \times N \times N$, where n_ω is the number of frequencies, and N is the number of degrees of freedom, is sometimes too large to keep in the RAM. In these cases, one could write the output matrix to a file in between computations. For smaller systems, where this is not necessary, this would significantly slow down the computation, as the disk memory is much slower to access.

In the case that the excitation spectral density does not depend on frequency, one could pre-calculate the part in brackets after the first @ in line 11, such that one only has to calculate it once. This can save a lot of time in the case of large systems and many frequencies sampled. This is however not useful for turbulent boundary layers, as in that case the excitation is of course frequency dependent.

If one is only interested in the response of a single degree of freedom of the structure, one can significantly speed up this process. This is done by only using the column corresponding to the degree of freedom of interest in the last matrix of the calculation, and the row of this degree of freedom in the first matrix of the calculation (for the exact matrix multiplications, see Equation 3.39, and for state-space Equation 3.68). If you then multiply the matrices from right to left, you are essentially doing matrix-vector multiplications instead of matrix-matrix multiplications. Matrix-vector multiplications are much faster than matrix-matrix multiplications. Below is an example of such a speed-up using the state-space method. The following code provides the response spectrum for a certain element r, s of the response matrix in state-space. `X` is the matrix of right eigenvectors, and

Y is the matrix of left eigenvectors. It can be seen here that we indeed only use column s of X and row r of Y.

```
def output_spectral_density_single_point(w_range, r, s, X, Y, M, eigenfrequencies,
    excitation_spectral_density_matrix):
    N = len(eigenfrequencies)
    P = len(M)
    B = numpy.vstack((numpy.zeros((P,P)), numpy.linalg.inv(M)))
    response = numpy.zeros(len(w_range), dtype = complex)

    for omega in enumerate(w_range):
        G = numpy.diag(numpy.array([1/(1j*omega - w_eig) for w_eig in eigenfrequencies]))

        temp = G @ (X).T.conj()[:,s]
        temp = B.T.conj() @ (Y @ temp)
        temp = B @ (excitation_spectral_density_matrix(omega) @ temp)
        temp = numpy.conj(G) @ ((Y).T.conj() @ temp)
        temp = X[r] @ temp

        response[count] = temp
    return (response)
```

BIBLIOGRAPHY

[1] OSPAR, *Overview of the impacts of anthropogenic underwater sound in the marine environment. ospar biodiversity series*, May 2009.

[2] B. Masterton, H. Heffner and R. Ravizza, 'The evolution of human hearing', *The Journal of the Acoustical Society of America* **45**, 966–85 (1969) 10.2514/1.C031405.

[3] U. Stöber and F. Thomsen, 'Effect of impact pile driving noise on marine mammals: a comparison of different noise exposure criteria', *The Journal of the Acoustical Society of America* **145**, 3252–3259 (2019) 10.1121/1.5109387.

[4] C. Erbe, S. A. Marley, R. P. Schoeman, J. N. Smith, L. E. Trigg and C. B. Embling, 'The effects of ship noise on marine mammals—a review', *Frontiers in Marine Science* **6**, – (2019) 10.3389/fmars.2019.00606.

[5] R. E. Kurt, H. Khalid, O. Turan, M. Houben, J. Bos and I. H. Helvacioglu, 'Towards human-oriented norms: considering the effects of noise exposure on board ships', *Ocean Engineering* **120**, 101–107 (2016) 10.1016/j.oceaneng.2016.03.049.

[6] C. C. Baker and A. K. Seah, 'Maritime accidents and human performance: the statistical trail', in Martech conference, singapore (2004), pp. 225–240.

[7] L. Li, Y. Cao and W. Zhang, 'Study on hull vibration and underwater radiation noise induced by propeller excitation considering shafting alignment', *The Journal of the Acoustical Society of America* **131**, 3507–3507 (2012) 10.1121/1.4709257.

[8] L. Miglianti, F. Cipollini, L. Oneto, G. Tani, S. Gaggero, A. Coraddu and M. Viviani, 'Predicting the cavitating marine propeller noise at design stage: a deep learning based approach', *Ocean Engineering* **209**, 107481 (2020) 10.1016/j.oceaneng.2020.107481.

[9] H. Seol, J.-C. Suh and S. Lee, 'Development of hybrid method for the prediction of underwater propeller noise', *Journal of Sound and Vibration* **288**, 345–360 (2005) 10.1016/j.jsv.2005.01.015.

[10] S. Sharma, K. Mani and V. Arakeri, 'Cavitation noise studies on marine propellers', *Journal of Sound and Vibration* **138**, 255–283 (1990) 10.1016/0022-460X(90)90542-8.

[11] G. M. Corcos, 'The structure of the turbulent pressure field in boundary-layer flows', *Journal of Fluid Mechanics* **18**, 353–378 (1964) 10.1017/S002211206400026X.

[12] R. Amiet, 'Noise due to turbulent flow past a trailing edge', *Journal of Sound and Vibration* **47**, 387–393 (1976) 10.1016/0022-460X(76)90948-2.

[13] S. Türkay and H. Akçay, 'A study of random vibration characteristics of the quarter-car model', *Journal of Sound and Vibration* **282**, 111–124 (2005) 10.1016/j.jsv.2004.02.049.

[14] J. W. Miles, 'On structural fatigue under random loading', *Journal of the Aeronautical Sciences* **21**, 753–762 (1954) 10.2514/8.3199.

[15] Z. Zeng, K. Zhu, X. He, W. Xu, L. Chen and P. Lou, 'Random vibration analysis of train moving over slab track on bridge under track irregularities and earthquakes by pseudoexcitation method', *Discrete Dynamics in Nature and Society* **2015**, 436567 (2015) 10.1155/2015/436567.

[16] J. J. Wijker, "Random vibrations in spacecraft structures design: theory and applications", Solid Mechanics and Its Applications (Springer Netherlands, 2009).

[17] L. Meirovitch, "Fundamentals of vibrations", McGraw-Hill higher education (McGraw-Hill, 2001).

[18] J. F. Hall, 'Problems encountered from the use (or misuse) of rayleigh damping', *Earthquake Engineering & Structural Dynamics* **35**, 525–545 (2006) 10.1002/eqe.541.

[19] J. Li and J. Chen, "Stochastic dynamics of structures" (Wiley, 2009).

[20] L. Meirovitch, "Principles and techniques of vibrations" (Prentice Hall, 1997).

[21] S. De Rosa and F. Franco, 'Exact and numerical responses of a plate under a turbulent boundary layer excitation', *Journal of Fluids and Structures* **24**, 212–230 (2008) 10.1016/j.jfluidstructs.2007.07.007.

[22] A. Leissa, "Vibration of plates", NASA SP (Scientific, Technical Information Division, National Aeronautics and Space Administration, 1969).

[23] N. Ottosen and H. Petersson, "Introduction to the finite element method" (Prentice Hall, 1992).

[24] J. Fish and T. Belytschko, "A first course in finite elements" (Wiley, 2007).

[25] E. Huggins, 'Speed of sound in metal pipes: an inexpensive lab', *The Physics Teacher* **46**, 13–14 (2008) 10.1119/1.2823993.

[26] L. Burill, 'Underwater propeller vibration tests', *London: North East Coast Institution of Engineers and Shipbuilders* **65** (1949).

[27] O. Zienkiewicz, R. Taylor and J. Zhu, "The finite element method: its basis and fundamentals" (Elsevier Science, 2005).

[28] M. Tanaka, G. Girard, R. Davis, A. Peuto and N. Bignell, 'Recommended table for the density of water between 0 c and 40 c based on recent experimental reports', *Metrologia* **38**, 301–309 (2001) 10.1088/0026-1394/38/4/3.

[29] A. Caiazzo, R. D'Amico and W. Desmet, 'Use of a generalized corcos model to predict flow-induced noise in a cavity-plate system', in Isma2016, leuven (Sept. 2016).

[30] F. L. dos Santos, L. Botero-Bolívar, C. Venner and L. D. de Santana, 'Modeling the turbulence spectrum dissipation range for leading-edge noise prediction', *AIAA Journal* **60**, 3581–3592 (2022) 10.2514/1.J061106.

[31] M. Karimi, L. Maxit, P. Croaker, O. Robin, A. Skvortsov, S. Marburg, N. Atalla and N. Kessissoglou, 'Analytical and numerical prediction of acoustic radiation from a

panel under turbulent boundary layer excitation', *Journal of Sound and Vibration* **479**, 115372 (2020) https://doi.org/10.1016/j.jsv.2020.115372.

[32] G. Williams, "Fourier acoustics: sound radiation and nearfield acoustical holography" (Elsevier Science, 1999).

[33] K. Been and W. Moon, 'Reconsideration on helmholtz-kirchhoff integral solutions for boundary points in radiation problems', *Acta Acustica united with Acustica* **105**, 827–837 (2019) 10.3813/AAA.919363.

[34] *Elmer*, https://www.csc.fi/web/elmer, Accessed: 05-09-2020.

[35] Q. Liang, C. Rodríguez, E. Egusquiza, X. Escaler, M. Farhat and F. Avellan, 'Numerical simulation of fluid added mass effect on a francis turbine runner', *Computers & Fluids* **36**, 1106–1118 (2007) 10.1016/j.compfluid.2006.08.007.

[36] *Actran*, https://www.mscsoftware.com/product/actran, Accessed: 07-09-2020.

[37] T. S. Miller, J. M. Gallman and M. J. Moeller, 'Review of turbulent boundary layer models for acoustic analysis', *Journal of Aircraft* **49**, 1739–1754 (2012) 10.2514/1.C031405.

[38] P. F. Mish and W. J. Devenport, 'An experimental investigation of unsteady surface pressure on an airfoil in turbulence—part 1: effects of mean loading', *Journal of Sound and Vibration* **296**, 417–446 (2006) 10.1016/j.jsv.2005.08.008.

[39] L. de Santana, *Semi-analytical methodologies for airfoil noise prediction*, PhD. Thesis, 2015.

[40] P. F. Mish, *Mean loading and turbulence scale effects on the surface pressure fluctuations occurring on a naca 0015 airfoil immersed in grid generated turbulence*, MSc. Thesis, 2001.

[41] R. Paterson and R. Amiet, 'Acoustic radiation and surface pressure characteristics of an airfoil due to incident turbulence', in *3rd aeroacoustics conference* (1976), 10.2514/6.1976-571.

[42] S. B. Pope, "Turbulent flows" (Cambridge University Press, 2000).